Interference Coordination in Heterogeneous Networks: Stochastic Geometry Based Modelling and Performance Analysis

Haonan Hu

Department of Electronic and Electrical Engineering
University of Sheffield

Supervisors: Prof. Jie Zhang, Dr. Xiaoli Chu
This dissertation is submitted for the degree of
Doctor of Philosophy

December 2018

This dissertation is dedicated to the memory of my grandfather who was my inspiration to pursue my doctoral degree, but he was unable to see my graduation.

Declaration

I hereby declare that except where specific reference is made to the work of others, the contents of this dissertation are original and have not been submitted in whole or in part for consideration for any other degree or qualification in this, or any other university. This dissertation is my own work and contains nothing which is the outcome of work done in collaboration with others, except as specified in the text and Acknowledgements. This dissertation contains fewer than 65,000 words including appendices, bibliography, footnotes, tables and equations and has fewer than 150 figures.

Haonan Hu
December 2018

Acknowledgements

I would like to express the deepest appreciation to my first supervisor, Prof. Jie Zhang, for his consistent guidances during my whole Ph.D. study. He has the substance of a genius, who always can provide insightful ideas for my research direction and valuable suggestions and comments for solving problems. He also inspired me to be an independent researcher, not only with hard working and good time management, but also with the positive attitude. I am also very grateful to my second supervisor, Dr. Xiaoli Chu, for her patience and dedication on polishing the writing and presentation of my works. She is a very talented researcher and is very kind to provide help on my research. I feel so fortunate to have the opportunity to work with them for four years, and without their guidance and persistent help, this dissertation would not have been possible.

I would also like to thank Chongqing University of Posts and Telecommunications and China Scholarship Council for their financial support.

The works in this dissertation are accomplished by cooperating with many excellent researchers. Chapter 3 is a collaborated work with Dr. Jialai Weng, Dr. Jiliang Zhang, Prof. Yang Wang and Prof. Jie Zhang. Chapter 4 is a joint work with Dr. Baoling Zhang, Dr. Qi Hong, Dr. Xiaoli Chu and Prof. Jie Zhang. The content in Chapter 5 is achieved jointly with Yuan Gao, Dr. Xiaoli Chu, Dr. Baoling Zhang and Prof. Jie Zhang. I am indebted to Dr. Jialai Weng and Dr. Jiliang Zhang, both of whom gave me a lot of helpful advices throughout my Ph.D. study. Despite the direct collaboration on this dissertation, I would like to thank Dr. Yue Wu and Dr. Wulin Liu, who provided constructive advices on my research. Appreciation to Dr. Baoling Zhang, Dr. Qi Hong, Dr. Hao Li, Weijie Qi, Kan Lin and Hui Zheng is due to not only the collaboration on some interesting ideas, but also the great fun when we hanged out together that makes these four years unforgettable.

I would like to express my gratitude to Prof. Qianbin Chen for his constant support on my study abroad and advices for my career development. Without his support, I can barely have the chance to finish my Ph.D. study.

Last but not the least, I want to thank my family and friends, who gave me many supports in the past four years. Specifically, I am very thankful to my fiance Ms. Ran Duan, who gave me full support and went through thick and thin together with me throughout the Ph.D. study.

Abstract

Recently data traffic has experienced explosive increase with the proliferation of wireless devices and the popularity of media-based free services. The academic and industry of mobile communications have predicted an estimated 1000x increase in traffic volume for the forthcoming 5G networks. This traffic explosion stimulates the deployment of heterogeneous networks (HetNets) with small cells (SCs) underlying in the traditional macrocells, which has been considered as a promising technique to contribute to the 1000x traffic capacity gain. Initially, licensed spectrum bands are expected to be used in SCs, thus the SC deployment introduces the cross-tier interference between SCs and macrocells, which degrades the downlink signal to interference plus noise ratio (SINR) of user equipments (UEs) severely, especially for the edge UEs in a ultra-densely deployed scenario. To alleviate this cross-tier interference between SCs and macrocells, unlicensed spectrum bands are advocated to be used in SCs. Specifically, with the aid of carrier aggregation, the 5 gigahertz (GHz) unlicensed band has become an option for SCs in the Long Term Evolution (LTE)-Unlicensed (LTE-U) scheme, but the 5 Ghz unlicensed band has already been used by WiFi networks. Thus downlink cross-tier interference also occurs between LTE-U and WiFi networks. Accordingly, downlink cross-tier interference is inevitable no matter licensed or unlicensed spectrum band (i.e., 5 GHz) is used in SCs, and interference coordination schemes, such as further enhanced inter-cell interference coordination (FeICIC) for macrocells and SCs, and Licensed Assisted Access (LAA) for WiFi networks and LTE-U networks, have been proposed to mitigate these cross-tier interferences. In this dissertation, we mainly focus on the modelling and performance analysis of HetNets with the aforementioned two interference coordination schemes (i.e., FeICIC and LTE-LAA) under the stochastic geometry framework.

Firstly, as the configuration of reduced power subframe (RPS)-related parameters was not well investigated in a two-tier HetNet adopting RPSs and cell range expansion (CRE), we derive the analytical expressions of the downlink coverage probability and rate coverage probability in such a HetNet. The optimal settings for the area of macrocell center regions, the area of SC range expansion regions, and the transmit power of RPSs for maximizing the rate coverage probability are analysed. As compared with the rate coverage probability in the two-tier HetNet with almost blank subframes (ABSs), which is proposed in the previous

version of FeICIC, i.e., the enhanced inter-cell interference coordination (eICIC), the results show that ABSs outperform RPSs in terms of the rate coverage probability in the two-tier HetNet with the optimal range expansion bias, but lead to a heavier burden on the SC backhaul. However, with static typical range expansion biases, RPSs provide better rate coverage probability than ABSs in the two-tier HetNet.

Secondly, the conventional FeICIC scheme ignores the potential of RPSs being adopted in both tiers of a two-tier HetNet without CRE, which is envisioned to improve the SINR level of edge UEs in both tiers. Accordingly, we study the downlink coverage probability and rate coverage probability of a two-tier HetNet applying with our proposed scheme. The results reveal that adopting RPSs in both tiers not only improves the coverage probabilities of edge UEs, but also increases the rate coverage probability of the whole two-tier HetNet.

Thirdly, in both previous works, strict subframe alignment (SA) was assumed throughout the whole network, which is difficult to maintain between neighbouring cells in reality. Consequently, we propose a novel subframe misalignment (SM) model for a two-tier HetNet adopting RPSs with SM offsets restricted within a subframe duration, and analyse the coverage probability under the effects of RPSs and SM. The numerical results indicate that the strict SA requirement can be relaxed by up to 20% of the subframe duration with a loss of below 5% in terms of the downlink coverage probability.

Lastly, since stochastic-geometry-based analysis of the coexisting LTE-LAA and WiFi networks, which adopt the carrier-sense multiple access with collision avoidance (CSMA/CA) as the medium access control (MAC) scheme and share multiple unlicensed channels (UCs), was missing, we analyse the downlink throughput and spectral efficiency (SE) of the co-existing LTE-LAA and WiFi networks versus the network density and the number of UCs based on the Matern hard core process. The throughput and SE are obtained as functions of the downlink successful transmission probability (STP), of which analytical expressions are derived for both LTE-LAA and WiFi UEs. The results show that the throughput and SE of the whole coexisting LTE-LAA and WiFi networks can be improved significantly with an increasing number of accessible UCs. Based on the numerical results, insights into the trade-off between the throughput and SE against the number of accessible UCs are provided.

All the derived results have been validated by Monte Carlo simulation in Matlab, and the conclusions observed from the results can provide guidelines for the future deployments of the FeICIC and LTE-LAA interference coordination schemes in HetNets.

List of publications

Published

[1] **H. Hu**, B. Zhang, Q. Hong, X. Chu, and J. Zhang, "Coverage Analysis of Reduced Power Subframes Applied in Heterogeneous Networks with Subframe Misalignment Interference," accepted in *IEEE Wireless Communications Letters*, March 2018.

[2] **H. Hu**, J. Weng and J. Zhang, "Coverage Performance Analysis of FeICIC Low-Power Subframes," *IEEE Transactions on Wireless Communications*, vol. 15, no. 8, pp. 5603-5614, August 2016.

[3] **H. Hu**, J. Weng, J. Zhang, J. Zhang, and Y. Wang, "Modelling and Analysis of Reduced Power Subframes in Two-Tier Femto HetNets," in *2016 IEEE 83rd Vehicular Technology Conference (VTC Spring)*, Nanjing, pp. 1-5, May 2016.

[4] Y. Gao, **H. Hu**, Y. Wu, X. Chu, and J. Zhang, "Energy Efficent and Fair Resource Allocation for LTE-Unlicensed Uplink Networks: A Two-sided Matching with Partial Information Approach," accepted in *Transactions on Emerging Telecommunications Technologies*, July 2018.

[5] Q. Liu, Z. Zhang, **H. Hu** and J. Shi, "Modeling and Analysis of One-Tier Ultradense Multiuser Networks," *IEEE Access*, vol. 6, pp. 13972-13979, April 2018.

[6] H. Zheng, J. Zhang, H. Li, Q. Hong, **H. Hu** and J. Zhang, "Exact Line-of-Sight Probability for Channel Modelling in Typical Indoor Environments," in *IEEE Antennas and Wireless Propagation Letters*, vol. 17, no. 7, pp. 1359-1362, July 2018.

[7] Q. H, J. Zhang, H. Zheng, H. Li, **H. Hu**, B. Zhang, Z. Lai, and J. Zhang. "The Impact of Antenna Height on 3D Channel: A Ray Launching Based Analysis," *Electronics*, vol. 7, no. 1, February 2018.

[8] H. Zheng, J. Zhang, **H. Hu**, and J. Zhang, "The Analysis of Indoor Wireless Communications by a Blockage Model in Ultra-dense Networks," accepted in *2018 IEEE 88th Vehicular Technology Conference (VTC Fall)*, Chicago, pp. 1-5, August 2018.

[9] J. Weng, W. Liu, **H. Hu**, X. Chu, and J. Zhang, "A mathematical formulation for MIMO channel map," in *2015 Loughborough Antennas Propagation Conference (LAPC)*, Loughborough, pp. 1-5, November 2015.

Submitted

[10] **H. Hu**, Y. Gao, X. Chu, B. Zhang, and J. Zhang, "On the Performance of LTE-LAA Networks Coexisting with WiFi Networks under Multiple Unlicensed Channels," under review in *IEEE Transactions on Wireless Communications*, May 2018.

[11] **H. Hu**, Y. Gao, J. Zhang, X. Chu, and J. Zhang, "On the Performance and Fairness of LTE-U Networks Coexisting with WiFi Networks sharing Multiple Unlicensed Channels," under review in *IEEE ICC 2019*, October 2018.

[12] Y. Gao, Y. Wu, **H. Hu**, X. Chu, and J. Zhang, "Licensed and Unlicensed Bands Allocation for Cellular Users: A Matching-based Optimization Approach", under review in *IEEE Wireless Communications Letters*, September 2018.

Table of contents

List of figures

List of tables

List of abbreviations

3GPP 3rd Generation Partnership Project

AO Actual Optimal

AP Access Point

BS Base Station

CAGR Compound Annual Growth Rate

CAPEX Capital Expenditure

CCDF Complementary Cumulative Distribution Function

CoMP Coordinated MultiPoint

CRE Cell Range Expansion

CRU Centre Region UE

CSAT Carrier Sensing Adaptive Transmission

CSI Channel State Information

CSMA/CA Carrier-Sense Multiple Access with Collision Avoidance

D2D Device-to-Device

EE Energy Efficiency

eICIC Enhanced Intercell Interference Coordination

ERU Edge Region UE

FBS Femtocell Base Station

FBS Femtocell Base Station

FeICIC Further enhanced Intercell Interference Coordination

FFR Fractional Frequency Reuse

FPS Full Power Subframe

FRPS Femto Reduced Power Subframe

GHz Gigahertz

HetNets Heterogeneous Networks

ICIC Intercell Interference Coordination

LAA Licensed Assisted Access

LAP LTE-LAA Access Point

LB Lower Bound

LBT Listen Before Talk

LOS Line-Of-Sight

LT Laplace Transform

LTE Long Term Evolution

LTE-U Long Term Evolution-Unlicensed

LUE LTE-LAA UE

M2M Machine-to-Machine

MAC Medium Access Control

MAP Medium Access Probability

MBS Macrocell Base Station

MHCP Matern Hard Core Process

MIMO Multiple-Input Multiple-Output

mmWave Millimetre Wave

MRPS Macro Reduced Power Subframe

MSMO Maximum Subframe Misalignment Offset

MUE Macro User Equipment

NLOS Non-Line-Of-Sight

NO Near Optimal

NOMA Non-Orthogonal Multiple Access

NPS Normal Power Subframe

OFDM Orthogonal Frequency-Division Multiplexing

OFDMA Orthogonal Frequency-Division Multiple Access

PBS Picocell Base Station

PDF Probability Density Function

PHP Poisson Hole Process

PS Protected Subframe

PUE Pico User Equipment

QPSK Quadrature Phase Shift Keying

RAT Radio Access Technology

RPS Reduced Power Subframe

RSS Received Signal Strength

SA Subframe Alignment

SC Small Cell

SDMA Spatial Division Multiple Access

SE Spectral Efficiency

SFR Soft Frequency Reuse

SINR Signal to Interference plus Noise Ratio

SIR Signal to Interference Ratio

SM Subframe Misalignment

SSE Spatial Spectral Efficiency

STH Spatial Throughput

STP Successful Transmission Probability

UC Unlicensed Channels

UE User Equipment

US Unprotected Subframe

VNI Visual Networking Index

VU Victim UE

WAP WiFi AP

WUE WiFi UE

Chapter 1

Introduction

1.1 Background

With the proliferation of wirelessly connected devices (e.g. smart phones and tablets) and the popularity of media-based free services, such as iTunes, YouTube, etc., mobile operators have experienced an exponential traffic growth in recent years. Mobile communication research and industry have been making efforts to meet an estimated 1000x increase requirement in traffic capacity for the forthcoming 5G networks. Although it is difficult to predict when the 1000x traffic growth will happen, tremendous growth in mobile data traffic has been observed in the past and it is expected to increase steadily in the future.

As observed by the Ericsson and the Cisco visual networking index (VNI) [1], global mobile traffic has grown steadily at a compound annual growth rate (CAGR) of 50 to 66 percent from 2012 to 2017, which has brought an eightfold to thirteen-fold traffic increase since 2012. According to the recently published report by the Cisco VNI [2], the global mobile data traffic will increase sevenfold between 2016 and 2021 at a CAGR of 46 percent, reaching 48.3 exabytes per month by 2021. In addition, by the year 2021, there will be 4.6 billion internet users, 27.1 billion connected network devices globally, and the total network traffic will reach 3.3 zettabytes annually, 82% of which will be video. This trend represents the largest challenge for mobile communication research and industry.

To overcome the 1000x traffic-growth challenge, some key enabling 5G technologies have been proposed, including massive multiple-input multiple-output (MIMO), millimetre wave (mmWave), small-cell (SC) deployment, filtered orthogonal frequency-division multiplexing (OFDM), full duplex communications, polar codes, spatial division multiple access (SDMA), native support of machine-to-machine (M2M) communications, etc. Most of these can be broadly classified into three main categories [3]: air interface improvements, more spectrum allocation, and network architecture improvements.

Firstly, air interface improvements are expected to provide a 3x-5x capacity gain for the mobile networks. The design of these improvements not only focuses on improving the traditional link-level spectrum efficiency (SE) using fundamental techniques, such as massive MIMO and new modulation or coding schemes, but also on allowing cooperation among BSs and UEs to enable better interference management to exploit system-level opportunistic gains, e.g., coordinated multipoint (CoMP) transmission and reception, non-orthogonal multiple access (NOMA), and three-dimensional MIMO.

Secondly, it is expected to provide a 5x-10x capacity gain by granting cellular networks access to the unlicensed spectrum bands. Last but not the least, the network architecture improvements, e.g., the heterogeneous networks (HetNets) with SCs and support of device-to-device (D2D) and M2M communications are expected to contribute most to the capacity enhancement, which could lead to a 90x-160x capacity gain.

1.2 Heterogeneous Networks

Among the network architecture improvements, the densification of SC deployment is the most promising contribution to capacity enhancements for 5G networks as the capacity is envisioned to increase linearly with respect to the SC density. SCs are small coverage areas served by low-transmit-power base stations (BSs) rather than macro BSs. This improves the frequency reuse and shortens the serving distance, thus increasing the network capacity. There are three main reasons for SC densification: Firstly, the densification of traditional macro BSs is only possible up to a point because of the limited deployment space in cities and the high capital expenditure (CAPEX) of associated infrastructures (e.g., monitor systems and cooling systems). As a result, it is difficult to ultra-densely deploy traditional macro BSs for the capacity improvement. Secondly, SC BSs can be treated as simplified traditional macro BSs with lower transmit power, which require almost no modifications in the air interface design. Thirdly, as 50 percent of phone calls and 70 percent of data services occur indoors [4], SC BSs, especially the femto BSs designed for indoor usage can provide better indoor coverage compared with macro BSs. Consequently, the traditional macro BSs and the low transmit power SC BSs form HetNets.

According to [4], HetNets can be defined as *networks with several tiers of different low-transmit-power BSs underlying traditional macrocells*. Based on the range of the transmit power, SCs are typically classified into three categories: microcells, picocells, and femtocells [5]. Typically, the maximum coverage radius of a microcell is two kilometres with a transmit power of 2 Watts and a maximum of several hundred users can be supported by each microcell. Microcells are often used to increase the outdoor network capacity for hot-spot scenarios,

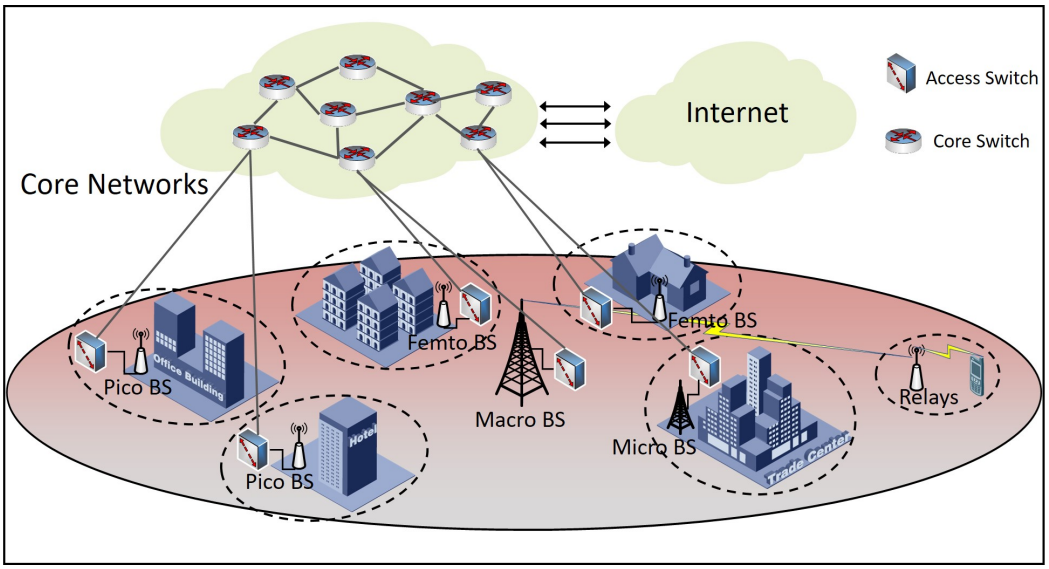

Fig. 1.1 The network architecture of HetNets

such as shopping centres, stadiums, or transportation hubs. Picocells are difficult to be precisely distinguished from microcells, but picocells are usually smaller than microcells and serve less than 100 users within a radio range of 300 m or less. The transmit power of the pico BSs ranges from 200 to 2000 mW. Picocells can be deployed for capacity improvement in traffic-intense outdoor scenarios and are frequently deployed indoors to improve poor wireless coverage within a building, e.g., shopping centres, office floors, or retail spaces. Femtocells are typically user-installed SCs that have the lowest CAPEX and are used to improve the coverage of a small area, e.g., residential spaces. The transmit power of femto BSs is typically 20 mW and the radius of a femtocell is less than 50 m. Unlike picocells and microcells, femtocells are designed to support only a dozen active users and are only capable of handling a few simultaneous calls.

Due to their deployment flexibility, lower maintenance costs, and ability to boost the network capacity of SCs, mobile operators are experiencing a growth in SC deployment [6]. According to the Small Cell Forum, around 67% of worldwide operators have already deployed indoor SCs (i.e., femtocells) and it was predicted that the number of deployed femtocells would increase from 4.3 million to 36.8 million by 2015. AT&T also announced that more than 40,000 outdoor SCs (i.e., picocells/metrocells) would be deployed by the end of 2015 [7]. In 2016 in the US, Verizon Wireless started to deploy SCs in several cities, including New York, Chicago, Atlanta, and San Francisco and in the UK, BT has already deployed over 50 outdoor trial sites of SCs.

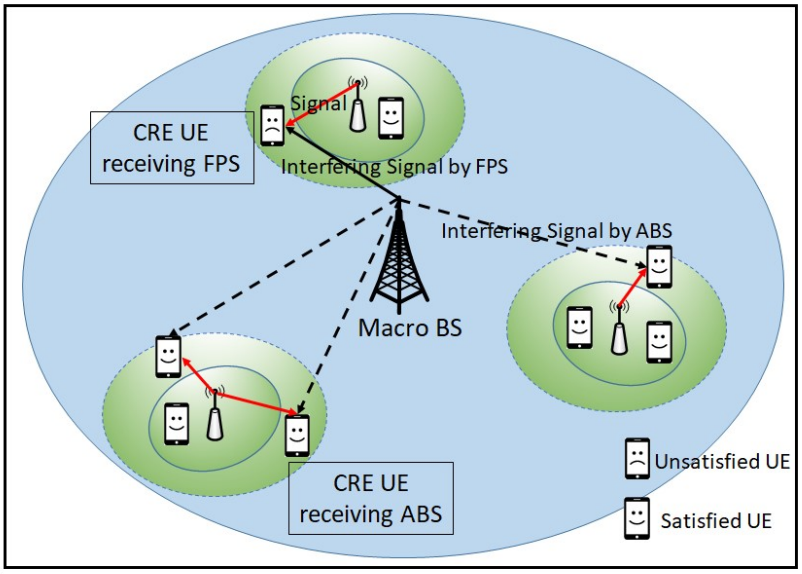

Fig. 1.2 An illustration of signals and interferences in the eICIC scheme

The architecture of HetNets is illustrated in Fig. 1.1 and shows that SCs provide last-mile wireless access to mobile Internet users by core networks via backhauls. For different kinds of SCs, wired and wireless solutions should be considered in terms of their deployment costs and feasibility [8]. Next, the main challenges of HetNets relating to this dissertation will be discussed.

1.3 Challenges in Heterogeneous Networks

The main challenges for the deployment of HetNets can be summarised as interference coordination, mobility management, backhaul design [8, 6, 7], and large-scale network performance evaluation [9]. In this dissertation, we only focus on interference coordination and large-scale network performance evaluation, and these will be discussed in the following section.

1.3.1 Interference Coordination

Interference coordination aims to reduce the interference that affects user equipments (UEs) or BSs using coordinated radio resource (i.e., frequency, time, power, and space) management. Initially, as SCs are encouraged to use licensed spectrum bands that have already been used by macro BSs, the *cross-tier interference* between BSs from different tiers is introduced, which degrades the signal to interference plus noise ratio (SINR) of UEs, especially for cell

edge UEs that already have a relatively low SINR. Additionally, due to the small coverage area of SCs, a limited number of UEs can associate with SC BSs, which is undesirable when macrocells are already overloaded. Cell range expansion (CRE) was proposed to overcome this load imbalance. This involves employing a range expansion bias that extends the coverage area of each SC without increasing their transmit power [6]. However, SC CRE UEs become vulnerable to interference from macro BSs. In Release 10 of the 3rd Generation Partnership Project (3GPP) standards, almost blank subframes (ABSs) [6] with no transmit power on both the data and control channels were proposed for the enhanced intercell interference coordination (eICIC) scheme to serve macrocell UEs. This allows SC CRE UEs to receive full power subframes (FPSs) in the same time slots as ABSs without suffering from significant cross-tier interference from macro BSs. The signals and interferences in the eICIC scheme are presented in Fig. 1.2. Nevertheless, this technique will cause significant capacity losses to macrocells. To reduce these capacity losses, in Release 11 of the 3GPP standards, reduced power subframes (RPSs) [10] with a relatively low transmit power compared to FPSs (as shown in Fig. 1.3) were proposed in the further eICIC (FeICIC) to serve macrocell centre region UEs (CRUEs), while mitigating the interference to SC CRE UEs. It was shown that the throughput of a whole two-tier network (i.e., picocells underlying macrocells with CRE) improves when ABSs are substituted with FPSs [11].

Nevertheless, employing relatively high-transmit-power RPSs will result in significant cross-tier interference on CRE UEs despite the total throughput enhancement, which translates into low SINR. In the worst cases, even basic modulations will be exacerbated. Furthermore, the desirable SINR does not necessarily mean a qualified downlink throughput, which is also determined by the number of allocated subframes directly. Accordingly, it becomes critical to analyse the SINR and the throughput of UEs by applying RPSs for cross-tier interference coordination in HetNets.

To alleviate the influence of interference from neighbouring cells, the use of RPSs requires strict subframe alignment (SA). This strict SA requirement cannot always be achieved, however, for two main reasons: Firstly, the SA between macrocells and SCs is achieved through control signal exchanges via the backhaul [12], which may be congested in a high density scenario. Secondly, the propagation delays from neighbouring cells are randomly distributed. As a result, subframes transmitted from neighbouring cells may be misaligned, namely subframe misalignment (SM). SM can cause the macrocell centre and SC CRE UEs to suffer increased interference from FPSs, which degrades their SINR performance. Therefore, the influence of SM on the SINR performance using RPSs in HetNets needs further investigation.

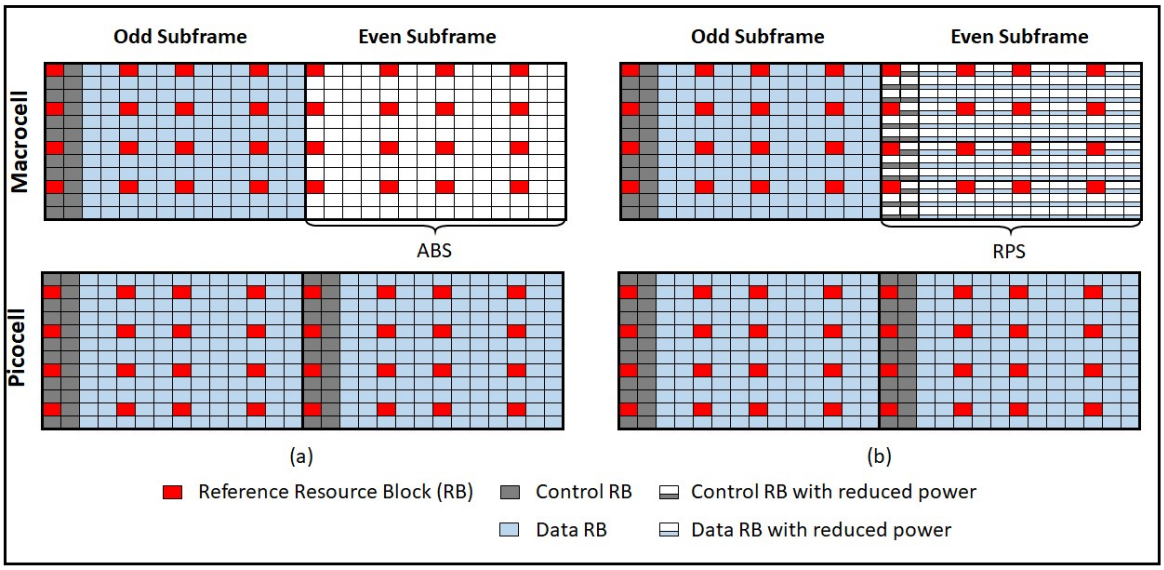

Fig. 1.3 Illustration of (a) ABSs and (b) RPSs that are used for time-domain (F)eICIC in 3GPP HetNets

As mentioned in Section 1.1, a combination of several technologies or schemes is required to achieve the 1000x capacity enhancement. Therefore, it is worthwhile to exploit additional gains by using extra spectrum bands with the deployment of SCs. Recently, due to the development of carrier aggregation, the utilisation of unlicensed spectrum bands has become a promising technique to gain capacity enhancement. In Releases 10-12 of the 3GPP standards [13], the Long Term Evolution (LTE)-Unlicensed (LTE-U) scheme was introduced, which encouraged LTE access points (APs) or BSs to access the 5 gigahertz (GHz) unlicensed band. The LTE-U scheme can potentially improve the SE of the WiFi-only network due to two aspeects: 1) The spatial SE can be increased by deploying LTE-U in LTE APs, especially in low-density WiFi APs (WAPs) scenarios; 2) Collisions among UEs when accessing the unlicensed band, which occur in WiFi networks because of the contention-based medium access control (MAC) protocol among UE, can be avoided by LTE-U via a centralised radio-resource-management protocol [14]. The 5 Ghz unlicensed band has already been used by WiFi networks, however, which means cross-tier interference between WiFi and LTE-U networks cannot be ignored.

To address this interference, the carrier-sensing adaptive transmission (CSAT) scheme, where adaptive duty cycles are used by LTE-U APs to leave certain time slots that only allow WAPs to access the unlicensed bands, was proposed by Qualcomm [15]. This proves that LTE-U APs can be good neighbours to WAPs if interference coordination schemes are applied in LTE-U networks. The 3GPP Release 13 standardised the LTE-Licensed Assisted Access

(LAA), which adheres to the requirement of the listen before talk (LBT) mechanism in the LTE-LAA APs (LAPs) [16]. The LTE-LAA has been mainly defined for the downlink and will be extended to the uplink in the enhanced-LAA in 3GPP Release 14 [17]. Nevertheless, in the literature, the performance of the coexisting LTE-LAA and WiFi networks has not been studied thoroughly, especially in the case of sharing multiple unlicensed channels (UCs). Consequently, the influence of the LAA scheme on the coexisting LTE and WiFi networks under a multi-UC scenario need further investigation.

Based on the above discussion, the cross-tier interference incorporated by SCs cannot be ignored, whether licensed or unlicensed spectrum bands are used. Interference coordination schemes are necessary to mitigate the cross-tier interference to improve network performance, and it is critical to evaluate the network performance with these interference coordination schemes.

1.3.2 Large-Scale Performance Evaluation

To evaluate the performance of a large-scale network, determining the network model, i.e., the BS locations, is a prerequisite. Traditional network models, such as the Wyner [18] and the hexagonal grid [19] models, are over-simplified for modelling LTE networks. The hexagonal grid model, the random model, and an actual deployment of 4G cellular network [9] are illustrated in Fig. 1.4. It can be seen that the traditional hexagonal grid model may no longer fit for the LTE network modelling. Firstly, adjacent BSs are no longer deployed at an equal distance in actual deployment, which is quite different from the distance property of the hexagonal grid model. Secondly, the BS locations vary significantly in different cities or regions, and SCs are highly likely to be customer-deployed (as shown in Fig. 1.5). Therefore, the randomness of BS locations should be incorporated into the network performance evaluation. In [9], it was claimed that the hexagonal grid model provides optimistic network performance as compared with the actual BS deployment, but Monte Carlo simulations need to be run numerous times to obtain a statistical result, which is both time-consuming and resource-consuming. In addition, the simulation results are intractable and provide limited insights into the network design. Therefore, we need new tools to analyse network performance with randomly deployed BSs.

Recently, stochastic geometry, which provides mathematical theories to model and analyse random point patterns, has been proven to be a powerful tool for large-scale network performance modelling. In stochastic geometry, the Poisson point process (PPP) is the most widely used spatial point process as it satisfies the three following conditions [20]: 1) The expected number of points existing in an arbitrarily bounded region follows the Poisson distribution; 2) For a collection of disjointed and bounded regions, the number of points in

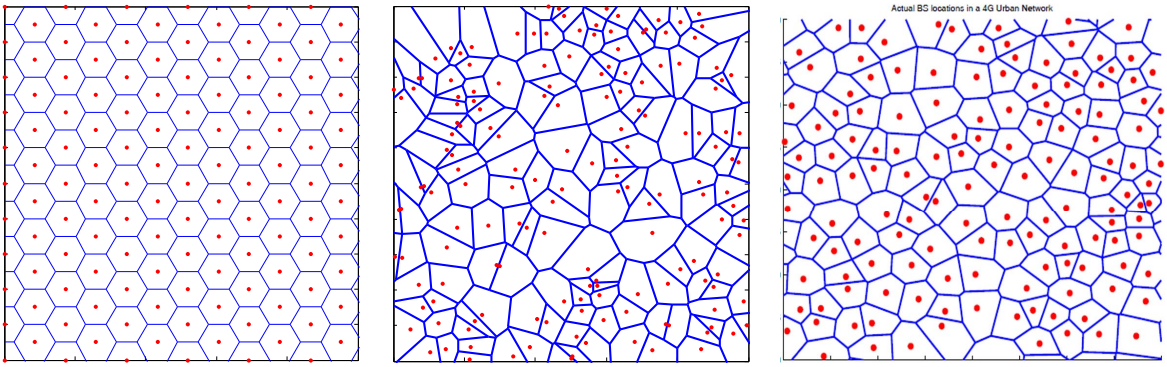

(a) Hexagonal grid model (b) Random model (c) Actual BS deployment[9]

Fig. 1.4 Comparison between the network models and the actual BS deployment, with red points showing the BS locations

each bounded region is completely independent of all others; and 3) The locations of BSs follow uniform distribution in bounded regions.

A comparison between the PPP model and the BS deployment in actual 4G networks in terms of the coverage probability, which is defined as the probability that the SINR of a typical UE is greater than a threshold, was given in [9]. It was shown that the PPP model gives a pessimistic coverage probability as compared with that given by the actual BS deployment and that the coverage-probability gap between the PPP model and actual BS deployment is comparable to that between the hexagonal grid model and the actual BS deployment. Furthermore, based on the database of BS locations in OpencellID, the coverage probabilities obtained by the PPP model, the hexagonal grid model, and actual worldwide BS deployment (e.g., London, Paris, Chicago, Los Angeles, Singapore, Hong Kong, etc.) were presented in [21]. This showed that the PPP model outperforms the hexagonal grid model in terms of the accuracy of the coverage-probability modelling for 4G networks. These results justified the effectiveness of the PPP in network performance modelling. Furthermore, there are four main advantages to use stochastic geometry. Firstly, explicit mathematical expressions of the statistical performance metrics can be obtained, which in most cases, especially with closed-form results, is more time-effective and less resource-consuming than the Monte Carlo simulation. Secondly, network design insights can be provided as the influence of specified parameters can be observed either directly by the explicit expression or by the numerical results. Thirdly, it provides a basis for comparisons between different interference coordination schemes or techniques in a randomly-deployed-BSs scenario. Last but not least, it is appropriate for the spatial modelling of SC BSs in HetNets [22].

Therefore, in this dissertation, stochastic geometry is utilised to analyse the aforementioned problems in Section 1.3.1. Additionally, the most frequently used definitions or

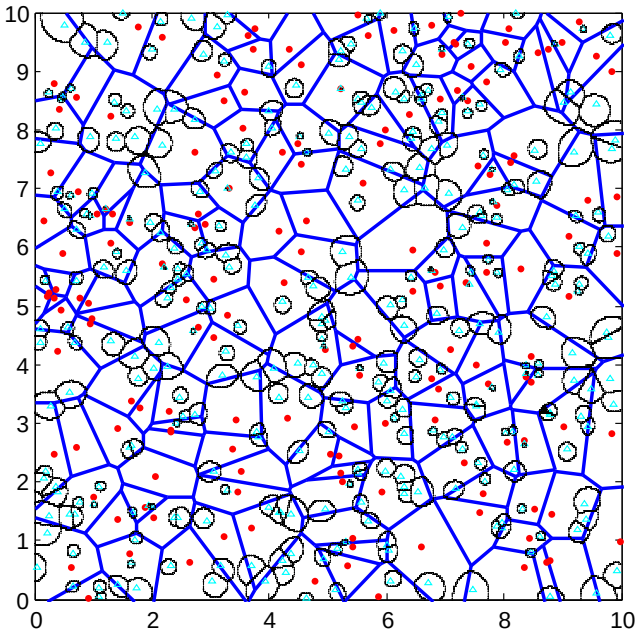

Fig. 1.5 A randomly deployed HetNet, with red points and blue triangles showing the locations of macro and SC BSs, respectively. The black circle around each blue triangle is the coverage area of each SC.

theorems, i.e., the definition of the PPP, Slivnyak's theorem, and the probability generating function for the PPP can be found at [P3, Definition 1.1.1], [P14, Theorem 1.4.5], and [P7, Proposition 1.2.2] in [23].

1.4 Contribution

Based on the discussions in Section 1.3, we focus on the large-scale performance modelling and analysis of HetNets with two interference coordination schemes, i.e., FeICIC RPSs and LTE-LAA, respectively, for the case of licensed and the 5 GHz unlicensed spectrum bands being used in SCs. The design guidelines for the corresponding parameters, such as range expansion bias, transmit power of RPSs, requirement of subframe alignment, BS density, etc., are provided. All the derived results are validated by the Monte Carlo simulation. The contribution of this dissertation can be briefly summarised as follows:

- **Modelling and performance analysis of applying FeICIC RPSs in HetNets with CRE**

  In a two-tier HetNet with CRE and RPSs, the analytical expressions of the coverage probability and the rate coverage probability that is defined as the average fraction

of UEs achieving a target rate are obtained in a one-dimensional integral form by assuming that BSs in both tiers follow two independent PPPs. Additionally, the near optimal values of the macrocell centre region bias (which determines the area of the macrocell centre regions) and the range expansion bias are obtained to maximise the rate coverage probability, which is close to the actual optimal values. Based on the optimal biases, a comparison of the two-tier HetNet using ABSs and RPSs is provided in terms of the coverage probability and the rate coverage probability.

- **Exploiting the potential of RPSs being used in both tiers of a two-tier HetNet without CRE**

  In a two-tier HetNet without CRE, we exploit the potential of RPSs being used in both tiers of BSs to further improve the signal to interference ratio (SIR) of macrocell edge UEs. Closed-form analytical expressions of the coverage probability and the rate coverage probability of the two-tier HetNet are derived. Furthermore, the rate coverage probabilities of the whole two-tier HetNet with the traditional FeICIC scheme and with our proposed scheme are compared.

- **Analysis of subframe misalignment using RPSs in HetNets**

  The effect of SM on the downlink coverage probability is analysed in a two-tier HetNet adopting RPSs. We propose a novel SM model with the misalignment offsets restricted within a specific range. Based on this proposed SM model, the downlink coverage probability for typical UE is derived under the stochastic geometry framework. By analysing the coverage degradation caused by SM, we provide design insights into the SA requirement for using RPSs in HetNets.

- **Performance analysis of LTE-LAA coexisting with WiFi networks that share multiple UCs**

  We provide performance analysis for a large-scale HetNet comprising of LAPs and WAPs that share multiple UCs and that both use the carrier-sense multiple access with collision avoidance (CSMA/CA) protocol as the medium access control (MAC) scheme. Analytical expressions of downlink successful transmission probabilities (STPs) are given, which are jointly determined by the downlink coverage probability of the UE and the medium access probability (MAP) of the serving AP. The latter is defined as the probability of a serving AP being granted transmission. Based on the STPs, we numerically analyse the effects of LAP density and the number of UCs on the throughput and SE. Moreover, by deriving the asymptotic throughput and SE as the LAP density approaches infinity, we provide insights into how the deployment density

of LAPs should be selected according to the number of UCs. Additionally, the fairness between the LTE-LAA and WiFi networks is analysed as a function of the radius of the LAP's sensing region.

1.5 Organisation

This dissertation is organised as follows: Chapter 2 comprehensively reviews the stochastic geometry-based network performance modelling and analyses in the literature, and then clarifies the motivations for the aforementioned four contributions in details. The modelling and performance analysis of applying FeICIC RPSs in a two-tier HetNet with and without CRE are investigated in Chapter 3. In Chapter 4, the effect of SM on the downlink coverage probability in a two-tier HetNet adopting RPSs is analysed. In Chapter 5, the STP, throughput, and SE of the coexisting LTE-LAA and WiFi networks sharing multiple UCs are investigated in terms of AP density and the number of UCs. The conclusion and ideas for future works are presented in Chapter 6.

Notations: Throughout this dissertation, we use $\mathbb{E}[\mathbf{X}]$ to denote the expectation of a random variable, $\mathbf{X}$, $\mathbb{P}(Y)$ to denote the probability of an event Y, and $\mathcal{L}_{\mathbf{X}}(s)$ to denote the Laplace transform of a random variable $\mathbf{X}$ with parameter s.

Chapter 2

Literature Review

In this chapter, we first review some of the existing investigations into the large-scale network performance modelling with stochastic geometry. Secondly, the existing studies on FeICIC RPSs are investigated. Then, we review the related works that have analysed the influence of time-domain asynchronisation on network performance and the existing studies on the LTE-U or LTE-LAA scheme for the coexisting LTE and WiFi networks sharing single or multiple UCs.

2.1 Stochastic-geometry-based Analysis of Large-scale Network Performance

Initially, stochastic geometry, especially the PPP, was used in the performance modelling of ad hoc and WiFi networks [24, 25] as the APs in these networks were assumed to be randomly distributed. In [9], the PPP was first used to model the downlink coverage probability of a homogeneous 4G cellular network. To obtain the closed-form coverage probability, three main assumptions were made: a) An omnidirectional single antenna was equipped in all BSs and UEs; b) The small-scale fading followed the Rayleigh fading, the pathloss followed the log-distance model and the large-scale shadowing was ignored; and c) UEs were always connected to their nearest BSs. Based on these assumptions, the distributions of the serving-BS-distance of a typical UE and the aggregate interference power suffered by this UE were obtained. The results showed that the PPP model was more tractable than the grid model and gave a pessimistic result (a lower bound), while the grid model provided an optimal result (an upper bound). Moreover, the coverage-probability gap between the PPP model and the actual BS deployment was comparable to that between the hexagonal grid model and the

actual BS deployment. The authors of [9] also called for extensive experiments to validate these analytical results.

In [21], the database of actual BS deployment in worldwide urban areas provided by the open source project *OpenCellID* was utilised to compare the coverage probability obtained from the actual deployment database with the PPP and hexagonal grid models. The results showed that the PPP model outperformed the hexagonal model in terms of the accuracy of coverage probability. Additionally, in [26], the accuracy of the PPP for modelling the actual cellular networks of two cities (i.e., London and Manchester) in the UK was further investigated. The building footprints, spatial blockages, and antenna patterns were taken into consideration in the validation. The results also confirmed the ability of the PPP to accurately analyse the performance metrics of cellular networks in a densely-deployed environment. These results indicated that using the PPP to model and analyse the performance metrics of 4G cellular networks was a valid option.

In [22], the PPP model was extended to the analysis of a K-tier HetNet (i.e., macrocells with underlying $K-1$ tiers of SCs). In contrast to homogeneous cellular networks ([9]), HetNets assume spatial-location independence of each tier and that each each UE is always associated with the BS which provides the highest received signal strength (RSS). Then, the explicit expressions of the downlink coverage probability and the average achievable rate of a typical UE associated with each tier were derived in this K-tier HetNet. Moreover, closed-form results were achieved by assuming that the pathloss exponents were the same throughout the K-tier HetNet. This work gives academics a benchmark for modelling and analysing HetNets. Based on [22], the frequency-domain-based intercell interference coordination (ICIC) scheme and the time-domain-based eICIC scheme were investigated in the literature [27–32].

The ICIC scheme is implemented in the frequency domain. In [27], the strict fractional frequency reuse (FFR) and the soft frequency reuse (SFR) were both investigated in an OFDMA cellular network with the PPP model. The main idea of FFR is to divide the whole spectrum band into several subbands to reduce the interference affecting edge UEs in neighbouring macrocells by preventing them to use the same subband. The PPP model causes the coverage area of a macrocell to become a random shape, which makes it impractical for the traditional distance-based method to determine the centre and edge regions of macrocells. Therefore, the centre and edge regions of macrocells were defined according to the SINR level of UEs, e.g., the edge region UEs has an SINR lower than the target SINR. The tractable expression of the coverage probability was derived for a comparison between the two FFR strategies, and the system design guidelines were summarised in terms of three aspects: coverage probability, SE, and sum rate. The results showed that strict FFR enhances the

network sum rate and that SFR improved the SE of the whole network. One year later, this work was extended into a two-tier HetNet scenario in [28]. However, closed-form expressions were not obtained, so the performance results were analysed numerically and a certain amount of time was needed for the integral calculation. The results showed that even in a HetNet, the use of strict FFR, which reserved some subbands for the UEs of each tier with low SINRs, can provide desirable gains in terms of coverage probability and throughput of UEs. As compared with strict FFR, some coverage losses occurred in edge UEs with SFR, but SFR allowed for more efficient use of the shared spectrum for both tiers.

The eICIC scheme is implemented in the time domain. The CRE mechanism was initially incorporated into the K-tier HetNet in [29]. The purpose of CRE is traffic offloading from macrocells to SCs through the introduction of a range expansion bias in SCs to attract more UEs to associat with them. This range expansion bias is used in the user association scheme, where the UE is associated with the BS that has the highest biased RSS. The coverage probability and average ergodic rate were both derived in integral form with different range expansion biases. Furthermore, the optimal biases for the best average ergodic rate were numerically analysed, and the results showed that the range expansion biases had a dramatic effect on the average ergodic rate. In [30], the optimal cell range biases for coverage performance in a K-tier HetNet were analysed. Specifically, the closed-form expression of the cell range bias for SCs in a two-tier HetNet was derived. Additionally, the explicit expression of rate coverage probability, which was defined as the probability of a typical UE that has rate greater than the target rate or the fraction of UEs that have rate greater than the target rate, was also derived. Based on this expression, the optimal cell range bias for the rate coverage probability was also analysed numerically. However, the aforementioned works did not take ABSs into account.

In [31], the performance of a two-tier HetNet with both CRE and ABSs was firstly analysed. Based on the proposed biased-RSS based user association strategy, the coverage area of the whole plane was divided into three regions: the macrocell coverage region, the original picocell coverage region and the expanded picocell coverage region. ABSs were only allocated to the UEs in the expanded picocell coverage region. A similar derivation in [30] was then applied to obtain the coverage performance of UEs in each of these three coverage regions. The results indicated that the fraction of ABSs and the range expansion biases both had a significant effect on the coverage and rate coverage probabilities, thus appropriate configurations for these are required to improve network performance. In [32], ABSs were used in a different way as compared with [31]. They were applied in SCs to improve the SINR of macrocell edge UEs that had dominant interferers (i.e., SC BSs) in their distance-based protected regions. The protected region of each UE was determined

based on a certain relationship between its closest distances to macrocell BSs and SC BSs. The coverage probability and rate of macrocell edge UEs were analysed with both closed- and open- acess-mode SC BSs. Moreover, the minimum required ABS number was also investigated to satisfy the rate requirement of macrocell edge UEs.

Although the adoption of ABSs can enhance the coverage and rate coverage probabilities for HetNets, this technique causes significant capacity losses in tiers using ABSs. Consequently, the FeICIC was proposed to alleviate the capacity losses by further exploiting the power domain. It advocates using RPSs instead of ABSs to serve macrocell centre region UEs, which can reduce the capacity losses without introducing severe interference to UEs in the expanded picocell coverage regions.

Despite the aforementioned works, stochastic geometry has also become popular in the large-scale performance evaluation of HetNets equipped with a variety of techniques, such as CoMP, MIMO, mmWave and cache-enabled HetNets.

a) CoMP: The main idea of CoMP is to exploit spatial domains to improve the SINR of edge UEs by mitigating the strongest interference from adjacent BSs [33]. In [34], the explicit expression of the coverage probability in a K-tier HetNet with a joint transmission scheme was derived. The joint transmission scheme allows a set of BSs from multiple tiers to jointly transmit signals to the same UE. It was claimed that if a maximum of two BSs were allowed to cooperate, a maximum of 30% coverage-probability gain can be achieved compared to without CoMP. To investigate the effect of channel state information (CSI) on CoMP, [35] analysed the coverage probability in a homogeneous network by allowing cooperation from a maximum of two BSs with variable levels of CSI. The results showed that the coverage probability can be notably improved even with imperfect CSI.

b) MIMO: HetNets with multiple antennas ware originally analysed in [36], and with the assumption of linear zero-forcing precoding, the sum of small-scale fading on the received power from multiple antennas to a typical UE follows the Gamma distribution [37]. Accordingly, the coverage expression was derived by the n_{th} derivation of the Laplace transform of the aggregate interference power in terms of two spatial transmission schemes: SDMA and single-user beamforming. The results showed that the full SDMA transmission scheme led to a lower coverage probability but higher area spectral efficiency (ASE) if the BSs in both tiers have the same number of antennas. In [38], an equivalent-in-distribution-based approach was proposed to analyse the performance of HetNets with MIMO, which is not only applicable to spatial multiplexing, but also receiver diversity, orthogonal space-time block coding, zero-forcing reception and zero-forcing precoding. Based on the aforementioned works, several performance metrics are analysed in [39–41]. In [39], the coverage probability and the ASE were analysed simultaneously. The author pointed out the trade-off between the

coverage probability and the ASE regarding the number of active tiers of the HetNet. An algorithm for finding the optimal BS density to maximise the ASE was also developed. In [40], the energy efficiency (EE) was analysed with constrained wireless backhaul, which was in the presence of both the uplink and downlink transmissions. The study concluded that the EE of the multiple-antenna-enabled HetNets was greater than that of homogeneous networks and was quite sensitive to the network load. The EE was also investigated in a different scenario in [41] where a HetNet's macrocell BSs were equipped with massive MIMO and the SC BSs were equipped with a single antenna. This scenario also advocated using flexible cell association, i.e., the CRE, which can significantly increase the ASE and EE simultaneously.

c) mmWave transmission: For mmWave transmission, the influence of building locations and sizes should be considered as they can determine whether the links between BSs and UEs are line-of-sight (LOS) links or non-line-of-sight (NLOS) links. In [42], the distribution of the buildings was modelled as a Poisson line process, which is leveraged from the random shape theory. All the buildings in the network were assumed to be rectangularly shaped, the centres of which follow the PPP. The size and orientation of each building followed an independent identical distribution, respectively. The explicit expression of blockage number for a known link was derived, which was used to obtain the probability of this known link being LOS or NLOS. However, single antenna was used in this work, which is impractical for the mmWave transmission. In [43], the directional beamforming for MIMO HetNets in mmWave transmissions was modelled to obtain the explicit expressions of coverage probability and rate for a typical UE. The results indicated that densely deployed networks with mmWave transmissions can achieve comparable coverage probability and much higher data rates than the conventional cellular networks.

d) Caching: Recently, caching popular content at the edge of HetNets has become a promising technique for improving the quality of UE service by reducing the latency and the burden of SC backhauls [44]. In [45], the optimisation of geographic content caching in a homogeneous network modelled following the PPP to maximise UE's hit probability was considered. The hit probability of UE was defined as the probability that the typical UE will find the content asked by it in one of the BSs this UE is covered by. The content popularity followed a Zipf distribution and the results indicated that the optimal policy can increase the hit probability of the whole network. This optimal policy did not always follow the standard policy of *cacheing the most popular content everywhere*. In [46], the tractable expression of successful transmission probability was derived in a HetNet, utilizing tools from stochastic geometry. The successful transmission probability was defined as the probability that a randomly requested file is successfully transmitted. Moreover, it was also assumed that the caching contents in macrocell BSs are identical and that in SC BSs they are randomly

distributed. The results showed that the successful transmission probability increased with an increase in cache size, but decreased with an increase in UE density.

The above discussion indicates that the tools of stochastic geometry can be utilized to analyse existing techniques, and could also be applied to future evolutions of techniques for SC deployment. On the other hand, there are some existing studues that look at the restrictions of the BS locations, to adjust the network model to be more fitting with the property of the actual BS deployment. In [47], the performance of an inter-tier dependent HetNet, where the macrocell-BS and picocell-BS locations followed a PPP and a Poisson hole process (PHP), respectively, was investigated. The PHP was formulated by restricting the active picocell BSs outside of an excluded region around the macrocell BSs. As the explicit characterisation of the aggregate interference power received by a typical UE is unknown for the PHP, the upper bound of the coverage probability was derived. Furthermore, a fitted Poisson cluster process was also applied to approximate the PHP. Through the simulation results, it was concluded that the performance of the inter-tier dependent PHP was closer to that of the actual deployment than the PPP model. This work was extended in [48] to consider not only the inter-tier dependent case, but also an intra-tier dependent case. In the intra-tier dependent case, macrocell BSs were modelled following a PPP and picocell BSs were modelled following a Matern cluster process because picocell-BS density may differ significantly in different regions. The results showed that the intra-tier dependent model was a more appropriate and accurate model for the HetNets with hotspot regions than the multi-tier independent PPP model. In [49], a summary of the existing approximation techniques used to obtain the approximated coverage probability for a PHP-based HetNet were presented, and novel tight upper and lower bounds of the coverage probability were also proposed. The results showed that the proposed bounded results outperformed other known bounds or approximations in terms of accuracy. Based on the PHP, the large-scale performance of cognitive radio [50–52] and D2D [53–55] networks was analysed. In cognitive radio networks, the PHP was used by restricting the active secondary transmitters outside an excluded region of primary UEs. In D2D networks, the holes in the PPP are excluded regions that may occurr around BSs where no D2D transmissions ara allowed because of the strong interference. Based on the cluster process, the large-scale performance of ad hoc networks and clustered networks was analysed in [56, 57], respectively. Moreover, by respectively modelling UEs with arbitrary movement trajectory and an improved random way-point mobility model [58], the handover performance was analysed in [59, 60].

According to the above literature review of stochastic geometry, we can conclude that stochastic geometry e.g. PPP has already been widely accepted in academia as a way of

analysing the large-scale performance of HetNets with various schemes due to its analytical tractability. Comprehensive reviews of stochastic geometry can be found in [61, 62].

2.2 Related Works of HetNets with RPSs

In Release 11 of the 3GPP standards, the FeICIC was proposed. This scheme advocates substituting ABSs with RPSs that are used by UEs in macrocell centre regions in coordinated time slots [63]. Before 2015, only a few studies had analysed the performance of HetNets using RPSs.

In [11], based on the baseline assumption of macro-pico deployment proposed in [64] (Table A.1-1), where macrocell BSs follow the hexagonal grid model with a maximum of 4 picocells deployed per macrocell, the cell-edge UE throughput (5% percentile) and the median of the UE throughput (50% percentile) were evaluated with various cell range biases, transmit powers, and fractions of RPSs. The results showed that the configurations of RPS fraction and transmit power strongly affected the achievable cell-edge and median UE throughput performance, and that the sensitivity to these configurations increases if large values of range expansion bias (e.g., 12 dB) are adopted. In addition, it was concluded that an optimal transmit power of RPSs for each combination of cell range bias and RPS fraction existed.

In [65], the cell-edge UE throughput, the median UE throughput, and the cell load were investigated with macrocells following the hexagonal grid model with both bursty and non-bursty traffic types. A comparison between ABSs and RPSs with several reduced transmit powers was also provided. The results showed that RPSs can increase both the cell-edge and median UE throughputs of the whole two-tier HetNet as compared with ABSs if small values of range expansion bias are applied. It was also shown that, with large values of range expansion biases (e.g., 12-14 dB), ABSs provided slightly higher cell-edge and median UE throughputs. A large value of range expansion bias increases the traffic load on SCs, however. It was also proposed that a constraint of quadrature phase shift keying (QPSK) on the modulation order of RPSs should be applied to minimise the influence of the reduced transmit power, which caused approximately 13% loss in the median UE throughput as compared with that obtained in non-modulation-constraint RPSs. In [66], an optimisation framework was developed for network capacity and rate fairness with range expansion bias and the fraction of RPSs (i.e., RPS duty cycle). The simulations were undertaken in an LTE network with practical simulation parameters and the system-level simulation results showed that significant gains can be achieved in terms of both network capacity and rate fairness.

The three studies mentioned above did not take the randomness of macrocell-BS locations into consideration. In [67], the sum UE throughput, sum-log UE throughput, and SE of a two-tier HetNet adopting RPSs were initially analysed with stochastic geometry. The coverage area of the whole plane was divided into four regions: macrocell centre regions, macrocell edge regions, original picocell regions, and expanded picocell regions. These regions were jointly determined by an absolute SINR threshold and a relative threshold related to the SINR of UEs served by FPSs and RPSs. A joint distribution of SINR was derived to further analyse the sum UE throughput and SE. The results showed that RPSs outperformed the ABSs and the FPSs in terms of the sum UE throughput and the proportional fairness (i.e., sum-log UE throughputs). Extended from this, in [68], the cell-edge UE throughput was analysed in a two-tier HetNet adopting RPSs, and a comparison between the stochastic-geometry-based theoretical results of the actual macrocell-BS deployment in London and the hexagonal grid model was presented. The results showed that the stochastic-geometry-based theoretical results outperformed the hexagonal grid model in terms of the accuracy of the cell-edge UE throughput as compared with the results obtained with the actual macrocell-BS deployment. The results were not in closed form, however, and as the user association was based on the SINR level, it is impractical to analyse the coverage performance in each tier based on the framework proposed in [67, 68]. Accordingly, the study of the coverage and rate coverage probability of HetNets with RPSs under the stochastic geometry framework was missing in the literature. Furthermore, the potential of adopting RPSs in both tiers of a two-tier HetNet without CRE was missing as well. These issues were therefore investigated.

Since the publications of our works (see Chapter 3), there have been several more studies that investigate the performance of HetNets with RPSs. In [69], a game-theory-based distributed algorithm for maximising the EE was proposed for an LTE-Advanced HetNet adopting ABSs or RPSs. This algorithm can also adapt itself to optimise various system optimisation targets, e.g., sum rate and proportional fairness maximization. The simulation results showed that with the proposed optimisation algorithm, the EE can be almost doubled and can see a 64% improvement for the use of RPSs and ABSs compared with no optimisation. In addition, RPSs can provide higher fairness in the UE throughput and better cell-edge UE throughput compared with ABSs. To further improve the EE and SE, a downlink-scheduler based on a cake-cutting algorithm was proposed. According to the simulation results, the EE and SE were increased by 10% as compared with that obtained with conventional schedulers.

Based on our work in Chapter 3, in [70], the EE of a two-tier HetNet adopting RPSs was further analysed together with an adaptive spectrum allocation scheme for the downlink transmission. The adaptive spectrum allocation scheme aimed to allocate proportional sub-

channels to a BS according to its traffic load. To analyse the EE, the sum power consumption of macrocell BSs was modelled as the combination of basic circuit power consumption to support sleep mode, baseband processing power consumption, radio frequency power consumption and backhaul power consumption. The results showed that RPSs with the proposed adaptive spectrum allocation scheme can significantly improve the coverage and EE of the whole network, especially with high SC densities. This work has been extended by the author in [71], in which a non-convex optimisation problem relating to the transmit power and fraction of RPSs, and the number of subchannels for the trade-off between EE and SE was formulated. A low-calculation-complexity iterative algorithm was also proposed to achieve the sub-optimal solution. Recently, RPSs have already been incorporated in the interference coordination among unmanned aerial BSs [72].

2.3 Related Works of the Analysis of Asynchronous Transmission

In its early stages, the analytical model for asynchronous transmission was developed for Aloha networks. In [73], the explicit expression of the downlink coverage probability in a wireless ad hoc network with non-slotted Aloha was derived. In such a network, the transmissions from different APs were not synchronised. Due to the asynchronous transmission, the aggregate interference power received by a typical UE became random. By averaging the received aggregate interference power in a packet duration, the closed-form coverage probability was obtained. The results exhibited that the pathloss exponent had a strong effect on the coverage-probability loss for the asynchronous Aloha network compared with the synchronous one, i.e., the coverage-probability loss was negligible in a low pathloss-exponent scenario, but in a high pathloss-exponent scenario, the coverage probability of an asynchronous Aloha network was worse than that of a synchronous Aloha network. This work was extended in [74] with the Poisson rain and Poisson renewal models, which further validated the aforementioned conclusion that no gain was observed from synchronisation in a scenario with small values of pathloss exponent. This gain gradually increased with an increase in the pathloss-exponent value. Based on the two studies above, in [75], the explicit expressions of coverage probability and network throughput were derived based on stochastic geometry in a full-duplex Aloha network with an asynchronous random-access policy. Based on these expressions, the transmission duration of each packet, self-interference cancellation, and the faction of full-duplex nodes were analysed in a full-duplex asynchronous Aloha network. In addition, the performance loss in the asynchronous Aloha network as com-

pared with the synchronous one was provided. The results illustrated that self-interference cancellation schemes are necessary for both synchronous and asynchronous full-duplex Aloha networks. In [76], the outage probability of an interference-limited homogeneous network with asynchronous frame transmission was derived in closed form. A general model to address the partial overlap with asynchronous frame transmission was proposed that can also be used in a synchronized network. Moreover, the effect of antenna height on the outage was also investigated through simulations. The results showed that with an increase in the concurrent transmission number, the outage probability with asynchronously transmitted frames approached some limits. Furthermore, a low antenna height provided a poor outage performance and after a certain height, with the increase in the antenna height, the enhancement in the outage performance became negligible.

Recently, the analysis of asynchronous transmission has been incorporated into cellular networks. In [77], a tractable system-level SINR model for an asynchronous orthogonal frequency-division multiple access (OFDMA) homogeneous network with spatially randomly distributed BSs was derived. To obtain this system-level SINR model, a link-level analysis of the received OFDMA symbol with a time-domain misalignment model following [78] was presented. Based on the system-level SINR model, the number of decodable BSs, the decoding probability of the nearest BS, and the network capacity were analysed in a homogeneous network lacking time synchronisation. Note that the time-domain misalignment was assumed to follow a Gaussian distribution with a mean of zero within a limited range to obtain the system-level SINR. The results showed that an optimal SINR detection threshold to maximize the network capacity existed, which is negligibly affected by the BS density.

In [79], the downlink coverage with asynchronous transmitted slots was studied in a two-tier HetNet. To capture the UE activity, two traffic patterns, i.e., slotted arrival and exponential interarrival, were introduced. For the slotted-arrival case, it was assumed that each BS independently determined to transmit at the start of each time slot with equal probability. For the exponential-interarrival case, it was assumed that the time duration between consequent packets transmitted by each BS was exponentially distributed, and that the transmit duration of these packets was identical. A comparison between HetNets with asynchronous and synchronous transmissions was presented in terms of the downlink coverage probability. The results showed that the coverage probability was less affected by asynchronous slots in high traffic-volume and low pathloss-exponent scenarios. Based on this work, in [80], the downlink and uplink coverage probabilities were derived for a co-channel multi-tier HetNet with decoupled user association. Furthermore, tight lower bounds with low calculation complexity for both downlink and uplink coverage probabilities were derived. The results showed that the synchronous case outperformed the asynchronous one in

terms of the uplink and downlink coverage probabilities at the cost of higher computational complexity.

The offsets between aynchronous transmitted slots may have arbitrarily large values in [79]. By employing existing time synchronization techniques via the backhaul, however, the offsets between asynchronous transmitted slots may not exceed the slot duration [77]. The offsets of asynchronous slots can be considered as the SM offsets as a subframe consists of two slots in an OFDMA network. Accordingly, the SM offsets are also restricted within a specific range, and the maximum value of this range is defined as the maximum subframe misalignment offset (MSMO). Moreover, none of the studies mentioned in Section 2.2 and this section analysed the influence of SM in the HetNets adopting RPSs and CRE. Therefore, we analyse the effect of SM with MSMO on the coverage probability in a two-tier HetNet adopting RPSs in Chapter 4.

2.4 Related Works of the LTE-U Networks Coexisting with WiFi Networks

There have already been investigations into the performance of an LTE-U/LAA network coexisting with a WiFi network. In [81], the UE throughput and satisfaction rate of the coexisting LTE-LAA and WiFi networks were analysed. UE satisfaction rate was defined as the channel utilisation time per UE. The LAPs adopted an LBT-based unlicensed-channel access scheme with adaptive channel sensing and usage times. The results showed that the coexisting LTE-LAA and WiFi networks outperformed the WiFi only network in terms of the satisfaction rate of UEs by traffic offloading between licensed and unlicensed bands. In [82], the fairness between the LTE-U/LAA and WiFi networks that coexisted via the CSAT and LBT mechanisms were analysed, where the LBT mechanism adopted the CSMA/CA protocol. The results indicated that for short-time transmissions, the LBT mechanism can provide a better level of fairness, and for long-time transmissions, the levels of fairness provided by both schemes are comparable. In [83], based on stochastic geometry, the density of successful transmissions and rate coverage probability were analysed in the coexisting LTE-U/LTE-LAA and WiFi networks under three mechanisms (i.e., continuous transmission, CSAT, and LBT adopting CSMA/CA protocol) deployed in LTE APs. The results showed that the LTE-LAA scheme with the LBT mechanism can provide the best rate coverage probability. In [84], the fairness between the LTE-U and WiFi networks based on CSAT was analysed under stochastic geometry framework, and the results revealed that a satisfactory level of fairness can be achieved by adjusting the duty cycle of non-transmitted subframes

in LTE-U networks. In [85], the medium access probability, coverage probability, and network throughput for both the downlink and uplink of LTE-U networks coexisting with IEEE 802.11ax WiFi networks under three mechanisms (i.e., continuous transmission, CSAT, and LBT adopting CSMA/CA protocol) were derived in analytical expression. Both the single-user and multiple-user operation modes of IEEE 802.11ax were investigated and the results indicated that for the IEEE 802.11ax WiFi network, the LTE-U or LAA network can be a good neighbour for different traffic types.

All the studies above mentioned only considered a single UC, however, and ignored general cases with multiple UCs. In [86], the network throughput of a large-scale LTE-LAA network coexisting with a WiFi network sharing multiple UCs was studied through simulation. The least power channel selection mechanism was adopted in the simulation, which made each AP select the channel with the least interference power. The simulation results showed that fair coexistence in terms of the throughput can be achieved in the LTE-LAA coexisting WiFi networks and that the channel selection mechanism was critical for alleviating the influence of the hidden node problem. In [87], the average throughput achieved by an LTE AP or a WiFi AP, with the availability of multiple UCs, was evaluated via Monte Carlo simulations. The results showed that the fairness between LTE-U/LAA and WiFi networks can be maintained through UC selection. In [88], the collision probabilities between LAPs and WAPs were analysed under multiple accessible UCs. The results showed that the access to the UCs of each LAP should be adapted to the WiFi traffic to guarantee a fair coexistence. The coverage probability and throughput of a typical UE that had an equal probability being an LTE UE or a WiFi UE were investigated in [89] under a multi-UC scenario. The results indicated that the coverage probability of a user increases with the number of accessible UCs.

Existing studies have also focused on optimising the performance or fairness of the LTE-U/LAA coexisting WiFi networks. In [90], a joint UE transfer and unlicensed resource allocation strategy based on the Nash bargaining solution was proposed to optimise the network throughput of the coexisting LTE-U and WiFi networks. The results demonstrated that by carefully allocating the time slots that allowed LTE-U BSs access and by choosing the transferred UE number, the throughput performance in cellular networks and WiFi networks can both be improved. In [91], a coalition-game-based AP selection algorithm was developed to improve the network throughput of the whole coexisting LTE-U and WiFi networks. These two studies both focused on the user association scheme to improve the throughput of the multi-UE LTE-U networks coexisting with WiFi networks. In [88], an adaptive channel access scheme was developed in the LTE-LAA networks coexisting with WiFi networks, which advocated LAPs selecting channels according to the WiFi traffic load on the unlicensed band and the available licensed bandwidth, to ensure fair coexistence

between LTE and Wi-Fi on the unlicensed bands. In [92], an adaptive energy detection scheme for LBSs was proposed to improve the coexistence throughput performance of WiFi and LTE-LAA networks. The results showed that the energy detection thresholds should be carefully designed, as a high threshold may cause frequent collisions whereas a low threshold may cause unnecessary back-off. In [93], by exploiting the degree of space (i.e., multiple signal classification direction of arrival estimation and null steering techniques), a scheme that enables LTE-U APs and WAPs to transmit simultaneously was proposed. The SINR and channel access durations were evaluated with this scheme based on simulations. The results showed that this scheme enabled the LTE-U APs to transmit simultaneously with nearby WAPs without causing significant interference to them, which increased the channel access opportunities for both kinds of radio access technology (RAT) APs. Therefore, it can be concluded that the LTE-U or LTE-LAA scheme can improve network performance with appropriate user association, resource allocation, or modifications in the MAC protocol. The optimisation of the LTE-U/LAA coexisting WiFi networks with the new MAC protocol, with dynamic spectrum management for uplink-downlink decoupling, indoor, and D2D transmission scenarios was repectively investigated in [94–98].

To the best of our knowledge, [89] is the only study that has analysed the performance of large-scale coexisting LTE-LAA and WiFi networks with multiple UCs under a stochastic-geometry framework, where both LAPs and WAPs accessed UCs via the CSMA protocol, ignoring collision avoidance. Therefore, the performance of large-scale coexisting LTE-LAA and WiFi networks both deploying the CSMA/CA protocol to access multiple UCs has not been sufficiently studied. Furthermore, the influence of the sensing-region radius of an LAP, which is determined by the sensing threshold of the received power in the CSMA/CA protocol adopted in the LBT-based LTE-LAA network has not been investigated in the coexisting LTE-LAA and WiFi networks with multiple UCs. Additionally, it is difficult to generalise the MAP, which is defined as the probability of a typical AP being granted transmission, under a single-UC scenario in [83, 84] to a general multi-UC case. Therefore, the coexisting LTE-LAA and WiFi networks in a multi-UC scenario need further investigation.

Chapter 3

Coverage and Rate Analysis of Applying RPSs in HetNets

[1]In this chapter, firstly, recall that the guidelines for the configuration of RPS-related parameters was not well investigated in the literature, thus we investigate the downlink coverage and rate performance of the FeICIC RPSs in a large-scale two-tier HetNet with CRE. Secondly, as the conventional FeICIC-RPS scheme ignores the potential of RPSs being adopted in both tiers of a two-tier HetNet without CRE to improve the SINR level of edge UEs, we study the downlink coverage probability and rate coverage probability of a two-tier HetNet without CRE but adopting our proposed scheme.

3.1 Applying RPSs in HetNets with CRE

In this section, initially, we propose a distance-based user association scheme in the two-tier HetNet with RPSs and CRE in terms of both power reduction factor and macrocell centre region bias. The distance-based user association scheme extends the dominant-interferer definition in [32]. The power reduction factor determines the transmit power of RPSs, and the macrocell centre region bias decides the centre-region area of each macrocell. Equipped with this user association scheme, the whole plane of the network can be divided into four regions: macrocell centre region, macrocell edge region, picocell range expansion region and picocell original coverage region. Then we derive an analytical expression of the downlink coverage probability and rate coverage probability in an integral form consisting of the SINR threshold, the power reduction factor, the duty cycle of RPSs, the pathloss exponents, the range expansion bias and the centre region bias. The coverage and rate coverage probabilities

[1]The content of this chapter is based on slightly revised versions of our two publications [99, 100]

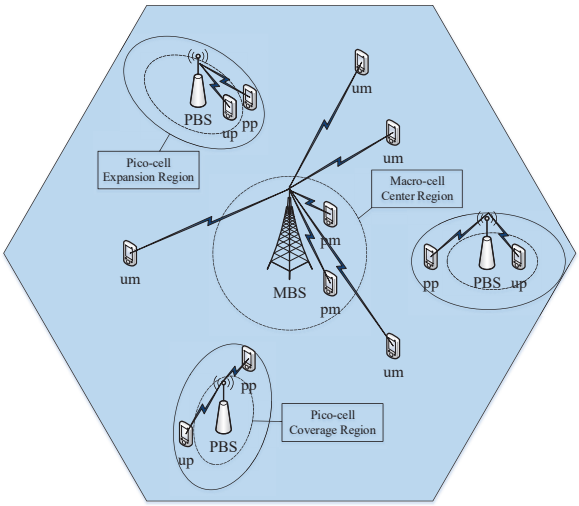

Fig. 3.1 Illustration of the user association strategy © 2016 IEEE

can be defined as the probabilities that the SINR and rate of a typical UE are greater than a threshold, respectively. The duty cycle of RPSs is the ratio of RPSs during the entire transmission. Additionally, an approximation of the Gauss hypergeometric function is applied to obtain the numerical integration results. Based on these numerical results, optimal values of the centre region bias and the range expansion bias are obtained for maximizing the rate coverage probability. Eventually, we compare the rate coverage performance obtained with optimal biases (i.e., centre region and range expansion biases) and static typical range expansion biases when RPSs and ABSs are respectively adopted in the two-tier HetNet.

The rest of this section is organized as follows: Section 3.1.1 and Section 3.1.2 introduce the system model and the user association strategy, respectively. Section 3.1.3 presents the derivation of the analytical results and the optimal bias ranges. Section 3.1.4 illustrates the simulation results before concluding in Section 3.1.5.

3.1.1 System Model

We consider a two-tier HetNet consisting of macrocells and picocells, following two independent PPPs, denoted by $\mathcal{M}$ and $\mathcal{P}$ with density λ_m and λ_p, respectively. They commonly share all the frequency resources. The full transmit power of macrocell BSs (MBSs) and picocell BSs (PBSs) are denoted by P_m and P_p, respectively. The macrocells adopt RPSs in centre areas, with the power reduction factor ρ. Otherwise, the MBSs and PBSs transmit at the fixed maximum power. With the assumption of Rayleigh fading, the received power of an arbitrary UE from a BS can be represented as $Phr^{-\alpha}$. The variable h denotes the small-scale fading attenuation on the received signal power following exponential distribution as $h \sim \exp(\mu)$.

The term $r^{-\alpha}$ is the pathloss, where r is the Euclidean distance and α is the pathloss exponent. The large-scale shadowing is ignored to avoid loss of tractability [29]. Moreover, every cell is assumed to employ a strict synchronization scheme [31]. Under this assumption, the UEs served by RPSs are not interfered by FPSs transmitted from other BSs, and vice versa. Otherwise, the macrocell centre-region UEs and the picocell range-expansion-region UEs will suffer severe interference from neighbouring MBSs. In particular when the PBSs are deployed at macrocell edge regions, their UEs still suffer strong interference from neighbouring MBSs. Therefore, the asynchronous case degrades the coverage performance of these UEs, the details of which will be investigated in Chapter 4. Similar to [10], we define RPSs and FPSs used in macrocells as protected subframes (PSs) and unprotected subframes (USs), respectively. The PSs and the USs are also defined in picocells although such subframes with different power do not exist. Based on the time slots as the PSs and USs transmitted in macrocells, the subframes transmitted in picocells at the same time slots as PSs in macrocells are defined as PSs, and the other subframes are defined as the USs. In such a case, the UEs can be classified into four groups: PS macrocell UEs (MUEs), US MUEs, PS picocell UEs (PUEs) and US PUEs. We use the index $l \in L = \{pm, um, pp, up\}$ to denote the four corresponding UE groups. Fig. 3.1 illustrates the four UE groups and their relationships to the four coverage regions in the two-tier HetNet. As shown in Fig. 3.1, UEs in macrocell centre region adopt PSs to mitigate interference from other BSs. In contrast, PSs in picocells are allocated to the range-expansion-region UEs, who receive weak signal power from their serving BSs. The other UEs will be allocated with the USs, i.e., the picocell original coverage region. Denoting the full-power aggregate interference from other MBSs and PBSs as I_m and I_p, respectively, and the thermal noise as σ^2, we give the SINR of a typical group-l UE as:

$$\Phi_l = \frac{\rho_l P_l h r_l^{-\alpha_l}}{\rho_l{}' I_{m_l} + I_{p_l} + \sigma^2}, \tag{3.1}$$

where $\rho_l = \rho$ only if $l = pm$, and $\rho_l{}' = \rho$ only if the UE utilizes PSs. Otherwise, $\rho_l = \rho_l{}' = 1$. Additionally, $I_{m_l} = I_{m/\{0\}}$ if $l = pm$ or um, and otherwise $I_{m_l} = I_m$, where $I_{\xi/\{0\}}$ denotes the received aggregate interference power from the tier-ξ excluding the serving BS, $\xi \in \{m, p\}$. For the aggregate interference power from PBSs I_{p_l}, $I_{p_l} = I_{p/\{0\}}$ if $l = pp$ or up, and otherwise $I_{p_l} = I_p$. Specifically, the SINR expressions of the four-group UEs are given as follows:

$$\begin{aligned} \Phi_{pm} &= \frac{\rho P_m h r_m^{-\alpha_m}}{\rho I_{m/\{0\}} + I_p + \sigma^2}, \qquad \Phi_{um} = \frac{P_m h r_m^{-\alpha_m}}{I_{m/\{0\}} + I_p + \sigma^2}, \\ \Phi_{pp} &= \frac{P_p h r_p^{-\alpha_p}}{\rho I_m + I_{p/\{0\}} + \sigma^2}, \qquad \Phi_{up} = \frac{P_p h r_p^{-\alpha_p}}{I_m + I_{p/\{0\}} + \sigma^2}, \end{aligned} \tag{3.2}$$

We assume that the locations of UEs follow another independent PPP, and the same-group UEs share the same spectrum resources in a round-robin manner [31]. Thus statistically the subframes can be considered to be allocated equally to the UEs in same group, as these UEs have equal probability to obtain each subframe. By information exchange between BSs and UEs, each BS knows which UEs are allocated with USs and which UEs are allocated with PSs. Also we assume that each BS knows which subframes are configured as PSs and USs. Consequently, the scheduler can run round-robin scheduling for PS and US UEs separately. Additionally, a full-buffer traffic model is assumed throughout the whole HetNet, thus each BS always has backlogged data waiting for transmission. To define the downlink rate together with the SINR expressions, we denote the RPS duty cycle (i.e, the proportion of RPSs) as β. As a result, the probability of a subframe being the PS and the US are β and $(1-\beta)$, respectively. Then the rate of a typical group-l UE can be formulated as:

$$R_l = \frac{\beta_l W}{N_l} \log_2(1+\Phi_l), \tag{3.3}$$

where β_l equals β and $1-\beta$ when the typical UE is served by PSs and USs, respectively. W is the spectrum bandwidth and N_l represents the number of serving UEs in group-l, which will be discussed in Section 3.1.3.

3.1.2 User Association Strategy

In this subsection, we will introduce a user association strategy, which gives the principle for classifying UEs into the aforementioned four groups. Note that the UE locations are assumed following another independent PPP. As a result, throughout our analysis, we assume that the typical UE is placed at the origin. It is reasonable because there is no difference in property observed either at a point of the PPP or at an arbitrary point, according to Slivnyak's theorem [101]. As a consequence, we can focus on the performance of this typical UE. By denoting the distances from this UE to its nearest MBS and PBS as r_m and r_p, respectively, the distance-based user association strategy is given in Proposition 3.1.

Proposition 3.1. *In a two-tier HetNet with CRE and RPSs, the serving BS and the allocated subframe type of a typical UE follow the relationships between r_m and r_p as follows:*

$$l = \begin{cases} pm, \ when \ k_c r_m \leq r_p, \\ um, \ when \ k_e r_m \leq r_p < k_c r_m, \\ pp, \ when \ k_p r_m \leq r_p < k_e r_m, \\ up, \ when \ k_p r_m > r_p, \end{cases} \tag{3.4}$$

where k_c, k_e and k_p are the macrocell centre region factor, the picocell range expansion factor and the picocell original coverage factor, respectively.

The centre-region area of each macrocell is completely dependent on k_c. A larger value of k_c results in a smaller size of the macrocell centre region. Therefore, the PS MUEs can be limited with close distances to their associated MBSs by employing a large enough value of k_c, even if their nearest interfering PBSs are distant. The value of k_e influences both the sizes of the picocell coverage region and the macrocell coverage region. The value of k_p determines the coverage bound between the picocell original coverage region and the picocell range expansion region. In the picocell original coverage region, a US PU receive stronger signal power from its associated PBS than any other interfering MBSs. Therefore, when a UE is deployed on the bound between the picocell original coverage and range expansion regions, its received signal power from the nearest MBS $P_m(k_p r_b)^{-\alpha_m}$ equals the signal power received from its associated PBS $P_p {r_b}^{-\alpha_p}$, where r_b is the distance between the UE at the bound and its associated PBS. If $\alpha_m = \alpha_p = \alpha$, the value of k_p is represented as $(P_p/P_m)^{1/\alpha}$. Otherwise, k_p has an approximation value of $(P_p/P_m)^{2/(\alpha_m+\alpha_p)}$ [32]. To obtain the association probability of the typical UE being classified into each of the four groups, the following lemma is proposed.

Lemma 3.1. *In two independent PPPs Θ_i and Θ_j with density λ_i and λ_j, respectively, if the closest distances from an arbitrary point to the two PPPs are denoted by r_i and r_j, then the probability of $r_i > k r_j$ is given as:*

$$\mathbb{P}(r_i > k r_j) = \frac{\lambda_j}{\lambda_j + k^2 \lambda_i}. \tag{3.5}$$

Proof. Note that the probability density function (PDF) of the nearest-point distance to an arbitrary point in the PPP Θ_j is $2\pi\lambda_j r \exp(-\pi\lambda_j r^2)$ [9]. The term $\mathbb{P}(r_i > k r_j)$ can be comprehended as the probability that there is no point is closer than $k r_j$ to the arbitrary point in Θ_i, which can be derived as follows:

$$\begin{aligned}
\mathbb{P}(r_i > k r_j) &= \mathbb{P}\{\text{no point closer than } k r_j | r_j\} \\
&= \int_0^\infty \exp(-\lambda_i \pi k^2 r^2) f_{r_j}(r) dr \\
&= 2\pi\lambda_j \int_0^\infty \exp(-\pi r^2(\lambda_i k^2 + \lambda_j)) r dr \\
&= \frac{\lambda_j}{\lambda_j + k^2 \lambda_i}.
\end{aligned} \tag{3.6}$$

□

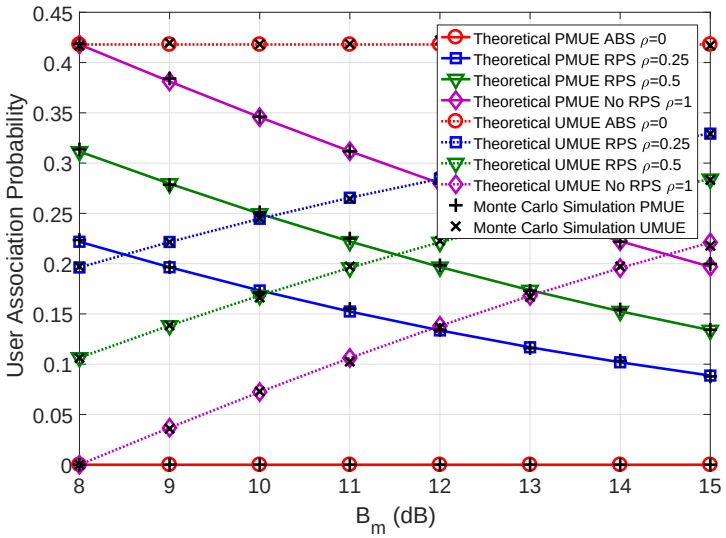

Fig. 3.2 User association probability of MUEs with various B_m values conditioned on $\lambda_p = 3\lambda_m$ © 2016 IEEE

The association probabilities for the US MUEs and the PS PUEs can be calculated by $\mathbb{P}(k_a r_m \leq r_p < k_b r_m) = \mathbb{P}(r_p > k_a r_m) - \mathbb{P}(r_p > k_b r_m)$, $k_a \in \{k_e, k_p\}$, $k_b \in \{k_c, k_e\}$. Combining (3.5) with the UE-group definition in (3.4), we have the association probabilities for the four UE groups as follows:

$$\begin{aligned} \text{Prob}(pm) &= \frac{\lambda_m}{\lambda_m + k_c^2 \lambda_p}, \qquad \text{Prob}(um) = \frac{\lambda_m \lambda_p (k_c^2 - k_e^2)}{(\lambda_m + k_c^2 \lambda_p)(\lambda_M + k_e^2 \lambda_p)}, \\ \text{Prob}(pp) &= \frac{\lambda_m \lambda_P (k_e^2 - k_p^2)}{(\lambda_m + k_e^2 \lambda_p)(\lambda_M + k_p^2 \lambda_p)}, \qquad \text{Prob}(up) = \frac{k_e^2 \lambda_p}{\lambda_m + k_p^2 \lambda_p}. \end{aligned} \tag{3.7}$$

In order to translate the variables k_c and k_e into an analogous form to k_p, we define k_c and k_e with the macrocell centre region bias B_m and picocell range expansion bias B_p as:

$$k_c = \left(\frac{B_m P_p}{\rho P_m}\right)^{\frac{2}{\alpha_m + \alpha_p}}, \quad k_e = \left(\frac{B_p P_p}{P_m}\right)^{\frac{2}{\alpha_m + \alpha_p}}. \tag{3.8}$$

Therefore, B_p and B_m can be written as:

$$B_m = \frac{\rho P_m}{P_p} (k_c)^{\frac{\alpha_m + \alpha_p}{2}}, \qquad B_p = \frac{P_m}{P_p} (k_e)^{\frac{\alpha_m + \alpha_p}{2}}. \tag{3.9}$$

In a special case, if $\rho = 0$, we define $k_c = \infty$, where its relationships to both k_e and B_m are broken. In that case, the PSs are configured as the ABSs proposed in the eICIC scheme. The

relationship of ρ, B_m, Prob(pm) and Prob(um) conditioned on the same pathloss exponent throughout the two-tier HetNet is shown in Fig. 3.2 with the optimal value of k_e obtained in Section 3.1.3. The results illustrate that the association probability of the PS MUEs improves (dotted curves) and that of the US MUEs declines (solid curves with black dots) while the variable B_m increases. The corresponding markers are Monte Carlo simulation results, which are close to the theoretical results.

After UEs being associated to BSs based on our proposed user association strategy, next we will discuss the PDF of the serving-BS distance. We consider a typical UE served by a tier-i BS. The two-dimensional Euclidean distance from the BS to this typical UE is denoted by r_i and the nearest distance from the interfering tier-j BSs is denoted by r_j. Thus, we have the following results regarding the distribution of the serving-BS distance.

Lemma 3.2. *In a two-tier HetNet with BS loations of both tiers following two independent PPPs, the PDF $f_{r_i}(r)$ of the serving-BS distance of a typical UE conditioned on $r_j > kr_i$ is*

$$f_{r_i|r_j>kr_i}(r) = 2\pi r(\lambda_i + k^2\lambda_j)\exp\left(-\pi r^2(\lambda_i + k^2\lambda_j)\right), \tag{3.10}$$

where r_i and r_j are the nearest distance from the UE to the tier-i BSs and the tier-j BSs, respectively, $i, j \in \{m, p\}$, $i \neq j$.

Proof. Using Bayes' rule, we have the probability of $r_i < R$ with condition $r_j > kr_i$ as:

$$\mathbb{P}\left(r_i < R | r_j > kr_i\right) = \frac{\mathbb{P}\left(r_i < R, r_j > kr_i\right)}{\mathbb{P}\left(r_j > kr_i\right)}. \tag{3.11}$$

The joint probability can be calculated as follows:

$$\begin{aligned}
\mathbb{P}\left(r_i < R, r_j > kr_i\right) &\overset{(a)}{=} \int_0^R \mathbb{P}(r_j > kr_i | r_i = r) f_{r_i}(r) dr \\
&\overset{(b)}{=} 2\pi\lambda_i \int_0^R r\exp(-\lambda_j \pi k^2 r^2)\exp(-\lambda_i \pi r^2) dr \\
&= \frac{\lambda_i}{\lambda_i + k^2\lambda_j}\left(1 - \exp(-\pi R^2(\lambda_i + k^2\lambda_j))\right),
\end{aligned} \tag{3.12}$$

where step (a) follows from the theorem of joint probability function and step (b) is derived from the probability of no point scattering in the region covered with radius kr_i in a PPP. Combining with Lemma 3.1, we have the conditional probability result as:

$$\text{Prob}\left(r_i < R | r_j > kr_i\right) = 1 - \exp(-\pi R^2(\lambda_i + k^2\lambda_j)). \tag{3.13}$$

Then after taking partial differentiation with respect to the variable R, we obtain (3.10). □

Using Lemma 3.2 and the UE-group definition in (3.7), we have the PDFs of the serving-BS distances for UEs of each group in (3.14).

$$\begin{cases} f_{pm}(r) = 2\pi r(\lambda_m + k_c^2\lambda_p)\exp\left(-\pi r^2(\lambda_m + k_c^2\lambda_p)\right) \\ f_{um}(r) = 2\pi r\dfrac{(\lambda_m + k_c^2\lambda_p)(\lambda_m + k_e^2\lambda_p)}{\lambda_p(k_c^2 - k_e^2)}\left[e^{-\pi r^2(\lambda_m + k_e^2\lambda_p)} - e^{-\pi r^2(\lambda_m + k_c^2\lambda_p)}\right] \\ f_{pp}(r) = 2\pi r\dfrac{(\lambda_m + k_e^2\lambda_p)(\lambda_m + k_p^2\lambda_p)}{\lambda_m(k_e^2 - k_p^2)}\left[e^{-\pi r^2(\lambda_m/k_e^2 + \lambda_p)} - e^{-\pi r^2(\lambda_m/k_p^2 + \lambda_p)}\right] \\ f_{up}(r) = 2\pi r(\lambda_m/k_p^2 + \lambda_p)\exp\left(-\pi r^2(\lambda_m/k_p^2 + \lambda_p)\right) \end{cases} \tag{3.14}$$

3.1.3 Performance Analysis

This subsection is our main analytical part. We derive the integral-form expression of the coverage and rate coverage probabilities with different pathloss exponents in the two tiers. Moreover, under the assumption of the same pathloss exponent throughout the two-tier HetNet, the analytical expression of the rate coverage probability is derived. At the end of this subsection, the optimization of bias values are discussed.

Coverage Probability

We define the coverage probability as the probability of a typical UE with SINR being larger than a target value, equivalent to the complementary cumulative distribution function (CCDF) of this typical UE's SINR. This coverage probability can also be comprehended as the fraction of UEs who have better SINR than the target value. In our analysis, we assume UEs and BSs are all static as a snapshot scene. Also, a UE can be allocated only with either PSs or USs. Then the coverage probability Λ of a typical UE is given as

$$\Lambda = \sum_{l \in L} \mathcal{P}_{cov}(l)\text{Prob}(l), \tag{3.15}$$

where $\mathcal{P}_{cov}$ is the coverage probability of a typical group-l UE. This coverage probability can be further transformed as:

$$\begin{aligned} \mathcal{P}_{\text{cov}}(l) &= \mathbb{P}(\Phi_l > \tau) \\ &\overset{(a)}{=} \int_R \mathbb{E}_I\left[\exp\left(\mu\frac{\tau r^{\alpha_l}}{\rho_l P_l}({\rho'}_l I_{M_l} + I_{P_l} + \sigma^2\right)\right] f_l(r)dr \\ &= \int_R \exp\left(\mu\frac{\tau r^{\alpha_l}}{\rho_l P_l}\sigma^2\right)\mathbb{E}_{I_M|l}\cdot\mathbb{E}_{I_P|l}\cdot f_l(r)dr, \end{aligned} \tag{3.16}$$

where step (a) is derived from the cumulative distribution function (CDF) of exponential distribution h. The expectation of the aggregate interference power from MBSs and PBSs, denoted by $\mathbb{E}_{I_M|l}$ and $\mathbb{E}_{I_P|l}$, are given as:

$$\begin{aligned}\mathbb{E}_{I_M|l} &= \mathbb{E}_{h,x}\left[\exp\left(-\frac{\mu\tau r^{\alpha_l}\rho'_l}{\rho_l P_l}\sum_{m\in M_l} P_m h_m {x_m}^{-\alpha_m}\right)\right],\\ \mathbb{E}_{I_P|l} &= \mathbb{E}_{h,x}\left[\exp\left(-\frac{\mu\tau r^{\alpha_l}\rho'_l}{\rho_l P_l}\sum_{n\in P_l} P_p h_n {x_n}^{-\alpha_p}\right)\right].\end{aligned} \tag{3.17}$$

Note that the distances of the nearest interfering BSs in both tiers have their lower limits as the open access mode is employed in picocells. By generally denoting the expectation of the aggregate interference power as $\mathbb{E}\left[\exp\left(-sI_\xi\right)\right]$ for the tier-ξ, where $I_\xi = P_\xi h {r_\xi}^{-\alpha_\xi}$ and $\xi \in \{m,p\}$, we have the result in Lemma 3.3.

Lemma 3.3. *In a two-tier HetNet with BS loations of both tiers following two independent PPPs, the Laplace transform $\mathcal{L}_{I_i}(s) = \mathbb{E}\left[\exp\left(-sI_i\right)\right]$ of the aggregate interference power from the tier-i BSs ($i \in \{m,p\}$) is*

$$\mathcal{L}_{I_i}(s) = \exp\left(-\pi\lambda_i\left(\frac{sP_i}{\mu}\right)^{\frac{2}{\alpha_i}} C\left((kr)^{\alpha_i}(\frac{s}{\mu})^{-1},\alpha_i\right)\right), \tag{3.18}$$

where function $C(a,b)$ is given as:

$$C(a,b) \approx \begin{cases} A(b) - a^{2/b}\left(1-\dfrac{2a}{b+2}\right), a<1,\\ B(b)a^{2/b-1}\left(1-\dfrac{(b-2)a^{-1}}{2b-2}\right), a\geq 1.\end{cases} \tag{3.19}$$

The functions $A(b)$ and $B(b)$ are defined as follows with $\Gamma(\cdot)$ being the Gamma function.

$$A(b) = \int_0^\infty (1+x^{b/2})^{-1}dx, \quad B(b) = -\frac{2\Gamma(2/b-1)}{b\Gamma(2/b)}. \tag{3.20}$$

Proof. The Laplace transform $\mathcal{L}_{I_i}(s)$ of the aggregate interference power I_i with the minimum interfering distance being kr can be transformed as follows:

$$\begin{aligned}\mathcal{L}_{I_i}(s) &= \mathbb{E}(\exp(-sI_i)) = \mathbb{E}\left(\prod_{i|r_i>kr}\exp(-sP_i h r_i^{-\alpha_i})\right)\\ &\overset{(a)}{=} \exp\left(-2\pi\lambda_i\int_{kr}^{\infty}(1-\mathbb{E}_h\left[\exp(-sP_i h u^{-\alpha_i})\right])udu\right),\end{aligned} \tag{3.21}$$

where step (a) follows from the probability generating function of a spatial homogeneous PPP [9]. By incorporating the PDF of h that follows $h\sim\exp(\mu)$, this Laplace transform can be translated into the following results:

$$\begin{aligned}\mathcal{L}_{I_i}(s) &= \exp\left(-2\pi\lambda_i\int_{kr}^{\infty}\frac{sP_i u^{-\alpha_i}}{sP_i u^{-\alpha_i}+\mu}udu)\right)\\ &\overset{(b)}{=} \exp\left(-\pi\lambda_i(\frac{sP_i}{\mu})^{\frac{2}{\alpha_i}}\int_{(kr)^2(\frac{sP_i}{\mu})^{\frac{-2}{\alpha_i}}}^{\infty}\frac{1}{1+t^{\frac{\alpha_i}{2}}}dt\right)\\ &= \exp\left(-\pi\lambda_i(\frac{sP_i}{\mu})^{\frac{2}{\alpha_i}}C((kr)^{\alpha_i}(\frac{sP_i}{\mu})^{-1},\alpha_i)\right),\end{aligned} \tag{3.22}$$

where step (b) is obtained by substituting $(\mu/sP_i)^{2/\alpha_i}u^2$ by t. Then by implying $C(a,b)=\int_{a^{2/b}}^{\infty}1/(1+t^{b/2})dt$, we achieve the final result in Lemma 3.3. Next, to reduce the calculation complexity, the approximation of $C(a,b)$ is investigated in terms of a. On one hand, for small parameter ($a<1$), the expression can be approximated as follows:

$$\begin{aligned}C(a,b) &= \int_0^{\infty}1/(1+t^{b/2})dt - \int_0^{a^{2/b}}1/(1+t^{b/2})dt\\ &\overset{(a)}{=} A(b) - t\cdot{}_2F_1\left(1,\frac{2}{b};1+\frac{2}{b};-t^{\frac{b}{2}}\right)\Big|_0^{a^{2/b}}\\ &\overset{(b)}{\approx} A(b) - a^{2/b}\left(1-\frac{2a}{b+2}\right),\end{aligned} \tag{3.23}$$

where $A(b)=\int_0^{\infty}(1+x^{b/2})^{-1}dx$ and ${}_2F_1(\cdot)$ is the Gauss hypergeometric function. Step (a) is obtained by the Wolfram symbolic integral calculator online and step (b) is the first-order series expansion of the Gauss hypergeometric function. The smaller the parameter a is, the closer match between the approximated and the actual values can be yielded. On the other hand, when a is larger than 1 ($a\geq 1$), we can approximate the result with $B(b)=-\frac{2\Gamma(2/b-1)}{b\Gamma(2/b)}$

as:

$$\begin{aligned} C(a,b) &\overset{(a)}{=} t\cdot {}_2F_1\left(1,\frac{2}{b};1+\frac{2}{b};-t^{\frac{b}{2}}\right)\Big|_{a^{2/b}}^{\infty} \\ &\overset{(b)}{=} B(b)a^{(2/b-1)}{}_2F_1(1,1-\frac{2}{b};2-\frac{2}{b};a^{-1}) \\ &\overset{(c)}{\approx} B(b)a^{(2/b-1)}\left(1-\frac{(b-2)a^{-1}}{2b-2}\right), \end{aligned} \tag{3.24}$$

where step (a) is obtained by the Wolfram symbolic integral calculator online and step (b) is achieved by combining (a) in (3.24) with equation (9) in [102]. Step (c) is obtained by the first-order series expansion of the Gauss hypergeometric function. □

Note that if the interference and signal are from BSs of the same tier, the minimum-interfering-BS distance is r. For simplicity, we assume that the thermal noise is approximately zero ($\sigma \sim 0$), which has negligible effect on the coverage probability and can be referred as an interference limited network [22]. Equipped with Lemma 3.3 and $\mathbb{E}[\exp(-sI_i)] = \mathcal{L}_{I_i}(s)$, we have the following results regarding the coverage probability of a typical UE in the two-tier HetNet.

Theorem 3.1. *In the two-tier HetNet with CRE and RPSs, following the user association strategy in* (3.4)*, the coverage probabilities of UEs in each group are given as follows:*

$$\begin{cases} \mathcal{P}_{cov}(pm) = \int_0^{\infty} e^{-\pi\left(D(\lambda_m,\alpha_m,r,\tau)+\lambda_p r^{\frac{2\alpha_m}{\alpha_p}}(\tau(\hat{P_m}\rho)^{-1})^{\frac{2}{\alpha_p}}C(k_c{}^{\alpha_p}r^{\alpha_p-\alpha_m}\rho\hat{P_m}\tau^{-1},\alpha_p)\right)} f_{pm}(r)dr, \\ \mathcal{P}_{cov}(um) = \int_0^{\infty} e^{-\pi\left(D(\lambda_m,\alpha_m,r,\tau)+\lambda_p r^{\frac{2\alpha_m}{\alpha_p}}(\tau\hat{P_m}^{-1})^{\frac{2}{\alpha_p}}C(k_e{}^{\alpha_p}r^{\alpha_p-\alpha_m}\hat{P_m}\tau^{-1},\alpha_p)\right)} f_{um}(r)dr, \\ \mathcal{P}_{cov}(pp) = \int_0^{\infty} e^{-\pi\left(D(\lambda_p,\alpha_p,r,\tau)+\lambda_m r^{\frac{2\alpha_p}{\alpha_m}}(\tau\rho\hat{P_m})^{\frac{2}{\alpha_m}}C(k_e{}^{-\alpha_m}r^{\alpha_m-\alpha_p}(\tau\rho\hat{P_m})^{-1},\alpha_m)\right)} f_{pp}(r)dr, \\ \mathcal{P}_{cov}(up) = \int_0^{\infty} e^{-\pi\left(D(\lambda_p,\alpha_p,r,\tau)+\lambda_m r^{\frac{2\alpha_p}{\alpha_m}}(\tau\hat{P_m})^{\frac{2}{\alpha_m}}C(k_p{}^{-\alpha_m}r^{\alpha_m-\alpha_p}(\tau\hat{P_m})^{-1},\alpha_m)\right)} f_{up}(r)dr, \end{cases} \tag{3.25}$$

where $\hat{P_m} = P_m/P_p$ *and* $D(\lambda,\alpha,r,\tau) = r^2\lambda\tau^{\frac{2}{\alpha}}C(\tau^{-1},\alpha)$.

Proof. Combining Lemma 3.3 with (3.16) and (3.17), we can achieve the results. □

The exponential part of the integration in each equation is obtained by the Laplace transform of the aggregate interference power from both tiers. Then we obtain the expectation of the coverage probability of the typical UE in each group by averaging on the serving BS distance. Equipped with these results, we have the coverage probability of a typical UE following (3.15). The closed-form results can be obtained when macrocells and picocells have the same pathloss exponent (α_m=α_p). Otherwise, we evaluate these results numerically.

Rate Performance

In this part, we focus on evaluating the rate coverage probability of a typical UE, which is defined as the probability of a typical UE that has a rate larger than the target rate. The expression of the rate coverage probability of a typical group-l UE is given by:

$$\mathbb{P}(R_l > \omega) = \mathbb{P}\left(\frac{\beta_l W}{N_l}\log_2(1+\Phi_l) > \omega\right), \tag{3.26}$$

where ω is the threshold of the downlink rate, W is the spectrum bandwidth, and N_l is the number of group-l UEs in a macrocell. The rate coverage probability can also be comprehended as the fraction of UEs in the two-tier HetNet achieving a target rate. In order to obtain the expected UE number of each group in the associated cell, we have the following result regarding to the expected number of UEs in a macrocell with the assumption of UE locations following an independent PPP with density of λ_u.

Lemma 3.4. *In a network with MBSs and UEs following two independent PPPs with densities of λ_m and λ_u, respectively, the expected UE number $\mathbb{E}(N)$ in a voronoi macrocell is λ_u/λ_m.*

Proof. As the ergodicity of the PPP [101], the mean coverage area of a voronoi macrocell is $\frac{1}{\lambda_m}$. Then the expectation UE number in a voronoi macrocell is $\frac{\lambda_u}{\lambda_m}$ as UE locations follow another independent PPP with density λ_u. □

Combining the Lemma 3.4 with user association probabilities in (3.7), the expected numbers of the four group UEs in a macrocell can be calculated by $\mathbb{E}(N_l) = \text{Prob}(l)\mathbb{E}(N)$. Then we have the rate coverage probability of a typical group-l UE in Theorem 3.2.

Theorem 3.2. *In the two-tier HetNet, the rate coverage probability $\mathcal{R}_{cov}(l)$ of a typical group-l UE can be approximated by a transformation of the coverage probability as:*

$$\mathcal{R}_{cov}(l) = \mathcal{P}_{cov}(l)|\tau = 2^{\frac{\omega N_l}{\beta_l W}} - 1. \tag{3.27}$$

Proof. From (3.26), the equation can be translated into the following result:

$$\mathbb{R}_{cov}(l) = \mathbb{E}_{N_l}\left[\text{Prob}\left(\Phi_l > 2^{\frac{\omega N_l}{\beta_l W}} - 1\right)\right]. \tag{3.28}$$

This has a similar form as the coverage probability. By substituting $2^{\frac{\omega N_l}{\beta_l W}} - 1$ with $g(\frac{\omega N_l}{\beta_l W})$, we have:

$$\mathbb{R}_{cov}(l) = \mathbb{E}_{N_l}\left[\mathcal{P}_{cov}(l)|\tau = g\left(\frac{\omega N_l}{\beta_l W}\right)\right]. \tag{3.29}$$

Table 3.1 NEW NOTATIONS IN Ω

Parameter	Value
g_l	$g\left(\frac{\omega\mathbb{E}(N_l)}{\beta_l W}\right)$
e_l	${g_l}^{\frac{2}{\alpha}} C({g_l}^{-1},\alpha)+1$
κ_l	$\hat{P_m}(\rho_l' g_l)^{-1}$
κ_l'	$(\hat{P_m}\rho_l' g_l)^{-1}$

However, equation (3.29) is difficult to calculate. In [30], the approximated rate coverage probability by exchanging the calculation order between the expectation and the integration has an offset limited within 5% as compared with the exact rate coverage probability, which validates the effectiveness of this approximation. Thus we get the final approximated value by exchanging the calculation order of the expectation and the integration as follows:

$$\mathbb{R}_{cov}(l) \approx \mathcal{P}_{cov}(l)|\tau = g\left(\frac{\omega\mathbb{E}(N_l)}{\beta_l W}\right). \tag{3.30}$$

□

Combining Theorem 3.2 with expected UE number of each group, we have the rate coverage probabilities of UEs in each group. Thus the rate coverage probability Ω of the whole two-tier HetNet can be calculated by $\Omega = \sum_l \text{Prob}(l)\mathcal{R}_{cov}(l)$. It represents the fraction of UEs in the whole network having a larger throughput than the threshold. Similar to the coverage probability, this rate coverage probability has a closed-form expression in (3.31) when $\alpha_m = \alpha_p \equiv \alpha$.

Optimal Bias Values

Under the assumption $\alpha_m = \alpha_p \equiv \alpha$, the rate coverage probability Ω has a closed-form expression in (3.31), with new notations introducing in Table 3.1 for notational simplicity, where $l \in \{cm, um, cp, up\}$.

$$\Omega = \left\{ \frac{1}{\theta k_c^2 + \theta\kappa_{pm}{}^{-\frac{2}{\alpha}} C(\kappa_{pm}k_c^{\alpha},\alpha) + e_{pm}} + \frac{1}{\theta k_e^2 + \theta\kappa_{um}{}^{-\frac{2}{\alpha}} C(\kappa_{um}k_e^{\alpha},\alpha) + e_{um}} - \right.$$
$$\frac{1}{\theta k_c^2 + \theta\kappa_{um}{}^{-\frac{2}{\alpha}} C(\kappa_{um}k_e^{\alpha},\alpha) + e_{um}} + \frac{1}{\theta^{-1}k_e^{-2} + \theta^{-1}\kappa'_{pp}{}^{-\frac{2}{\alpha}} C(\kappa'_{pp}k_e^{-\alpha},\alpha) + e_{pp}} -$$
$$\left. \frac{1}{\theta^{-1}k_p^{-2} + \theta^{-1}\kappa'_{pp}{}^{-\frac{2}{\alpha}} C(\kappa'_{pp}k_p^{-\alpha},\alpha) + e_{pp}} + \frac{1}{\theta^{-1}k_p^{-2} + \theta^{-1}\kappa'_{up}{}^{-\frac{2}{\alpha}} C(\kappa'_{up}k_p^{-\alpha},\alpha) + e_{up}} \right\} \tag{3.31}$$

Recall that the optimal bias values are defined for maximizing the rate coverage probability, thus the optimal values of k_c and k_e can be written as the following form:

$$[{k_c}^{opt}, {k_e}^{opt}] = \arg\max_{k_c,k_e}\{\Omega(k_c,k_e)\}. \tag{3.32}$$

As the biases B_m and B_p always have upper and lower limits, the values of k_c and k_e also have limited ranges according to (3.8). Moreover, as the terms κ_l, κ_l' and e_l include both k_c and k_e, the objective function is too complicated to obtain a closed-form optimal values. Thus the optimal values of k_c and k_e can only be analysed numerically. However, the procedure is exhaustive because of the two-dimensional search space. In order to reduce the time and resource for searching, we proposed a new method to obtain the near optimal (NO) values by a single iteration method. The main idea is translating the search space into several one-dimension spaces. In the following, first we propose an NO value for k_c related to k_e based on the SINR property of PS MUEs and US MUEs. Then we substitute the value of k_c with this k_e-related value in (3.32) to obtain the NO value of k_e. Eventually the NO value of k_c is calculated with the substitution of the NO value of k_e in (3.32). The details of this single-iteration method are given below.

When considering the effect of k_c on the rate coverage probabilities of MUEs, we treat the value of k_e as a constant. As a result, the number of the MUEs is determined, denoted by N_{mue}. Then the maximization problem of the rate coverage probabilities can be formulated as a maximization problem of the minimum rate coverage, which is given as follows:

$$\begin{aligned} &\max_{N_l}\{\min\{\mathcal{R}_{cov}(um), \mathcal{R}_{cov}(pm)\}\} \\ s.t.\quad &N_{um} + N_{pm} = N_{mue}. \end{aligned} \tag{3.33}$$

Without the explicit SINR values, this problem is difficult to resolve. Fortunately, if we assume the SINR of a PS MUE is identical to that of a US MUE, the maximum minimum rate coverage probability is achieved following the relationship of user association probabilities of PS MUEs and US MUEs:

$$\frac{\text{Prob}(pm)}{\text{Prob}(um)} = \frac{\beta}{1-\beta}. \tag{3.34}$$

For notational simplicity, we replace β' with $\frac{\beta}{1-\beta}$. Furthermore, combining (3.34) with the user association probability in (3.7), we have the following relationship of k_c and k_e as:

$$k_c' = \sqrt{{k_e}^2 + \frac{\lambda_m + {k_e}^2\lambda_p}{\lambda_p \beta'}}. \tag{3.35}$$

As resource allocation contributes more than SINR when the optimal rate coverage probability is obtained intuitively, the value of k_c' can be deemed as the initial NO value of k_c. Equipped

$$\hat{k}_e^{opt} = \underset{k_c=k_c', k_e}{\arg\max} \left[\frac{1}{\theta k_e^2 + \theta \kappa_{um}{}^{-\frac{2}{\alpha}} C(\kappa_{um} k_e^{\alpha}, \alpha) + e_{um}} - \frac{1}{\theta k_c^2 + \theta \kappa_{um}{}^{-\frac{2}{\alpha}} C(\kappa_{um} k_e^{\alpha}, \alpha) + e_{um}} \right.$$
$$\left. + \frac{1}{\theta^{-1} k_e^{-2} + \theta^{-1} \kappa_{pp}'{}^{-\frac{2}{\alpha}} C(\kappa_{pp}' k_e^{-\alpha}, \alpha) + e_{pp}} - \frac{1}{\theta^{-1} k_p^{-2} + \theta^{-1} \kappa_{pp}'{}^{-\frac{2}{\alpha}} C(\kappa_{pp}' k_e^{-\alpha}, \alpha) + e_{pp}} \right]. \tag{3.36}$$

with this k_c', the NO value of k_e, denoted by $\hat{k}_e^{opt}$ can be evaluated numerically by (3.36). This is because the first term and last term in (3.31) exclude variable k_e. Therefore, by combining the value of ${k_e}^{opt}$ with (3.32), the NO value of k_c, $\hat{k}_c^{opt}$, can also be obtained numerically by the following result.

$$\hat{k}_1^{opt} = \underset{k_c, k_e=\hat{k}_2^{opt}}{\arg\max} \left[\frac{1}{\theta k_c^2 + \theta \kappa_{pm}{}^{-\frac{2}{\alpha}} C(\kappa_{pm} k_c^{\alpha}, \alpha) + e_{pm}} - \frac{1}{\theta k_c^2 + \theta \kappa_{um}{}^{-\frac{2}{\alpha}} C(\kappa_{um} k_e^{\alpha}, \alpha) + e_{um}} \right]. \tag{3.37}$$

Thus the NO values of k_c and k_e are obtained by this single-iteration method. Interestingly, the NO values are very close to the actually numerical optimal results when the search of the optimal k_e starts with k_c in (3.35). Equipped with these optimal values and the definition of B_p and B_m in (3.9), the comparisons between the NO values and the actual optimal (AO) values of the picocell range-expansion bias and the macrocell centre-region bias are illustrated in Fig. 3.3 and Fig. 3.4, respectively.

Fig. 3.3 illustrates the AO values and NO values of the picocell range-expansion bias B_p with the rate threshold being 100 and 200 kbps. The results show that the gaps between the NO and AO values of this bias are negligible. It proves the effectiveness of our proposed single-iteration method. The comparison between the proposed NO values and AO values of the macrocell centre-region bias B_m is illustrated in Fig. 3.4, also with the rate threshold being 100 and 200 kbps. The results show that when the power reduction factor ρ is small (0.1 and 0.25), the difference between these NO and AO values of B_m is negligible. However, with the increase of the transmit power of RPSs (0.5), the gap between them increases but never exceeds 2 dB. As shown in the rate-coverage-probability comparison in Fig. 3.5, this gap contributes so little that the rate coverage probability of a typical UE with the NO and AO values of biases are almost the same. The reason is that the small offsets on B_m have negligible effect on the rate coverage probability when the bias B_m is relatively large. Consequently, it is reasonable to consider the results achieved from the single-iteration method as the optimal values for B_m and B_p.

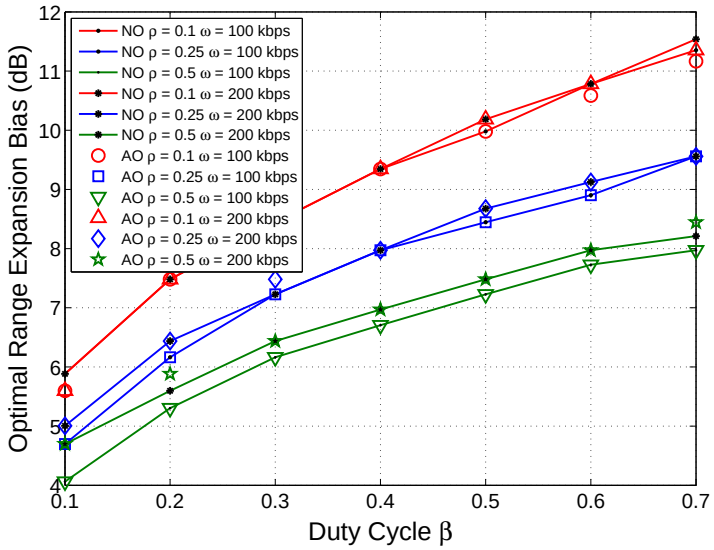

Fig. 3.3 The optimal range expansion biases with varieties of power reduction factor ρ, and the rate threshold $\omega = 100$ and 200 kbps ©2016 IEEE

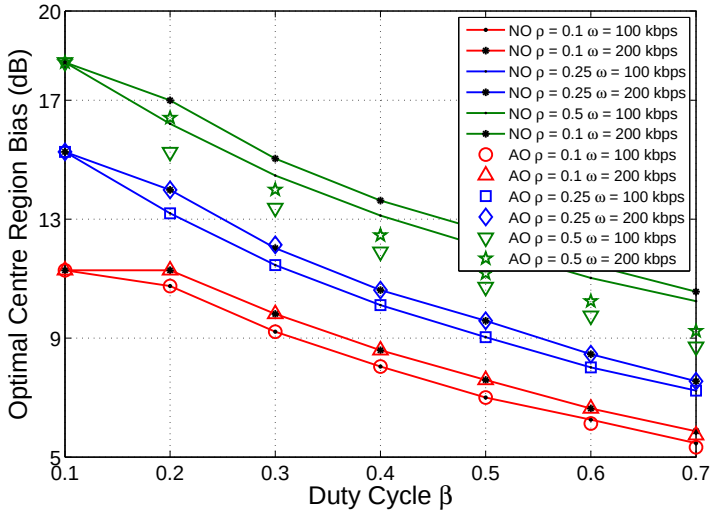

Fig. 3.4 The optimal centre region biases with varieties of ρ, and the rate threshold $\omega = 100$ and 200 kbps ©2016 IEEE

3.1.4 Simulation Results and Discussion

In this subsection, we present the theoretical results of the coverage probability and the rate coverage probability derived in Section 3.1.3 and validate these results with Monte Carlo simulations. Furthermore, the effects of the power reduction factor and duty cycle on the coverage and rate coverage probabilities are investigated numerically. The simulated network is assumed to be a square area of 25 km^2. We sample $10,000$ times where BSs are deployed following the PPP model and the typical UE is deployed at the origin. A realization of spatial locations and coverage area of BSs is illustrated in 3.6, in which red dots and blue triangles denote MBSs and PBSs respectively. The purple and black circle around each PBS respectively represent the original and the expanded coverage area by CRE. The black circle around each MBS is the centre area of the corresponding macrocell. The simulation parameters are summarized in Table 3.2.

In Fig. 3.7, we compare the coverage probabilities of a typical UE with several typical pathloss exponents (i.e., α_m and α_p equal 2.5 or 3.0). The results obtained by Monte Carlo simulations match the theoretical results, especially when the pathloss exponents are equal in both tiers. It proves the correctness of our proposed model. Moreover, the network with lower picocell pathloss exponent outperforms that with lower macrocell pathloss exponent in terms of the coverage probability. This has two causes. The first cause is the CRE of picocells. When macrocells has lower pathloss exponent, then the CRE UEs suffer stronger interference from MBSs. Also, with relatively higher pathloss exponent of picocells, the

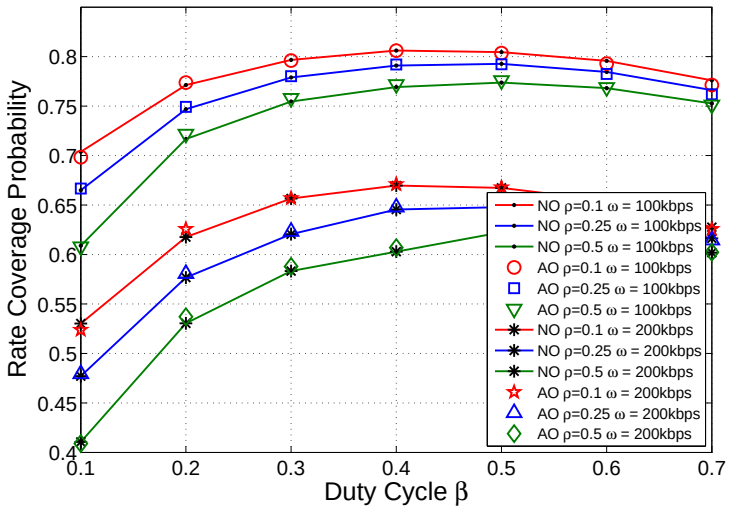

Fig. 3.5 The rate coverage probability of a typical UE in the two-tier HetNet with NO and AO biases ©2016 IEEE

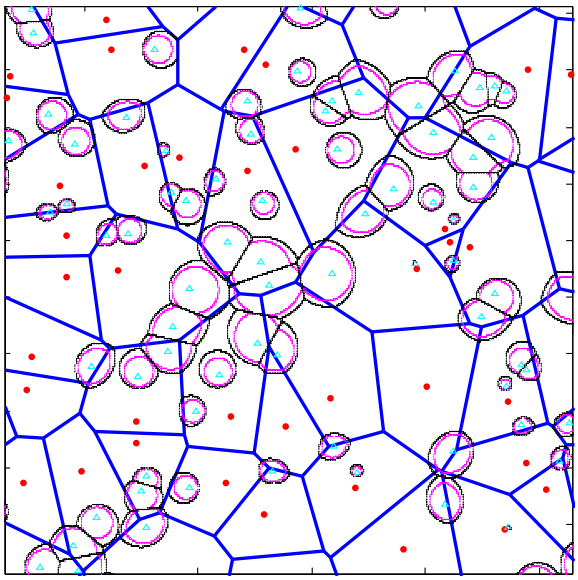

Fig. 3.6 A realization of spatial locations and coverage area of BSs in the HetNet with CRE and RPSs, in which red dots and blue triangles denote MBSs and PBSs respectively. The purple and black circle around each PBS respectively represent the original and the expanded coverage area by CRE. The black circle around each MBS is the centre area of the corresponding macrocell.

Table 3.2 NOTATIONS AND SIMULATION VALUES

Parameter	Description	Value
$\mathcal{S}$	Square range	$5000 \times 5000\ m^2$
W	Spectrum bandwidth	5 MHz
λ_m	Density of MBS	$1.27e^{-6}\ /m^2$
λ_p	Density of PBS	$3\lambda_m$
λ_u	Density of UEs	$30\lambda_m$
P_m	Maximum transmit power of MBSs	43 dB
P_p	Maximum transmit power of PBSs	30 dB
α_m	Macrocell pathloss exponent	2.5 and 3.0
α_p	Picocell pathloss exponent	2.5 and 3.0
β	RPS duty cycle	0.5
μ	Exponential distribution factor	1
k_c	Macrocell centre-region factor	${k_c}^{opt}$
k_e	Picocell range-expansion factor	${k_e}^{opt}$
k_p	Picocell original coverage-region factor	$(\frac{P_p}{P_m})^{\frac{2}{\alpha_m+\alpha_p}}$
B_m	Macrocell centre-region bias ($\rho \neq 0$)	$\frac{\rho P_m}{P_p}(k_c)^{\frac{\alpha_m+\alpha_p}{4}}$
B_p	Picocell range-expansion bias	$\frac{P_m}{P_p}(k_e)^{\frac{\alpha_m+\alpha_p}{4}}$

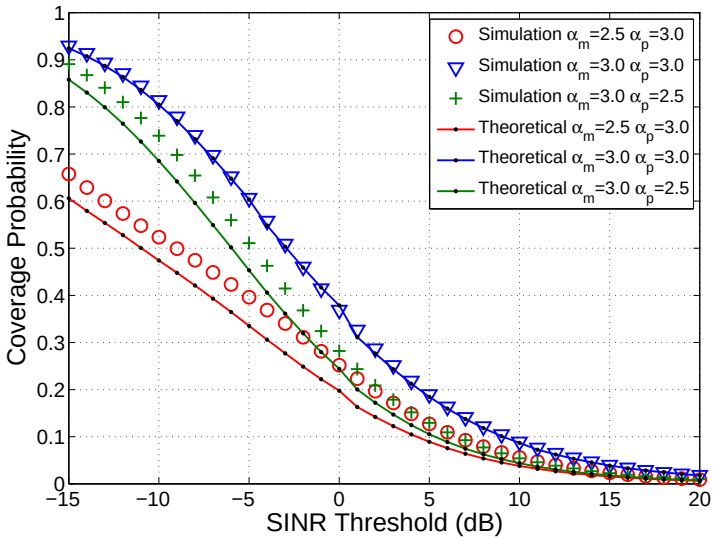

Fig. 3.7 Validation of coverage probabilities of a typical UE versus the SINR threshold with several pathloss exponents ©2016 IEEE

CRE UEs receive weaker signals. The second cause is that the MBS has a higher transmit power. Under the same circumstance, MBSs cause higher interference than PBSs.

Fig. 3.8 shows the rate coverage probability of a typical UE with several typical pathloss exponents (i.e., α_m and α_p equal 2.5 or 3.0). Similar to the coverage probability, the

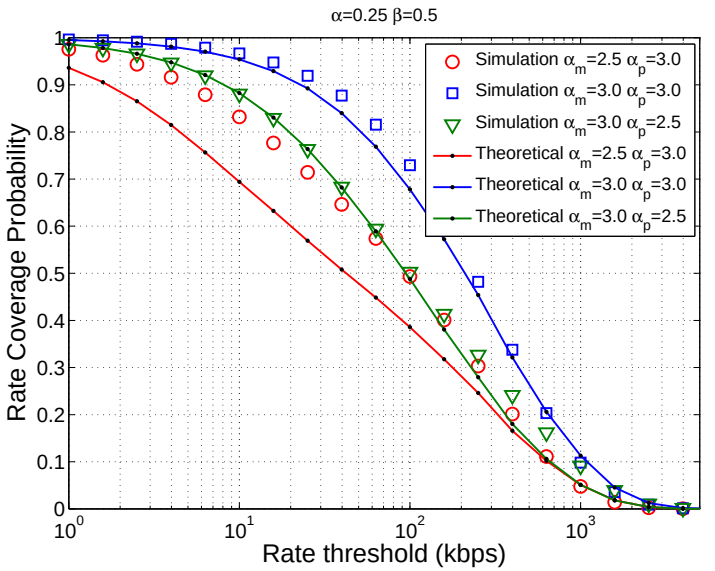

Fig. 3.8 Validation of rate coverage probabilities of a typical UE versus the SINR threshold with several pathloss exponents ©2016 IEEE

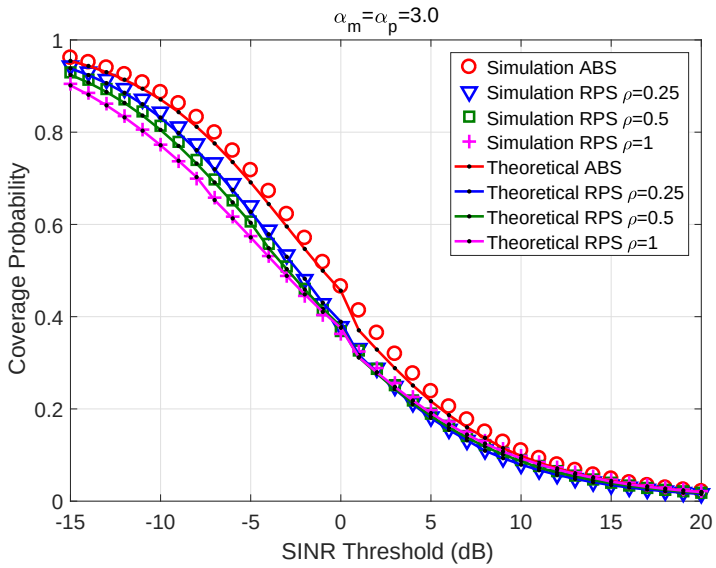

Fig. 3.9 The coverage probabilities of a typical UE versus SINR threshold with several power reduction factors ©2016 IEEE

theoretical results (solid curves with black dots) closely match the Monte-Carlo-simulation results (only markers), especially when the pathloss exponents of both tiers are the same. There are two main reasons for choosing 100 or 200 kbps as the threshold: Firstly, the comparable values of the rate coverage threshold are also used in [30] and [31]. Secondly, a relatively decent rate coverage probability can be provided with the threshold being 100 or 200 kbps. As compared with the actual system, the rate coverage probability is still too low mainly because of the system model we use. Specifically, we assume that single input single out put antenna is equipped in each BS while in reality multiple antennas are equipped in each MBS. Additionally, only one subchannel is assumed and in multiple-subchannel case, the suffered interference can be reduced. Moreover, the value of pathloss exponent may be low. Thus the rate coverage is poorer in our system model as compared with that in reality.

In Fig. 3.9, we compare the coverage probabilities of a typical UE with several RPS transmit powers (i.e., $\rho = 0, 0.25, 0.5$ and 1). The results show that the coverage probability with ABSs is better than that with RPSs. This is because the CRE UEs suffer no interference from MBSs when applying ABSs in the HetNet, they always have a better SINR than that when applying RPSs. In addition, RPSs also degrade the SINR of the macrocell centre-region UEs. Moreover, for small SINR thresholds ($\tau < 0$), as the power reduction factor increases, the coverage probability declines. The SINR deterioration is caused by the increasing interference from MBSs. On the other hand, for large SINR thresholds, there is nearly no difference with different RPS transmit powers except for the ABS case. The reason is the poor coverage probabilities of CRE UEs. When the SINR threshold $\tau > 5$, their coverage

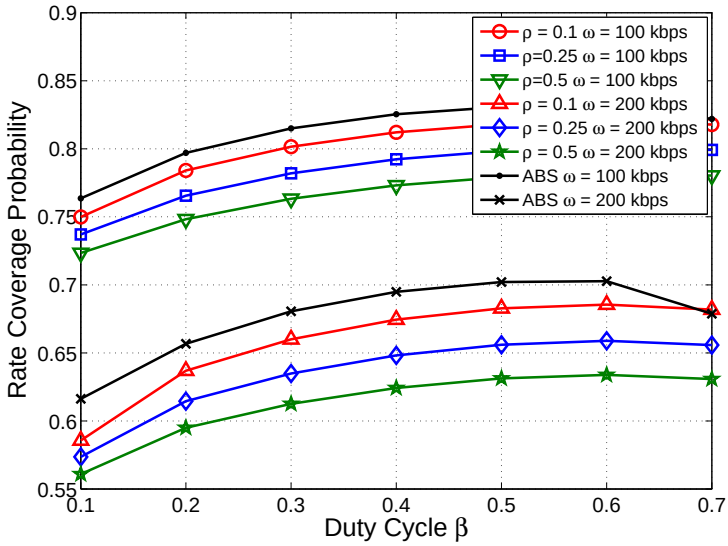

Fig. 3.10 The rate coverage probabilities of a typical UE versus duty cycle β in terms of optimal biases with target rate being 100 and 200 kbps ©2016 IEEE

probabilities are close to zero. The coverage probability enhancement with the increase of the RPS transmit power is caused by the improved PS MUE performance.

Fig. 3.10 illustrates the theoretical rate coverage probabilities of a typical UE versus the RPS duty cycle β with several typical power reduction factors (i.e., $\rho = 0.1, 0.25$, and 0.5) and the rate threshold ω being 100 and 200 kbps under the optimal B_m and B_p. As shown in the results, the best rate coverage probability is always achieved when β is approximate 0.6. Moreover, this rate coverage probability yields the best performance when using ABSs. In the ABS case, the CRE UEs have the best SINR as they suffer no interference from MBSs. Therefore, a larger picocell range-expansion area results in more UEs having better SINR and rate. However, in such a case, more UEs are attracted to the picocells, as shown in Fig. 3.11. This figure illustrates the ratio between the number of MUEs and PUEs per cell when the optimal rate coverage probability is achieved. Using ABSs always have more UEs associated with PBSs as compared with using RPSs. This means a heavier burden on the backhaul of picocells. However, in reality, picocells may have a limited backhaul while the macrocell backhaul is remarkably larger than picocell backhaul. In the following, we investigate the rate coverage probability with several typical fixed values of picocell range-expansion bias B_p.

In Fig. 3.12, we compare the rate coverage probabilities of a typical UE versus duty cycle β with several typical values of B_p (i.e., 3 dB, 7 dB and 12 dB). The rate threshold is set as 100 kbps. Different from the results with optimal biases, the rate coverage probabilities

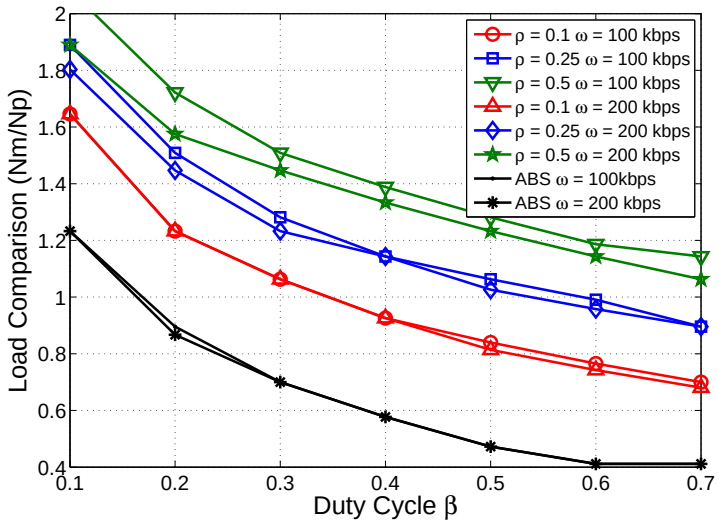

Fig. 3.11 The load compasison versus duty cycle β in terms of the optimal biases with target rate being 100 and 200 kbps ©2016 IEEE

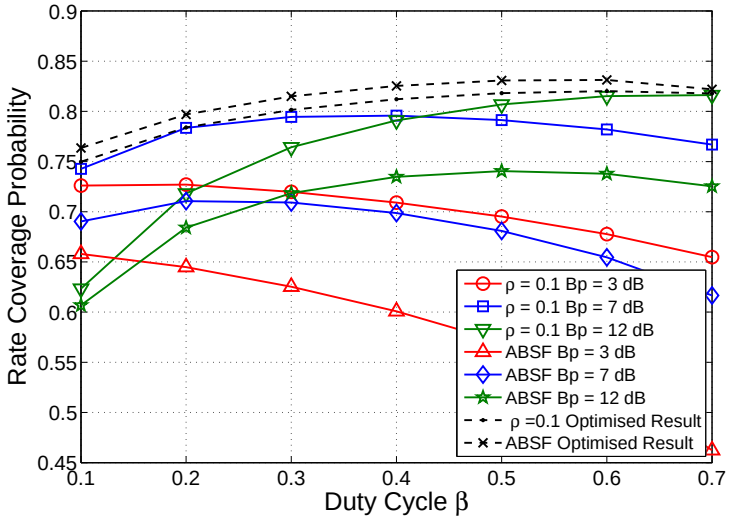

Fig. 3.12 The rate coverage probabilities of a typical UE versus duty cycle β with $\omega = 100$ kbps ©2016 IEEE

obtained with RPSs are better than that with ABSs. On one hand, when the picocell range-expansion bias is static, in particular when it is small, the RPSs with a relative low transmit power have limited effects on the rate performance of the CRE UEs. On the other hand, the rate of the macrocell centre-region UEs increases by sharing more spectrum resources.

In Fig. 3.13, the rate coverage probabilities of a typical UE is analysed versus the power reduction factor ρ, with the typical values of B_p (i.e., 3 dB, 7 dB and 12 dB) and the rate threshold ω being 100 and 200 kbps. On one hand, the results show that a sharp increase occurs when the ρ varies from 0. Intuitively, compared with the ABSs, the RPSs provide better rate coverage probabilities for the macrocell edge-region UEs by sharing more spectrum, but worse rate coverage probabilities for the CRE UEs. In our case, the transmit power of RPSs is low, thus the rate-coverage-probability gain in macrocells exceeds that loss in picocells, which results in the sharp increase of the rate coverage probability. On the other hand, interestingly, the performance remains almost constant with various ρ ($\rho \neq 0$) values when the B_p is relatively low. In such a low B_p case, the number of the CRE UEs is small, and by allocating some more resources to these UEs, the rate-coverage-probability loss due to their degraded SINR is made up. In other words, by adjusting the RPS duty cycle β, the coverage performance is not affected by ρ when the B_p is low (under 7 dB in our simulation). However, a large value of B_p results in more UEs to camp to picocell range-expansion regions, which will be significantly interfered when the RPS transmit power

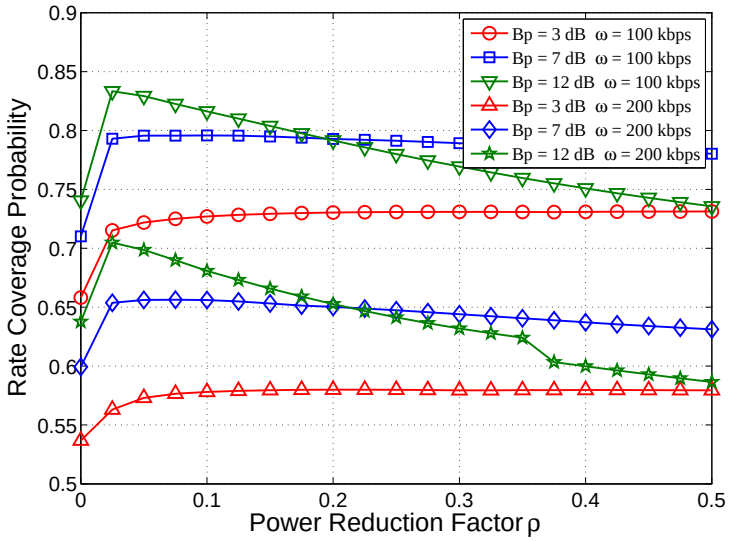

Fig. 3.13 The rate coverage probabilities of a typical UE versus power reduction factor ρ with fixed B_p and target rate ω being 100 and 200 kbps ©2016 IEEE

is large. Therefore, the rate coverage probability declines with the increase of ρ when B_p is large.

3.1.5 Conclusion

In the first section, we have obtained the analytical results to calculate the coverage and rate coverage probabilities employing FeICIC-RPSs and CRE in a two-tier HetNet. Following the results, the rate coverage performance is analysed with the biases, the power reduction factor and the duty cycle. We conclude that with the optimal macrocell centre and picocell range-expansion biases, the ABSs outperform the RPSs in terms of both coverage and rate coverage probabilities, which can be observed in Fig. 3.10. As the ABS case has a larger optimal picocell range expansion bias, more UEs will be attracted to the CRE regions. This will result in a heavier backhaul burden on picocells, which in reality may have limited backhaul capability. From Fig. 3.12, if the picocell range-expansion bias is static and not optimal, the RPSs in turn outperform the ABSs in terms of rate coverage probability by sharing more spectrum resource in the macrocell edge region. Additionally, when the picocell range -expansion bias is relatively low (under 7 dB), the power reduction factor has negligible effect on the rate coverage probability when the duty cycle is optimised.

3.2 Exploiting RPSs in Two-tier HetNets without CRE

In the second section, we develop a tractable model for the analysis of RPSs adopted in both tiers of a two-tier HetNet without CRE (i.e., macrocells and femtocells) by assuming the locations of MBSs and femtocell BSs (FBSs) following two independent PPPs. Existing works only adopted RPSs in macrocells, which did not exploit their full potential to improve the macrocell edge-region UEs' Signal to Interference Ratio (SIR) level. Moreover, different from the work in Section 3.1, the user association strategy is divided into two steps: the serving tier is determined by the highest RSS and the subframe allocation is decided by the SIR level. A closed-form coverage probability is derived by the joint Laplace transformation of the aggregate interference power, which is validated by Monte Carlo simulations. Through numerical analysis, we find that our proposed scheme not only increases the coverage probabilities of macrocell edge-region UEs, but also improves the rate coverage of the whole two-tier HetNet.

Accordingly, three contributions of this work can be summarised: We are the first to analyse the performance of RPSs applying in both macrocells and femtocells under the stochastic geometry framework. Moreover, we jointly adopt the RSS and the SIR in the

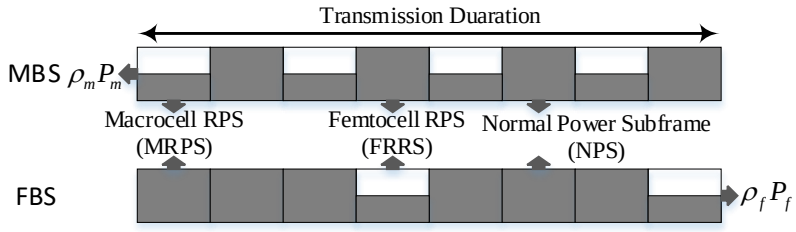

Fig. 3.14 The subframe types in a transmission duration ©2016 IEEE

user association strategy to derive the closed-form coverage probability. This result can be easily extended to a K-tier HetNet. Finally, our proposed scheme enhances the coverage probabilities of macrocell edge-region UEs and the rate coverage probability of the whole two-tier HetNet.

The rest of the this section is organised as follows: In Section 3.2.1, the system model and the derivation of the coverage and the rate coverage probabilities of a typical UE are introduced. Section 3.2.4 validates the derived coverage probability with the Monte Carlo simulation. Then the coverage probability of a typical macrocell edge-region UE and the rate coverage probability of the whole two-tier HetNet are analysed numerically.

3.2.1 System Model

In this work, a two-tier HetNet composed of traditional MBSs and the lower maximum-transmit-power FBSs that operate in open access mode is considered. MBSs form tier-m and FBSs form tier-f, the locations of which follow two independent PPPs [9, 22], with homogeneous densities of λ_m and λ_f, respectively. For an arbitrary UE x_k, its distances to MBSs and FBSs are denoted by R_{m,x_k} and R_{f,x_k}, where $R_{m,x_k} = \{r_{m,k}^{(0)}, r_{m,k}^{(1)}, \ldots, r_{m,k}^{(N_m)}\}$ and $R_{f,x_k} = \{r_{f,k}^{(0)}, r_{f,k}^{(1)}, \ldots, r_{f,k}^{(N_f)}\}$. The variables N_m and N_f denote the numbers of MBSs and FBSs, respectively. Without loss of generality, we assume that $r_{i,k}^{(0)}$ is the closest distance in R_{i,x_k}, $i \in \{m, f\}$. Therefore, $r_{i,k}^{(0)}$ is the serving-BS distance if x_k is served by the tier-i BS. A UE's received signal power can be denoted by $P_t h r^{-\alpha}$, where P_t is the transmit power of the BS, variable h is the small-scale fading on the received power following the exponential distribution ($h \sim \exp(1)$), and r is its Euclidean distance to the BS. The variable α is the pathloss exponent, and in this work we assume that the pathloss exponents in both tiers are the same as α.

By applying RPSs in both tiers, the subframes are classified into three groups as shown in Fig. 3.14: Macrocell RPSs (MRPSs), femtocell RPSs (FRPSs) and normal power subframes (NPSs). MRPSs in tier-m are the reduced-transmit-power subframes ($\rho_m P_m$) while in tier-

f they are the subframes with full transmit power at the same time slots as the MRPSs transmitted in tier-m. These subframes are allocated to the tier-m UEs near to their serving BSs while to the tier-f edge-region UEs. The FRPSs follow the reverse pattern of the MRPSs, as FRPSs in the tier-f are transmitted with a reduced transmit power $\rho_f P_f$. The parameters P_m and P_f represent the maximum transmit power on each subframe of MBSs and FBSs, respectively. The NPSs are FPSs, which are allocated to mid-distance-range UEs. Moreover, MRPSs and FRPSs occur at different time slots to avoid interference with each other. The fraction of MRPSs in the whole subframe duration is denoted by β_m and that of FRPSs is β_f. Thereby, the fraction of NPSs is $1-\beta_m-\beta_f$. Furthermore, strict time synchronisation is assumed throughout this two-tier HetNet. Under this assumption, the UEs served by subframes of each group only suffer interference from the same-group subframes transmitted from other BSs.

Because of the derivation similarity of coverage probability of a typical UE in tier-m and tier-f, we only provide the details of the coverage-probability derivation for a typical tier-m UE in the rest of this section. Moreover, the effect caused by the thermal noise is negligible in an interference limited network [101], thus we focus on the SIR Γ^m of a typical tier-m UE using the three group subframes, which are given as follows:

$$\begin{aligned}
\Gamma^m_{\text{MRPS}} &= \frac{\rho_m P_m h^{(0)}_{m,k} r^{(0)-\alpha}_{m,k}}{\sum\limits_{i\in N_m/\{0\}} \rho_m P_m h^{(i)}_{m,k} r^{(i)-\alpha}_{m,k} + \sum\limits_{i\in N_f} P_f h^{(i)}_{f,k} r^{(i)-\alpha}_{f,k}}, \\
\Gamma^m_{\text{FRPS}} &= \frac{P_m h^{(0)}_{m,k} r^{(0)-\alpha}_{m,k}}{\sum\limits_{i\in N_m/\{0\}} P_m h^{(i)}_{m,k} r^{(i)-\alpha}_{m,k} + \sum\limits_{i\in N_f} \rho_f P_f h^{(i)}_{f,k} r^{(i)-\alpha}_{f,k}}, \\
\Gamma^m_{\text{NPS}} &= \frac{P_m h^{(0)}_{m,k} r^{(0)-\alpha}_{m,k}}{\sum\limits_{i\in N_m/\{0\}} P_m h^{(i)}_{m,k} r^{(i)-\alpha}_{m,k} + \sum\limits_{i\in N_f} P_f h^{(i)}_{f,k} r^{(i)-\alpha}_{f,k}},
\end{aligned} \tag{3.38}$$

where $h^{(n)}_{m,k}$ is the small scale fading on the received power between the n-th MBS and the UE x_k. The SIR expression for tier-f UEs can be formulated analogously.

3.2.2 User Association

The UE positions are modelled following aother independent PPP with density λ_u. According to the Slivayak's theorem, the UE positions have no effect on the property observed from PPP-based deployed networks [101]. Thereby, we place the UE at the origin [9] throughout our analysis. Then the UE is categorised by the following two steps based on the average

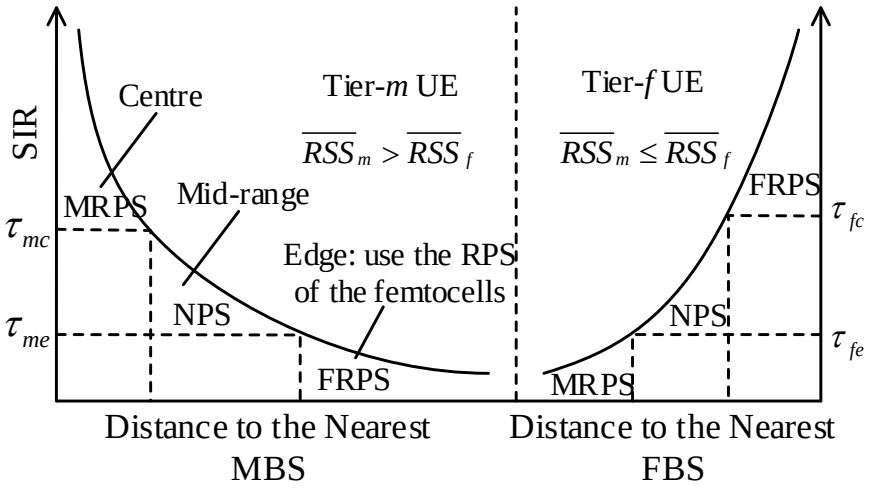

Fig. 3.15 User association strategy with allocation of the subframes ©2016 IEEE

RSS and the SIR, as shown in Fig. 3.15. For notational simplicity, we substitute the variable $r_{i,k}^{(n)}$ with $r_{i,n}$.

Step I: The UE served by the MBS or the FBS is determined by the maximum average RSS transmitted with NPSs [29] as follows:

$$\begin{cases} P_m r_{m,0}^{-\alpha} > P_f r_{f,0}^{-\alpha} & \text{as} \quad \text{Tier-}m \text{ UE} \\ P_m r_{m,0}^{-\alpha} \leqslant P_f r_{f,0}^{-\alpha} & \text{as} \quad \text{Tier-}f \text{ UE} \end{cases} \tag{3.39}$$

The variable $r_{i,0}$ denotes the nearest distance from the typical UE to the tier-i BSs.

Step II: The UE served by which group of subframes is determined by the SIR value with both tiers using NPSs. For example, in a macrocell, when the SIR of the typical UE using the NPS is higher than a threshold τ_{mc}, it will be allocated with MRPSs as a macrocell centre-region UE. And if it is lower than another threshold τ_{me}, the UE will be allocated with FRPSs as a macrocell edge-region UE. Otherwise, the UE remains to be served by the NPS as a macrocell mid-range-region UE. The subframe-allocation strategy used in a femtocell reverses in the allocation of MRPSs and FRPSs, which is shown in Fig.3.15. This strategy in the macrocell is given as follows:

$$\begin{cases} \Gamma_{\text{NPS}} > \tau_{mc} \quad as \quad \text{Macrocell Centre-region UE} \quad using \quad \text{MRPSs}, \\ \Gamma_{\text{NPS}} < \tau_{me} \quad as \quad \text{Macrocell Edge-region UE} \quad using \quad \text{FRPSs}, \\ \text{Otherwise} \quad as \quad \text{Macrocell Mid-range-region UE} \quad using \quad \text{NPSs}. \end{cases} \tag{3.40}$$

In the rest of this subsection, we discuss the user association probability with the results from existing works [29, 31]. According to [31], the probabilities of a typical UE being in

tier-m and tier-f, denoted by $\mathcal{P}^m$ and $\mathcal{P}^f$, respectively, are given by:

$$\mathcal{P}^m = \frac{1}{1+\widehat{A}_m}, \quad \mathcal{P}^f = \frac{1}{1+\widehat{A}_f}. \tag{3.41}$$

For notational simplicity, we define $\widehat{P}_i = \frac{P_{i^\neg}}{P_i}$, $\widehat{\lambda}_i = \frac{\lambda_{i^\neg}}{\lambda_i}$ and $\widehat{A}_i = \widehat{\lambda}_i \widehat{P}_i^{\frac{2}{\alpha}}$, where i denotes for the tier-i and $i \cup i^\neg = \{m, f\}$ (e.g., $\widehat{P}_m = \frac{P_f}{P_m}$). The probabilities of the tier-m UE using MRPSs and FRPSs, respectively denoted by $\mathcal{P}^m_{\text{MRPS}}$ and $\mathcal{P}^m_{\text{FRPS}}$, can be formulated as the following results [29]:

$$\begin{cases} \mathcal{P}^m_{\text{MRPS}} = \dfrac{1}{D(\tau_{mc}, 1, \widehat{A}_m) + 1 + \widehat{A}_m} \\ \mathcal{P}^m_{\text{FRPS}} = \dfrac{D(\tau_{me}, 1, \widehat{A}_m)}{(D(\tau_{me}, 1, \widehat{A}_m,) + 1 + \widehat{A}_m)(1 + \widehat{A}_m)} \end{cases} \tag{3.42}$$

where the function $D(\tau, \rho, A)$ is given as:

$$D(\tau, \rho, A) = \tau^{\frac{2}{\alpha}} C(\tau^{-1}, \alpha) + A(\tau\rho^{-1})^{\frac{2}{\alpha}} C(\rho\tau^{-1}, \alpha), \tag{3.43}$$

with the function $C(a, b)$ given as:

$$C(a, b) = \int_0^\infty \frac{1}{1 + t^{\frac{b}{2}}} dt - a^{\frac{2}{b}} {}_2F_1(1, \frac{2}{b}; 1 + \frac{2}{b}; -a). \tag{3.44}$$

${}_2F_1(\cdot)$ is the *Gauss hypergeometry function*. The probability of the tier-m UE using NPSs can be obtained by $\mathcal{P}^m - \mathcal{P}^m_{\text{MRPS}} - \mathcal{P}^m_{\text{FRPS}}$. Equipped with the probabilities of the tier-m UEs using each type of subframes, the coverage probabilities of these tier-m UEs are derived in the next subsection.

3.2.3 Main Results

Coverage Probability

The coverage probability is defined as the probability of the typical UE having a larger SIR than a threshold τ, i.e., $\mathbb{P}(\Gamma > \tau)$. Next, we will give the closed-form results of the coverage probabilities of the tier-m UE using the three types of subframes. The probabilities for the tier-f UE can be evaluated similarly. By defining the function $J(\tau, A)$ as $\frac{D(\tau,1,A)}{D(\tau,1,A)+1+A}$, we give the coverage probability of the tier-m UE using NPSs in Theorem 3.3.

Theorem 3.3. *In the two-tier HetNet without CRE, the coverage probability Γ^m of a typical tier-m UE using NPSs is given by:*

$$\mathbb{P}(\Gamma^m > \tau|\text{NPS}) = \frac{\text{J}(\tau_{\text{mc}}, \widehat{\text{A}}_{\text{m}}) - \text{J}(\max(\tau_{\text{me}}, \min(\tau, \tau_{\text{mc}})), \widehat{\text{A}}_{\text{m}})}{\text{J}(\tau_{\text{mc}}, \widehat{\text{A}}_{\text{m}}) - \text{J}(\tau_{\text{me}}, \widehat{\text{A}}_{\text{m}})}. \tag{3.45}$$

Proof. The coverage probability is a conditional probability, which can be translated into the expression in (3.46) as follows:

$$\mathbb{P}(\Gamma^m > \tau|\text{NPS}) \triangleq \mathbb{P}(\Gamma^m_{\text{NPS}} > \tau|\Gamma^m_{\text{NPS}} < \tau_{mc}, \Gamma^m_{\text{NPS}} > \tau_{me}). \tag{3.46}$$

By using the Baye's rule, we have

$$\mathbb{P}(\Gamma^m > \tau|\text{NPS}) = \frac{(\Gamma^m_{\text{NPS}} < \tau_{mc}) - (\Gamma^m_{\text{NPS}} < \min(\tau_{me}, \max(\tau_{mc}, \tau)))}{(\Gamma^m_{\text{NPS}} < \tau_{mc}) - (\Gamma^m_{\text{NPS}} < \tau_{me})}, \tag{3.47}$$

which can be translated into (3.45) by combining with (3.42). □

As the results of the tier-*m* using the other two types of subframes resemble but differ significantly from that tier UE using NPSs, their coverage probabilities are given together in Theorem 3.4.

Theorem 3.4. *In the two-tier HetNet witout CRE, the coverage probabilities of the tier-m UE using MRPSs and FRPSs are given in* (3.48) *and* (3.49)*, respectively.*

$$\mathbb{P}(\Gamma^m > \tau|MRPS) = \frac{D(\tau_{mc}, 1, \widehat{A}_m) + 1 + \widehat{A}_m}{\widehat{A}_m G(\tau_{mc}, \rho_m^{-1}\tau) + G(\tau_{mc}, \tau) - H(\tau_{mc}, \tau) - \widehat{A}_m H(\tau_{mc}, \rho_m^{-1}\tau) + 1 + \widehat{A}_m} \tag{3.48}$$

$$\mathbb{P}(\Gamma^m > \tau|FRPS) = \frac{D(\tau_{me}, \rho_m, \widehat{A}_m) + 1 + \widehat{A}_m}{D(\tau_{me}, \rho_m, \widehat{A}_m)} \times \left[\frac{1 + \widehat{A}_m}{D(\tau, \rho_f^{-1}, \widehat{A}_m) + 1 + \widehat{A}_m} - \frac{1 + \widehat{A}_m}{\widehat{A}_m G(\tau_{me}, \rho_f \tau) + G(\tau_{me}, \tau) - H(\tau_{me}, \tau) - \widehat{A}_m H(\tau_{me}, \rho_f \tau) + 1 + \widehat{A}_m} \right] \tag{3.49}$$

Proof. We only give the derivation of the coverage probability of the tier-*m* UE using FRPSs, as that of this typical UE using MRPSs can be derived similarly. Then the coverage probability of the tier-*m* UE using FRPSs is defined as the following expression:

$$\mathbb{P}(\Gamma^m > \tau|\text{FRPS}) \triangleq \frac{\mathbb{P}(\Gamma^m_{\text{FRPS}} > \tau, \Gamma^m_{\text{NPS}} < \tau_{me})}{\mathbb{P}(\Gamma^m_{\text{NPS}} < \tau_{me})}. \tag{3.50}$$

Equipped with (3.42), the denominator can be obtained as:

$$\mathbb{P}(\Gamma^m_{\text{FPS}} < \tau_{me}) = \frac{D(\tau_{me}, 1, \widehat{A}_m)}{D(\tau_{me}, 1, \widehat{A}_m) + 1 + \widehat{A}_m}. \tag{3.51}$$

Then we focus on the result of the numerator. It can be translated into the following expression as:

$$\begin{aligned} &\mathbb{P}\left(\frac{P_m h_m'^{(0)} r_{m,0}^{-\alpha}}{I'_m + \rho_f I'_f} > \tau, \frac{P_m h_m^{(0)} r_{m,0}^{-\alpha}}{I_m + I_f} < \tau_{me}\right) \\ =&\mathbb{P}\left(h_m'^{(0)} > \frac{\tau r_{m,0}^{\alpha}}{P_m}(I'_m + \rho_f I'_f), h_m^{(0)} < \frac{\tau_{me} r_{m,0}^{\alpha}}{P_m}(I_m + I_f)\right). \end{aligned} \tag{3.52}$$

The interference caused by the i-th tier is represented as $I_i = \sum_k P_i h_i^{(k)} r_i^{(k)}$, where $h_m'^{(k)}$ and $h_f'^{(k)}$ represent the small scale fading effect on the received power of FRPSs, which are independent to the $h_m^{(k)}$ and $h_f^{(k)}$. And because of this independence, the above expression can be evaluated as follows:

$$\begin{aligned} &\mathbb{P}(\Gamma^m_{\text{FRPS}} > \tau, \Gamma^m_{\text{NPS}} < \tau_{me}) \\ =&\int_{R_d} \left(\mathbb{E}_{I'}\left[e^{-\frac{\mu\tau r^{\alpha}}{P_m}(I'_m + \rho_f I'_f)}\right] - \mathbb{E}_{I,I'}\left[e^{-\frac{\mu\tau r^{\alpha}}{P_m}(I'_m + \rho_f I'_f)} e^{-\frac{\mu\tau_{me} r^{\alpha}}{P_m}(I_m + I_f)}\right]\right) f_{r_{m,0}}(r) dr. \end{aligned} \tag{3.53}$$

The result of the first term in (3.53) can be calculated as:

$$\mathbb{E}_{I'}\left[e^{-\frac{\mu\tau r^{\alpha}}{P_m}(I'_m + \rho_f I'_f)}\right] = \frac{1 + \widehat{A}_m}{D(\tau, \rho_f^{-1}, \widehat{A}_m) + 1 + \widehat{A}_m}. \tag{3.54}$$

Therefore, if we achieve the result of the second term in (3.53), we can have the final coverage probability of the tier-m UE using FRPSs. The second term can be interpreted as a general expression as $\mathbb{E}_{I,I'}\left[e^{-s_p I_p - s_m I_m} e^{-s'_p I'_p - s'_m I'_m}\right]$, which is the joint Laplace transform of the terms I_m, I'_m, I_p and I'_p. Because of the positions of MBSs and FBSs are independent, the second term can be translated as follows:

$$\mathbb{E}_{I,I'}\left[e^{-s_p I_p - s_m I_m} e^{-s'_p I'_p - s'_m I'_m}\right] = \mathbb{E}_{I_m, I'_m}\left[e^{-s_m I_m - s'_m I'_m}\right] \mathbb{E}_{I_p, I'_p}\left[e^{-s_p I_p - s'_p I'_p}\right]. \tag{3.55}$$

Therefore, if we have the result of the first term in (3.55), the second term can be easily obtained by some extra work. We can have the following result of the first term as:

$$\mathbb{E}_{I_m,I'_m}\left[e^{-s_m I_m - s'_m I'_m}\right] \overset{(a)}{=} \exp\left(-2\pi\lambda_m \int_r^\infty \left[1 - \frac{1}{1+\frac{P_m s_m}{\mu}u^{-\alpha}}\frac{1}{1+\frac{P_m s'_m}{\mu}u^{-\alpha}}\right] udu\right), \tag{3.56}$$

where step (a) follows from the probability generating function [101]. On the other hand, the general integral expression in (3.56) $\int_r^\infty \left[1 - \frac{1}{1+au^{-\alpha}}\frac{1}{1+bu^{-\alpha}}\right] udu$ can be evaluated as the following result:

$$\int_r^\infty \left[1 - \frac{1}{1+au^{-\alpha}}\frac{1}{1+bu^{-\alpha}}\right] udu = G(a,b) - \frac{r^2}{2}H(ar^{-\alpha}, br^{-\alpha}), \tag{3.57}$$

where the function $G(a,b)$ and $H(a,b)$ are given as follows:

$$G(a,b) = \frac{a^{\frac{2}{\alpha}} - b^{\frac{2}{\alpha}}}{(a-b)\mathrm{sinc}(2\pi/\alpha)}, \tag{3.58}$$

$$H(a,b) = \frac{a\,{}_2F_1(1,\frac{2}{\alpha};\frac{2+\alpha}{\alpha};-a^{-1}) - b\,{}_2F_1(1,\frac{2}{\alpha};\frac{2+\alpha}{\alpha};-b^{-1})}{a-b}. \tag{3.59}$$

Equipped with these results, we have the following result of the second term in (3.53):

$$\begin{aligned}&\mathbb{E}_{I,I'}\left[e^{-\frac{\mu\tau r^\alpha}{P_m}(I'_m+\rho_f I'_f)}e^{-\frac{\mu\tau_{me}r^\alpha}{P_m}(I_m+I_f)}\right]\\ =&\frac{1+\widehat{A}_m}{\widehat{A}_m G(\tau_{me},\rho_f\tau)+G(\tau_{me},\tau)-H(\tau_{me},\tau)-\widehat{A}_m H(\tau_{me},\tau\rho_f)+1+\widehat{A}_m}\end{aligned} \tag{3.60}$$

Then incorporating this result into (3.53) and (3.50), the final result can be achieved. □

Rate Coverage

The rate coverage probability $\widetilde{R}_{z,l}$ is defined as the fraction of tier-l UEs using subframe type z in the two-tier HetNet achieving a target rate ξ, where $l \in \{m,f\}$ and $z \in \{\mathrm{MRPS},\mathrm{FRPS},\mathrm{NPS}\}$. Equipped with coverage probabilities of tier-m and tier-f UEs using the three types of subframes, the rate coverage probability can be evaluated by [31]:

$$\widetilde{R}_{z,l} = \mathbb{P}(\Gamma^m > 2^{\frac{\widetilde{N}_{z,l}\xi}{W\widetilde{\beta}_{z,l}}} - 1), \tag{3.61}$$

where $\widetilde{N}_{z,l}$ is the expected number of tier-l UEs using subframe type z, which is given as:

$$\widetilde{N}_{z,l} = \mathcal{P}_z^l \frac{\lambda_u}{\lambda_l}. \tag{3.62}$$

The variable $\beta_{z,l}$ is the ratio between the group-z subframe used by tier-l UEs and the whole transmission duration. If we denote the variable $X = \{\text{MRPS}, \text{FRPS}, \text{NPS}\}$, then the rate coverage probability of the whole two-tier HetNet is given in Corollary 3.1.

Corollary 3.1. *The rate coverage probability $\widetilde{R}_{cov}$ of a typical UE in the two-tire HetNet without CRE can be obtained as:*

$$\widetilde{R}_{cov} = \sum_{l \in \{m,f\}, z \in X} \mathcal{P}_z^l \widetilde{R}_{z,l} \tag{3.63}$$

3.2.4 Simulation Results

Validation

Firstly, we validate the derived coverage probabilities of tier-m and tier-f UEs using the three types of subframes with Monte Carlo simulation. The Monte-Carlo-simulation results are obtained by running $10,000$ realizations of BS locations in Matlab. The simulation parameters are given in Table 3.3. In each simulation, the BSs of both tiers are deployed following two independent PPPs in a square range of 400 km^2 and the typical UE is located at the origin. Moreover, the serving BS of the typical UE is determined following the two-step user association strategy (i.e., (3.39) and (3.40)) and the SIR of this UE is calculated by (3.38). From our previous study in Chapter 3, we found that in our system model there no more than 30% of the UE having a larger SINR threshold than 3 dB, thus we set 3 dB as the centre region threshold. Additionally, in reality, it is considered an edge region if the SINR is lower than 0 dB, and in our system model, there will be approximately 30% of UEs having a SINR threshold smaller than -3 dB. As a result, we choose the SIR threshold of the edge region as -3 dB. Actually, the selection of the threshold will be another interesting research topic, which can be considered as one of our future work.

Fig. 3.16 depicts the comparison of the derived results and the Monte-Carlo-simulation results of the coverage probabilities for a typical tier-m and tier-f UE. The results show that the proposed results match the Monte-Carlo-simulation results, validating the correctness of our proposed tractable model. On the other hand, the tier-m UE using FRPSs performs worst in the coverage probability, even if the transmit power of FRPSs reduces to 50%. As a result, the SIR performance of such a UE requires improvement.

Table 3.3 NOTATIONS AND SIMULATION VALUES

Parameter	Description	Value
α	Pathloss exponent	3
P_m, P_f,	Transmit powers	46 dBm, 30 dBm
ρ_m, ρ_f	Reduced power factors	-10 dB, -3 dB
$\tau_{mc} = \tau_{fc}$, $\tau_{me} = \tau_{fe}$	Region thresholds	3 dB, -3 dB

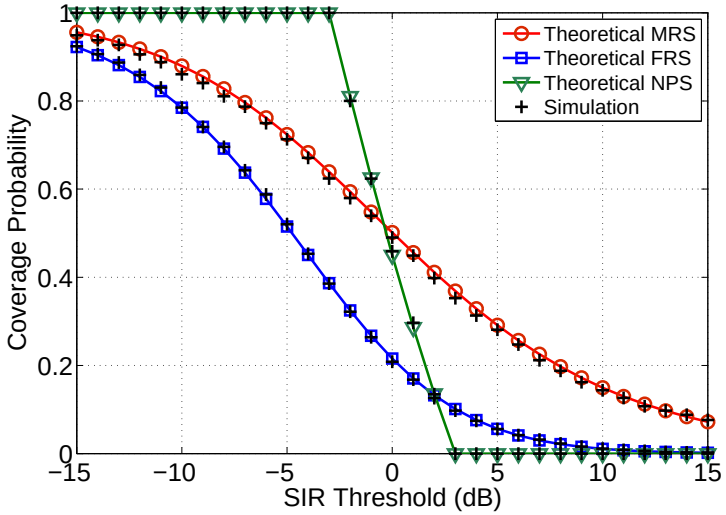

(a) macrocell

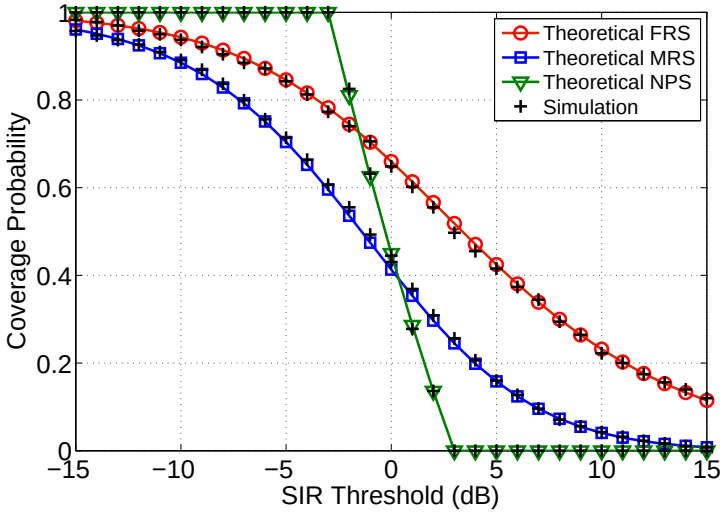

(b) femtocell

Fig. 3.16 Validation of the coverage probabilities of tier-m and tier-f UEs ©2016 IEEE

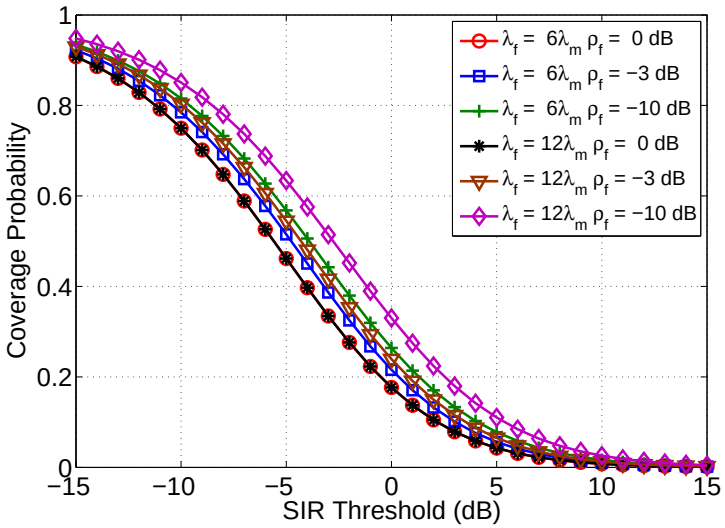

Fig. 3.17 The coverage probability of the macrocell edge-region UE with several FBS densities and power reduction factors ©2016 IEEE

Analysis

Secondly, we analyse the effect of FRPS transmit power on the coverage probability of the macrocell edge-region UEs. In Fig. 3.17, we compare the coverage probability of the macrocell edge-region UE with several typical FBS densities (i.e., $6\lambda_m$ and $12\lambda_m$) and power reduction factors (i.e., 0 dB, -3 dB and -10 dB). The results show that the macrocell edge-region UE's SIR significantly improves especially with lower FRPS transmit power in a more densely-deployed scenario. Interestingly, the performance remains in a denser scenario when the power reduction facotr is 0 dB in the femtocell, which can be proved by substituting the ρ_f with 1 in (3.49). Therefore, applying RPSs in femtocells is a promising technique to improve the macrocell edge-region UE's coverage performance.

Next we discuss the rate coverage probability of a typical UE in the two-tier HetNet. Equiped with the numerical results in (3.63), we obtained the optimal results with parameter ρ_m, β_m and β_f by a three-dimensional linear search method. Then we compare this optimal result with the conventional FeICIC scheme [99], with a variety of the power reduction factors ρ_f in femtocells as shown in Fig. 3.18. The frequency bandwidth of the system is 10 MHz, the expected UE number is 100, and the rate threshold is 100 kbps per UE. The results illustrate that our proposed scheme outperforms the traditional FeICIC scheme in terms of the rate coverage probability. This improvement has two reasons. One is the adoption of RPSs, providing a $3\% \sim 4\%$ gain of the rate coverage probabilities of all UEs. The other reason is the increasing number of resources allocated to the macro edge-region UEs, enhancing

their rate coverage probabilities by 6% $\sim$ 10%. We can infer from the result that the more dense deployment of the network, the larger rate coverage enhancement by adopting RPSs in femtocells.

3.2.5 Conclusion

In this section, we have proposed an analytical framework for applying RPSs both in the macrocells and the femtocells. The numerical results reveal that the macro edge-region UE's coverage-probability gains can be up to 20% by introducing RPSs in femtocells, and the rate coverage probability can obtain a maximum of 15% gain.

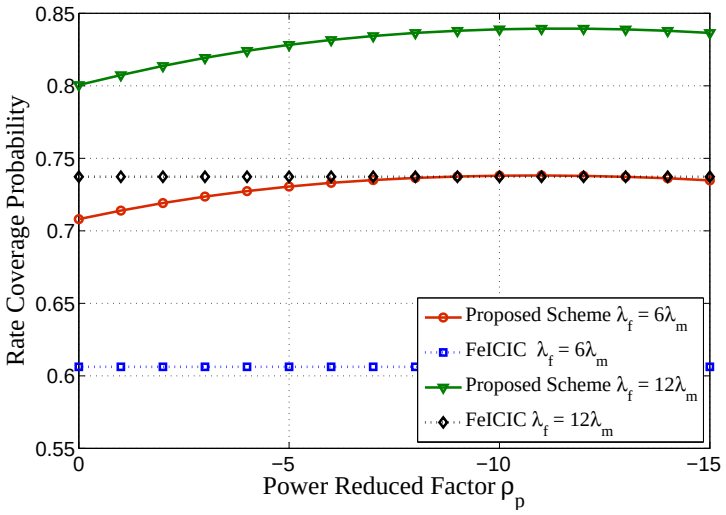

Fig. 3.18 The rate coverage probability of a typical UE with the target rate being 100 kbps under our proposed scheme and the FeICIC ©2016 IEEE

Chapter 4

Subframe Misalignment Analysis of RPSs in HetNets with CRE

4.1 Introduction

In Chapter 3, strict SA was assumed in both works. However, this assumption of strict SA cannot always be satisfied, as the SA between macrocells and SCs is achieved through control signal exchanges via the backhaul [12], which may be congested in a high SC density scenario. In addition, the random propagation delays of subframes transmitted from neighbouring cells can lead to misaligned interfering subframes, namely SM. Because of SM, macrocell centre and SC CRE UEs may suffer increased interference from FPSs, which degrades their coverage performance. As aforementioned in Chapter 2, existing work [79] studied the downlink coverage with asynchronous slots where the offsets of unsynchronised slots may take arbitrarily large values. It ignored the fact that the offsets of unsynchronised slots may not exceed a slot duration [77] by employing existing time synchronization techniques via the backhaul. The offsets of unsynchronised slots can be considered as the SM offsets, since a subframe consists of two slots in an orthogonal frequency-division multiple access (OFDMA) network. Accordingly, the SM offsets are also restricted in a specific range, and the maximum value of this range is defined as the maximum subframe misalignment offset (MSMO).

[1]In this chapter, we propose an SM model with the misalignment offsets restricted by the MSMO, which is a more practical misalignment model than that in [79]. Based on this proposed SM model, the downlink coverage probability for a typical UE is derived based on stochastic geometry and validated through Monte Carlo simulation. By analysing the

[1]The content of this chapter is based on a revised version of our publication [103]

coverage degradation caused by SM versus the subframe duration, we provide design insights into the SA requirement for using RPSs in HetNets.

4.2 System Model

We consider a two-tier HetNet, indexed by the set $\mathcal{K} = \{1,2\}$, where macrocell BSs form tier 1 and SC BSs form tier 2. BSs in different tiers may vary in terms of the transmit power P_i, the deployment density λ_i, the power reduction factor ρ_i, and the duty cycle β_i, $i \in \mathcal{K}$. The power reduction factor determines the transmitt power of RPSs, which can be denoted by $\rho_i P_i$. The duty cycle is defined as the proportion of RPSs in the total transmission duration, which can also be treated as the probability of a subframe transmitting as an RPS. The positions of the two tier BSs are modelled following two independent spatial PPPs, denoted by $\Phi = \{\Phi_1, \Phi_2\}$. The locations of UEs are modelled as another independent spatial PPP. According to Slivnyak's theorem [9], we assume a typical UE located at the origin without loss of generality. The location of the j-th BS in the i-th tier is denoted by $\mathbf{x}_{i,j}$, and its distance to the typical UE is given by $r_{i,j} = ||\mathbf{x}_{i,j}||$. The corresponding pathloss is given by $r_{i,j}^{-\alpha_i}$, where α_i is the i-th tier pathloss exponent. Moreover, independent Rayleigh fading is assumed for each link, thus the fading power gain $h_{i,j}$ on the link from the j-th BS in the i-th tier to the typical UE follows an exponential distribution $h_{i,j} \sim \exp(1)$. Next the user association strategy will be introduced for the two-tier HetNet.

4.2.1 User Association

As SCs adopt the CRE to attract more UEs to associate with them, we can assume that BSs in the i-th tier use the range expansion bias $B_i (i \in \mathcal{K})$ for CRE. It is worthy mentioning $B_1 = 1$ because there is no range shrinking or expansion for macrocells. The typical UE is associated with the nearest BS in the k-th tier, where $k = \arg\max_{i \in \mathcal{K}} B_i P_i r_{i,0}^{-\alpha_i}$, $r_{i,0}$ is the distance between the typical UE and the nearest BS in the i-th tier. To determine the subframe allocation, this k-th tier typical UE is classified as a centre region UE (CRU) or an Edge Region UE (ERU) based on the following strategy:

$$\begin{cases} \text{CRU, If } P_k r_{k,0}^{-\alpha_k} > M_k^i P_i r_{i,0}^{-\alpha_i}, i \in \mathcal{K}/\{k\}, \\ \text{ERU, Otherwise.} \end{cases} \tag{4.1}$$

M_k^i is defined as the centre region bias, which decides the centre region area of a k-th tier cell. The value of M_k^i should be larger than B_i/B_k, so that the centre region area of a k-th tier cell is smaller than the range-expanded coverage area of a k-th tier cell (influenced by

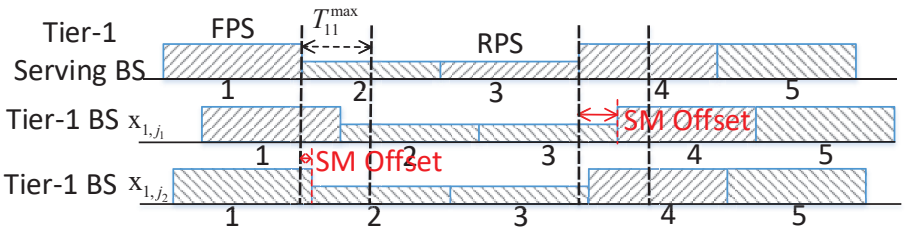

Fig. 4.1 SM between tier-1 serving BS and tier-1 interfering BSs ©2018 IEEE

B_i/B_k), and the resulting value of $A_k^{\mathrm{R}}/A_k^{\mathrm{F}}$ is comparable to that of $\beta_k/(1-\beta_k)$, where A_k^{R} and A_k^{F} respectively denote the probabilities of the typical UE being a CRU and an ERU [99]. For SCs, the centre region factor is set at $M_2^1 = 1$, so that the centre area is the same as the original coverage area without CRE. CRUs and ERUs in each tier are respectively allocated with RPSs and FPSs, and the tier-1 RPSs and FPSs share the same transmitting slots with the tier-2 FPSs and RPSs, respectively. This is because that ERUs should be protected by BSs in the other tier transmitting RPSs. For example, the tier-2 ERUs suffer the FPS interference from other tier-2 BSs, and suffer the RPS interference from the tier-1 BSs. Consequently, the duty cycles follow $\beta_2 = 1-\beta_1$.

4.2.2 Interference Caused By Subframe Misalignment

A full buffer traffic model is assumed for each BS, i.e., each BS always has data to transmit. Fig. 4.1 shows that due to SM, a serving subframe for a tier-1 typical UE suffers interference from two consecutive subframes transmitted by a tier-1 BS. It can be extended to a more general case that a serving subframe for the k-th tier typical UE suffers interference from two consecutive subframes transmitted by an i-th tier BS. We assume that the MSMO $T_{ki}^{\max}$ between an i-th tier interfering BS and a k-th tier UE does not exceed the subframe duration T_p, i.e., $T_{ki}^{\max} \leq T_p$ [77]. The SM offset between an i-th tier BS and the k-th tier typical UE is modelled as a uniformly distributed random variable in the range of $[0, T_{ki}^{\max}]$ [75, 79, 80, 104]. The assumption of a uniform distribution for the subframe misalignment offsets is mainly for analytical tractability. Other distributions, e.g. Gaussian distribution, can be analysed similarly following the steps in this thesis. We define $N_{ki} = T_p/T_{ki}^{\max}$ as the maximum SM factor. BSs in the same tier share the same value of N_{ki}. The SIR of the serving subframe for the k-th tier typical UE is given by:

$$\Gamma_k^t = \frac{P_k^t h_{k,0} {r_{k,0}^t}^{-\alpha_k}}{\sum_{i\in\mathcal{K}}\sum_{\mathbf{x}_{i,j}\in\Phi_i/\{\mathbf{x}_{k,0}\}} P_i \Delta_{i,j}^{k,t} h_{i,j} r_{i,j}^{-\alpha_i}}, \tag{4.2}$$

where $t \in \{\mathrm{R},\mathrm{F}\}$. If $t = \mathrm{R}$, then the typical UE is a CRU served by RPSs; otherwise it is an ERU served by FPSs. $P_k^{\mathrm{R}} = \rho_k P_k$, $P_k^{\mathrm{F}} = P_k$, and $\Delta_{i,j}^{k,t}$ is the random bias caused by SM on the received interference power from the j-th BS in tier i to the k-th tier CRU or ERU. Accordingly, the SIR of a CRU and an ERU in the k-th tier can be represented as follows:

$$\Gamma_k^{\mathrm{R}} = \frac{\rho_k P_k h_{k,0} {r_{k,0}^t}^{-\alpha_k}}{\sum_{i\in\mathcal{K}} \sum_{\mathbf{x}_{i,j}\in\Phi_i/\{\mathbf{x}_{k,0}\}} P_i \Delta_{i,j}^{k,\mathrm{R}} h_{i,j} r_{i,j}^{-\alpha_i}} \tag{4.3}$$

$$\Gamma_k^{\mathrm{F}} = \frac{P_k h_{k,0} {r_{k,0}^t}^{-\alpha_k}}{\sum_{i\in\mathcal{K}} \sum_{\mathbf{x}_{i,j}\in\Phi_i/\{\mathbf{x}_{k,0}\}} P_i \Delta_{i,j}^{k,\mathrm{F}} h_{i,j} r_{i,j}^{-\alpha_i}} \tag{4.4}$$

Because the SM offsets of BSs in the same tier are independent and identically distributed, the random biases $\Delta_{i,1}^{k,t}, \Delta_{i,2}^{k,t} \cdots$ on the received interference power from the same-tier BSs follow the same distribution. It indicates that the BS index (i.e., the subscript j) in $\Delta_{i,j}^{k,t}$ can be omitted in the final results by the moment generating function on the aggregate interference power [20], thus we denote $\Delta_{i,j}^{k,t}$ by $\Delta_i^{k,t}$.

For the two consecutive interfering subframes transmitted by an i-th tier BS, there are four different possible combinations: FPS and FPS, FPS and RPS, RPS and FPS, and RPS and RPS. Note that the type of one of the two consecutive interfering subframes can be determined because the SM offsets do not exceed the subframe duration. For example, if the typical UE is a tier-1 CRU, then one of the two consecutive subframes must be an RPS from an interfering tier-1 BS, and must be an FPS from an interfering tier-2 BS. Herein we categorise the random bias $\Delta_i^{k,t}$ as the RPS random bias $\Delta_k^{\mathrm{R}}(i)$ or the FPS random bias $\Delta_k^{\mathrm{F}}(i)$ if the determined subframe in the two consecutive subframes is found to be an RPS or an FPS, respectively. According to the subframe allocation described in the user association strategy, we can determine the transformation between $\Delta_i^{k,t}$ and $\Delta_k^{t'}(i)$, $t' \in \{\mathrm{R},\mathrm{F}\}$, as follows:

$$\Delta_i^{k,\mathrm{R}} = \begin{cases} \Delta_k^{\mathrm{R}}(i), i = k \\ \Delta_k^{\mathrm{F}}(i), i \neq k \end{cases}, \quad \Delta_i^{k,\mathrm{F}} = \begin{cases} \Delta_k^{\mathrm{F}}(i), i = k \\ \Delta_k^{\mathrm{R}}(i), i \neq k \end{cases}. \tag{4.5}$$

The randomness in $\Delta_k^{\mathrm{R}}(i)$ and $\Delta_k^{\mathrm{F}}(i)$ is caused by the undetermined subframe in the two consecutive interfering subframes. For the FPS random bias, according to reference [74], the random bias on the average interference power $\Delta_k^{\mathrm{F}}(i)$ can be calculated as:

$$\Delta_k^{\mathrm{F}}(i) = \frac{1}{T_p} \int_{T_0}^{T_0+T_p} \sigma_i(t) dt, \tag{4.6}$$

where T_0 is the starting time of the observing subframe, and $\sigma_i(t)$ is the random bias function, which equals 1 if the interfering subframe is an FPS, and equals ρ_i otherwise. The serving subframe suffers the interference from two consecutive subframes, and one of these two consecutive subframes can be confirmed as the FPS. If the other undermined interfering subframe is an FPS, then $\Delta_k^{\mathrm{F}}(i) = 1$; otherwise, $\Delta_k^{\mathrm{F}}(i) = 1-(1-\rho_i)\mathcal{T}/T_p$, where $\mathcal{T}$ is the length of subframe misalignment offset, following a uniform distribution in $[0, T_p/N_{ki}]$. Thus we have $\Delta_k^{\mathrm{F}}(i)$ following a uniform distribution in the range of $[1-\frac{1-\rho_i}{N_{ki}}, 1]$ if the other interfering subframe is an RPS. For the RPS random bias, if the undetermined subframe is an FPS, then $\Delta_k^{\mathrm{R}}(i)$ follows a uniform distribution in the range of $[\rho_i, \rho_i+\frac{1-\rho_i}{N_{ki}}]$, which can be obtained in a similar way as the FPS random bias. Because the PDF of a discrete value y can be denoted by the Dirac delta function as $\delta(\xi-y)$, and the PDF of a uniform distribution ξ within the range of $[l_1, l_2]$ can be denoted by $\frac{1}{l_1-l_2}\mathbf{1}_{\xi\in(l_1,l_2)}$, the PDFs of $\Delta_k^{\mathrm{F}}(i)$ and $\Delta_k^{\mathrm{R}}(i)$ are given as:

$$f_{\Delta_k^{\mathrm{F}}(i)}(\xi) = (1-\beta_i)\delta(\xi-1) + \frac{\beta_i N_{ki}}{1-\rho_i}\mathbf{1}_{\xi\in[1-\frac{1-\rho_i}{N_{ki}},1]}, \tag{4.7}$$

$$f_{\Delta_k^{\mathrm{R}}(i)}(\xi) = \beta_i\delta(\xi-\rho_i) + \frac{(1-\beta_i)N_{ki}}{1-\rho_i}\mathbf{1}_{\xi\in[\rho_i,\rho_i+\frac{1-\rho_i}{N_{ki}}]}, \tag{4.8}$$

where $\mathbf{1}_z$ is the indicator function, which equals 1 if the subscript z is true, and otherwise equals 0.

4.3 Coverage Analysis

In this section, we derive the downlink coverage probability of the two-tier HetNet employing RPSs under SM. The coverage probability is defined as the probability that the SIR of the typical UE is greater than a threshold τ, which can be denoted by:

$$p_{\mathrm{cov}}(\lambda_1, \lambda_2, \mathbf{N}, \tau) = \sum_{k\in\mathcal{K}}\sum_{t\in\{\mathrm{R},\mathrm{F}\}} A_k^t \mathbb{P}(\Gamma_k^t > \tau), \tag{4.9}$$

where $\mathbf{N} = \{N_{11}, N_{12}, N_{21}, N_{22}\}$. In order to obtain the result, The PDFs of the distance to the serving BS, conditioned on the typical tier-k UE being a CRU or an ERU, i.e., $f_{r_{k,0}^{\mathrm{R}}}(r)$ and $f_{r_{k,0}^{\mathrm{F}}}(r)$, should be derived first, which is given in Lemma 4.1 as below.

Lemma 4.1. *The conditional serving-BS-distance PDFs of a tier-k CRU and ERU are respectively given as:*

$$\begin{cases} f_{r^R_{k,0}}(r) = \mathcal{D}(k, M^1_k, M^2_k, r)/A^{\mathrm{R}}_k, \\ f_{r^F_{k,0}}(r) = (\mathcal{D}(k, \widehat{B}^k_1, \widehat{B}^k_2, r) - \mathcal{D}(k, M^1_k, M^2_k, r))/A^{\mathrm{F}}_k, \end{cases} \tag{4.10}$$

where $\widehat{B}^k_i = B_i/B_k$, $i \in \mathcal{K}$, $\widehat{P}^k_i = P_i/P_k$, $\widehat{\alpha}^k_i = \alpha_i/\alpha_k$. By denoting y_1 and y_2 as two variables, we define function $\mathcal{D}(k, y_1, y_2, r)$ as

$$\mathcal{D}(k, y_1, y_2, r) = 2\pi\lambda_k r \exp(-\pi \sum_{i\in\mathcal{K}} \lambda_i (y_i \widehat{P}^k_i)^{2/\alpha_i} r^{2/\widehat{\alpha}^k_i}). \tag{4.11}$$

The probabilities A^R_k and A^F_k can be obtained in a way similar to Lemma 1 in [31] as $A^R_k = \int_0^\infty \mathcal{D}(k, M^1_k, M^2_k, r)dr$ and $A^F_k = \int_0^\infty \mathcal{D}(k, \widehat{B}^k_1, \widehat{B}^k_2, r)dr - A^R_k$, respectively.

Proof. The probability of the typical UE associating with the k-th tier BS can be calculated as:

$$\begin{aligned} &\mathbb{P}\left(\text{The typical UE belongs to the } k\text{-th tier}\right) \\ &= \mathbb{P}\left(B_k P_k r_{k,0}^{-\alpha_k} > B_i P_i r_{i,0}^{-\alpha_i}\right) \quad (i \neq k) \\ &= \mathbb{P}\left(r_{i,0} > (\widehat{B}^k_i \widehat{P}^k_i)^{1/\alpha_i} r_{k,0}^{1/\alpha^k_i}\right) \\ &= \mathbb{E}_{r_{k,0}}\left[\exp(-\lambda_i \pi (\widehat{B}^k_i \widehat{P}^k_i)^{2/\alpha_i} r_{k,0}^{2/\alpha^k_i})\right] \\ &= \int_0^\infty \mathcal{D}(k, \widehat{B}^k_1, \widehat{B}^k_2, r)dr. \end{aligned} \tag{4.12}$$

Based on this derivation, the probability of the k-th tier UE being a CRU can be obtained as $A^{\mathrm{R}}_k = \int_0^\infty \mathcal{D}(k, M^1_k, M^2_k, r)dr$. In order to calculate the serving-BS-distance PDF conditioning on the k-th typical UE being a CRU, the following probability is derived as:

$$\begin{aligned} &\mathbb{P}\left(r_{k,0} > \mu | \text{the } k\text{-th typical UE being a CRU}\right) \\ =&\mathbb{P}\left(r_{k,0} > \mu, \text{the k-th typical UE being a CRU}\right)/A^{\mathrm{R}}_k \\ =&\int_\mu^\infty \mathcal{D}(k, M^1_k, M^2_k, r)dr/A^{\mathrm{R}}_k. \end{aligned} \tag{4.13}$$

Then we take partial differentiation in terms of μ, the conditional serving-BS-distance PDFs for a k-th tier CRU can be obtained as $\mathcal{D}(k, M^1_k, M^2_k, r)/A^{\mathrm{R}}_k$. For the k-th tier ERU, its

Table 4.1 NOTATIONS FOR SIMPLICITY

Notation	Value
s_k^t	$\tau r^{\alpha_k}/P_k^t$
$m_i^{k,t}$	$s_k^t P_i$
$n_i^{k,t}$	$(m_i^{k,t})^{-\frac{2}{\alpha_i}}(d_i^{k,t})(r)^2$
$\omega_i^{k,t}$	$s_k^t P_i u^{-\alpha_i}$

serving-BS-distance PDF can be obtained from the following probability calculation:

$$\begin{aligned}
&\mathbb{P}\left(r_{k,0}>\mu|\text{the } k\text{-th typical UE being an ERU}\right)\\
&\overset{(a)}{=}\mathbb{P}\left(r_{k,0}>\mu,\text{the k-th typical UE being an ERU}\right)/A_k^{\mathrm{F}}\\
&=\left(\int_{\mu}^{\infty}\mathcal{D}(k,B_k^1,B_k^2,r)dr-\int_{\mu}^{\infty}\mathcal{D}(k,M_k^1,M_k^2,r)dr\right)/A_k^{\mathrm{F}}.
\end{aligned}\tag{4.14}$$

By partial differentiating in terms of μ, the the conditional serving-BS-distance PDFs for a k-th tier ERU can be obtained. Consequently, the results in (4.10) can be obtained. □

Based on these conditional serving-BS-distance PDFs, the coverage probability of a tier-k CRU or ERU under SM is given in Theorem 4.1. The notations used for simplification is summarised in Table 4.1.

Theorem 4.1. *The downlink coverage probability of the typical UE in the k-th tier (as a CRU if $t=\mathrm{R}$ and as an ERU if $t=\mathrm{F}$) under SM is given as:*

$$\mathbb{P}(\Gamma_k^t>\tau)=\int_{r>0}\exp\left(-2\pi\lambda_i\sum_{i\in K}\mathcal{F}_{\Delta_i^{k,t}}(s_k^t(r))\right)f_{r_{k,0}^t}(r)dr,\tag{4.15}$$

where $s_k^t(r)=\tau r^{\alpha_k}/P_k^t$. For notational simplicity, s_k^t is used to replace $s_k^t(r)$ in the following. The function $\mathcal{F}_{\Delta_i^{k,t}}(s_k^t)$ can be transformed into $\mathcal{F}_{\Delta_k^R(i)}(s_k^t)$ or $\mathcal{F}_{\Delta_k^F(i)}(s_k^t)$ based on transformation between $\Delta_i^{k,t}$ and $\Delta_k^{t'}(i)$(4.5) as follows:

$$\mathcal{F}_{\Delta_i^{k,R}}=\begin{cases}\mathcal{F}_{\Delta_k^R(i)},i=k\\ \mathcal{F}_{\Delta_k^F(i)},i\neq k\end{cases},\quad \mathcal{F}_{\Delta_i^{k,F}}=\begin{cases}\mathcal{F}_{\Delta_k^F(i)},i=k\\ \mathcal{F}_{\Delta_k^R(i)},i\neq k\end{cases}.\tag{4.16}$$

Furthermore, the functions $\mathcal{F}_{\Delta_k^R(i)}(s_k^t)$ *and* $\mathcal{F}_{\Delta_k^F(i)}(s_k^t)$ *can be represented as:*

$$\mathcal{F}_{\Delta_k^R(i)}(s_k^t) = \beta_i \mathcal{G}_i(m_i^{k,t}, n_i^{k,t}) + (1-\beta_i) m_i^{k,t\,\frac{2}{\alpha_i}} \mathcal{H}_i(\rho_i, \rho_i + \frac{1-\rho_i}{N_{ki}}, n_i^{k,t}), \tag{4.17}$$

$$\mathcal{F}_{\Delta_k^F(i)}(s_k^t) = (1-\beta_i) \mathcal{G}_i(m_i^{k,t}, n_i^{k,t}) + \beta_i m_i^{k,t\,\frac{2}{\alpha_i}} \mathcal{H}_i(1 - \frac{1-\rho_i}{N_{ki}}, 1, n_i^{k,t}), \tag{4.18}$$

where $m_i^{k,t} = s_k^t P_i$, $n_i^{k,t} = (m_i^{k,t})^{-\frac{2}{\alpha_i}} (d_i^{k,t}(r))^2$, $d_i^{k,t}(r)$ *is the minimum interfering distance given by:*

$$d_i^{k,t}(r) = \begin{cases} (\widehat{P}_i^k M_k^i)^{\frac{1}{\alpha_i}} r^{\frac{1}{\widehat{\alpha}_i^k}}, i \neq k, t = R, \\ (\widehat{P}_i^k \widehat{B}_i^k)^{\frac{1}{\alpha_i}} r^{\frac{1}{\widehat{\alpha}_i^k}}, i \neq k, t = F, \\ r, \quad otherwise. \end{cases} \tag{4.19}$$

The function $\mathcal{H}_i(b,c,y)$ *is given in* (4.20) *as:*

$$\mathcal{H}_i(b,c,y) = \frac{y^{\frac{\alpha_i+2}{2}}}{(\alpha_i+2)(b-c)} \left[y^{-\frac{\alpha_i}{2}} \left(\frac{1}{2}(\alpha_i+2)(c-b) + \mathcal{C}_i(b,c,y) \right) + \log \left(\frac{1+by^{-\frac{\alpha_i}{2}}}{1+cy^{-\frac{\alpha_i}{2}}} \right) \right], \tag{4.20}$$

with the function $\mathcal{C}_i(b,c,y)$ *represented as:*

$$\mathcal{C}_i(b,c,y) = c\phi\left(-cy^{-\frac{\alpha_i}{2}}, 1, -\frac{2}{\alpha_i}\right) - b\phi\left(-by^{-\frac{\alpha_i}{2}}, 1, -\frac{2}{\alpha_i}\right), \tag{4.21}$$

where $\phi(\cdot)$ *denotes the Lerch's Transcendent function [105]. Denoting* ${}_2F^1(\cdot)$ *as the Gauss hypergeometric function, the function* $\mathcal{G}_i(a,y)$ *in* (4.17) *and* (4.18) *is given as:*

$$\mathcal{G}_i(a,y) = \frac{2a^{\frac{2}{\alpha_i}} y^{1-\frac{\alpha_i}{2}}}{\alpha_i - 2} {}_2F^1\left(1, 1-\frac{2}{\alpha_i}; 2-\frac{2}{\alpha_i}; -y^{-\frac{\alpha_i}{2}}\right). \tag{4.22}$$

Proof. According to the definition, the coverage probability of the k-th tier UE can be calculated as:

$$\mathbb{P}(\Gamma_k^t > \tau) = \int_{r>0} \prod_{i \in \mathcal{K}} \mathbb{E}\left[\exp\left(-s_k^t I_{i,k}^t\right)\right] f_{r_{k,0}}^t(r) dr, \tag{4.23}$$

where $I_{i,k}^t$ denotes the aggregate interference power of the i-th tier BSs on the k-th tier CRU or ERU. Then the result is transformed into a form with the product of Laplace Transforms (LTs) of the aggregate interference power of each tier. The LT $\mathcal{L}_{I_{i,k}^t}(s_k^t), i \in \mathcal{K}$, can be represented as:

$$\mathcal{L}_{I_{i,k}^t}(s_k^t) = \exp(-2\pi\lambda_i \int_{d_i^{k,t}(r)}^{\infty} (1 - \mathbb{E}_{h,\Delta}[e^{-s_k^t P_i h_i \Delta_i^{k,t} u^{-\alpha_i}})]) u du), \tag{4.24}$$

which is obtained by the moment generating function [20]. Note that the minimum interfering distance $d_i^{k,t}(r)$ has remarkable effect on the final result. Accordingly, in the following, we will discuss the derivation of the values of $d_i^{k,t}(r)$ shown in (4.19).

Following the user association strategy, if the serving tier and the interfering tier are the same (i.e., $i=k$), then $d_i^{k,t}=r_{k,0}$, where $r_{k,0}$ is the serving BS distance. If $i\neq k$ and the UE is a CRU, then we have $P_k r_{k,0}^{-\alpha_k} > M_k^i P_i r_{i,0}^{-\alpha_i}$ (i.e., $r_{i,0} > (\widehat{P}_i^k M_k^i)^{\frac{1}{\alpha_i}} r_{k,0}^{\frac{1}{\widehat{\alpha}_i^k}}$) and thus $d_i^{k,t}=(\widehat{P}_i^k M_k^i)^{\frac{1}{\alpha_i}} r_{k,0}^{\frac{1}{\widehat{\alpha}_i^k}}$. If $i\neq k$ and the UE is an ERU, then we have $B_k P_k r_{k,0}^{-\alpha_k} > B_i P_i r_{i,0}^{-\alpha_i}$ (i.e., $r_{i,0} > (\widehat{P}_i^k \widehat{B}_i^k)^{\frac{1}{\alpha_i}} r_{k,0}^{\frac{1}{\widehat{\alpha}_i^k}}$), and thus $d_i^{k,t}=(\widehat{P}_i^k \widehat{B}_i^k)^{\frac{1}{\alpha_i}} r_{k,0}^{\frac{1}{\widehat{\alpha}_i^k}}$. Therefore, the expression of $d_i^{k,t}(r)$ in (4.19) can be achieved by substituting $r_{k,0}$ with r, which is caused by the average calculation on the serving-BS distance. Consequently, we can focus on the calculation of the term in the integration of (4.24). For denotational simplicity, we define

$$\mathcal{F}_{\Delta_i^{k,t}}(s_k^t)=\int_{d_i^{k,t}(r)}^{\infty}(1-\mathbb{E}_{h,\Delta}[e^{-s_k^t P_i h_i \Delta_i^{k,t} u^{-\alpha_i})}])u du,$$

then the LT $\mathcal{L}_{I_i}(s_k^t)$ can be denoted by $\mathcal{L}_{I_i}(s_k^t)=\exp(-2\pi\lambda_i \mathcal{F}_{\Delta_i^{k,t}}(s_k^t))$. Based on the transformation between $\Delta_i^{k,t}$ and $\Delta_k^{t'}(i)$ as in (4.5), the expectation $\mathbb{E}_{h,\Delta}[\exp(-\omega_i^{k,t} h_i \Delta_i^{k,t})]$ in (4.24) can be calculated as follows with $\omega_i^{k,t}=s_k^t P_i u^{-\alpha_i}$:

$$\mathbb{E}_{\Delta}[\mathbb{E}_{h_i}[\exp(-\omega_i^{k,t}\Delta_k^{t'}(i)h_i)]]=\mathbb{E}_{\Delta}\left[\left(1+\omega_i^{k,t}\Delta_k^{t'}(i)\right)^{-1}\right]\triangleq\Theta(\omega_i^{k,t},\Delta_k^{t'}(i)). \tag{4.25}$$

Based on (4.7) and (4.8), the expectation $\Theta(\omega_i^{k,t},\Delta_k^{t'}(i))$ can be calculated as follows with t' respectively being F and R:

$$\Theta(\omega_i^{k,t},\Delta_k^{t'}(i))=\begin{cases}(1-\beta_i)\dfrac{1}{1+\omega_i^{k,t}}+\beta_i\displaystyle\int_{1-\frac{1-\rho_i}{N_k i}}^{1}\frac{1}{1+\omega_i^{k,t}\xi}\frac{N_{ki}}{1-\rho_i}d\xi, & t'=\mathrm{F},\\ \beta_i\dfrac{1}{1+\rho_i\omega_i^{k,t}}+(1-\beta_i)\displaystyle\int_{\rho_i}^{\rho_i+\frac{1-\rho_i}{N_{ki}}}\frac{1}{1+\omega_i^{k,t}\xi}\frac{N_{ki}}{1-\rho_i}d\xi, & t'=\mathrm{R}.\end{cases} \tag{4.26}$$

By calculating the integrals in (4.26), we have:

$$\Theta(\omega_i^{k,t},\Delta_k^{t'}(i))=\begin{cases}(1-\beta_i)\dfrac{1}{1+\omega_i^{k,t}}+\beta_i\dfrac{\ln(1+\omega_i^{k,t})-\ln(1+(1-\frac{1-\rho_i}{N_{ki}})\omega_i^{k,t})}{(1-(1-\frac{1-\rho_i}{N_{ki}}))\omega_i^{k,t}}, & t'=\mathrm{F}\\ \beta_i\dfrac{1}{1+\rho_i\omega_i^{k,t}}+(1-\beta_i)\dfrac{\ln(1+(\rho_i+\frac{1-\rho_i}{N_{ki}})\omega_i^{k,t})-\ln(1+\rho_i\omega_i^{k,t})}{((\rho_i+\frac{1-\rho_i}{N_{ki}})-\rho_i)\omega_i^{k,t}}, & t'=\mathrm{R}\end{cases} \tag{4.27}$$

The result in (4.27) can be represented with a general form in terms of the value of t' as:

$$\Theta(\omega_i^{k,t},\Delta_k^{t'}(i))=\tilde{\beta}_i^{t'}\frac{1}{1+a\omega_i^{k,t}}+(1-\tilde{\beta}_i^{t'})\frac{\ln(1+b\omega_i^{k,t})-\ln(1+c\omega_i^{k,t})}{(b-c)\omega_i^{k,t}}, \tag{4.28}$$

where $\{\tilde{\beta}_i^{\mathrm{R}},\tilde{\beta}_i^{\mathrm{F}}\}=\{\beta_i,1-\beta_i\}$, $a\in\{\rho_i,1\}$, $b\in\{\rho_i,1-\frac{1-\rho_i}{N_{ki}}\}$, and $c\in\{\rho_i+\frac{1-\rho_i}{N_{ki}},1\}$. Therefore, the function $\mathcal{F}_{\Delta_i^{k,t}}(s_k^t)$ can always be transformed as the following form:

$$\mathcal{F}_{\Delta_i^{k,t}}(s_k^t)\triangleq\mathcal{F}_{\Delta_k^{t'}(i)}(s_k^t)=\int_{d_i^{k,t}(r)}^{\infty}(\tilde{\beta}_i^{t'}\mathcal{Q}_i^1(a)+(1-\tilde{\beta}_i^{t'})\mathcal{Q}_i^2(b,c))udu, \tag{4.29}$$

where $\mathcal{Q}_i^1(a)=1-1/(1+a\omega_i^{k,t})$, and $\mathcal{Q}_i^2(b,c)$ is given by:

$$\mathcal{Q}_i^2(b,c)=1-\frac{\ln(1+c\omega_i^{k,t})-\ln(1+b\omega_i^{k,t})}{(c-b)\omega_i^{k,t}}. \tag{4.30}$$

Specifically, the values of parameters a, b and c are determined by i, k and t', which are summarised as below:

$$\begin{cases}a=1, \quad b=1-\dfrac{1-\rho_i}{N_{ki}}, \quad c=1, \quad \text{if} \quad t'=\mathrm{F},\\ a=\rho_i, \quad b=\rho_i, \quad c=\rho_i+\dfrac{1-\rho_i}{N_{ki}}, \quad \text{if} \quad t'=\mathrm{R}.\end{cases} \tag{4.31}$$

The closed-form result of function $\int_{d_i^{k,t}(r)}^{\infty}\mathcal{Q}_i^1(a)udu$ can be easily obtained as $\mathcal{G}_i(a,n_i^{k,t})$ [99]. Moreover, we have:

$$\int_{d_i^{k,t}}^{\infty}\mathcal{Q}_i^2(b,c)udu=\frac{m_i^{k,t}{}^{\frac{2}{\alpha_i}}}{\alpha_i}\int_0^{n_i^{k,t}{}^{-\frac{2}{\alpha_i}}}\left[1-\frac{\ln(1+c\omega)-\ln(1+b\omega)}{(c-b)\omega}\right]\omega^{-\frac{2+\alpha_i}{\alpha_i}}d\omega \tag{4.32}$$

which can be transformed into $\frac{m_i^{k,t}{}^{\frac{2}{\alpha_i}}}{\alpha_i}\mathcal{H}_i(b,c,n_i^{k,t})$, with function $\mathcal{H}$ expressing in (4.20) by symbolic integration in Wolfram Mathematica. Equipped with $\mathcal{G}_i(a,n_i^{k,t})$ and $\mathcal{H}_i(b,c,n_i^{k,t})$,

Table 4.2 NOTATIONS OF FUNCTIONS

Functions	Description
$\mathcal{S}_k^t(\tau)$	Coverage probability
$\mathcal{F}_{\Delta_i^{k,t}}(s_k^t)$	For denoting the coverage probability
$\mathcal{G}_i(a,x)$	For representing $\mathcal{F}_{\Delta_i^{k,t}}(s_k^t)$
$\mathcal{H}_i(b,c,x)$	For representing $\mathcal{F}_{\Delta_i^{k,t}}(s_k^t)$
$\mathcal{C}_i(b,c,x)$	For representing $\mathcal{H}_i(b,c,x)$
$\mathcal{Q}_i^1(a)$	For generally calculating $\mathcal{F}_{\Delta_i^{k,t}}(s_k^t)$
$\mathcal{Q}_i^2(b,c)$	For generally calculating $\mathcal{F}_{\Delta_i^{k,t}}(s_k^t)$
$\mathcal{L}_{I_{i,k}^t}(s_k^t)$	The Laplace Transformation
$\phi(\cdot)$	Lerch's Transcendent function
${}_2F^1(\cdot)$	Gauss hypergeometric function
$\mathcal{U}(\cdot)$	Uniform Distribution
$\delta(\cdot)$	Dirac delta function
$\mathbf{1}$	Indicator function

the result of function $\mathcal{F}_{\Delta_i^{k,t}}(s_k^t)$ can be achieved. As a result, we can obtain the LTs of the aggregate interference power $L_{I_i}(s_k^t)$, $i \in \mathcal{K}$, as in (4.24). Then by incorporating the result of $L_{I_i}(s_k^t)$ into (4.23), the result in Theorem 4.1 can be yielded. □

The coverage probability in (4.15) can be calculated numerically with a one-dimensional integration if pathloss exponents of the two tiers are different. Therefore, the coverage probability of a typical UE, i.e., $\sum_{k\in\mathcal{K}}\sum_{t\in\{\mathrm{R,F}\}} A_k^t \mathbb{P}(\Gamma_k^t > \tau)$, can be analysed. The functions newly defined in this work has been summarised in Table 4.2.

4.4 Simulation Results

The simulated network area is a square of 400 km^2, with the tier-1 BS density λ_1 being 1 node/km^2. We simulate 10,000 realizations of the BS locations following the PPP, where the UE is deployed at the origin, to obtain the CCDF of the coverage probability. Note that in a full buffered traffic network, the MSMOs between a tier-2 BS and the typical UE of each tier (i.e., N_{12} and N_{22}) have no effect on the coverage probability, thus they can be neglected in the discussion. We assume that the MSMOs between a tier-1 BS and the typical UE of each tier, i.e., N_{11} and N_{21}, have the same value to simplify the discussion. Besides, a typical tier-1 CRU and tier-2 ERU are respectively referred to as a tier-1 victim UE (VU) and a tier-2 VU, as they will suffer from increased interference due to SM. The values and corresponding definitions of the simulation parameters are given by Table 4.3 unless otherwise specified. In

Table 4.3 NOTATIONS AND SIMULATION VALUES

Parameter	Description	Value
$\mathcal{K}$	Tier sets	$\mathcal{K}=\{1,2\}$
t	RPS or FPS case	$t\in\{\mathrm{R},\mathrm{F}\}$
i, j	Tier and BS indexes	$i\in\mathcal{K}$
λ_1, λ_2	BS densities	$\lambda_1=1$ node/km^2
P_1, P_2	Transmitting powers	$P_1=100P_2$
ρ_1, ρ_2	Power reduction factors	$[\rho_1,\rho_2]=[0.1 \text{ or } 0.3,1]$
β_1, β_2	Duty cycling ratios	$[\beta_1,\beta_2]=[0.5,0.5]$
$\mathbf{x}_{i,j}$	BS position	
Φ_1, Φ_2	Sets of tier-1 and tier-2 PPPs	
α_1, α_2	Pathloss exponents	$[\alpha_1,\alpha_2]=[3,4]$
B_1, B_2	Range expansion factors	$B_2=4B_1$
$M_k^i(i\neq k)$	centre region factors	$[M_1^2,M_2^1]=[20,1]$
$h_{i,j}$	Power attenuation of small scale fading	$h_{i,j}\sim\exp(1)$
k	The serving tier	
A_k^{R}, A_k^{F}	Association probabilities	
Δ	Random bias caused by SM	
Γ_k^t	SIR expression	
τ	SIR threshold	0 dB
T_p	Subframe duration	
$T_{ki}^{\max}$, N_{ki}	Maximum SM offset, Maximum SM factor	
$d_i^{k,t}$	Minimum interference distance	

the following, how to choose the values of the centre region bias and the range expansion is explained.

Intuitively, the centre region bias M_k^i should be larger than $\widehat{B}_i^k=B_i/B_k$, to ensure that the centre region area of a k-th tier cell is smaller than the range-expanded coverage area of a k-th tier cell. Typically, the range of the range expansion factor is between 0 dB and 10 dB. As a result, we configure the range expansion bias as 6 dB, i.e., $B_2=4B_1$. Note that the appropriate setting of the centre region bias needs to consider parameters such as transmit power, cell range expansion bias, pathloss exponent, and BS density, and would be an interesting research problem, but it is out of the scope of this chapter. Some initial discussions of the centre-region-bias optimization can be found in Chapter 3. According to these discussions, an intuitive principle for choosing the centre region bias is that the resulting value of $A_k^{\mathrm{R}}/A_k^{\mathrm{F}}$ is comparable to the ratio of RPS duty cycle and FPS duty cycle (i.e. $\beta_k/(1-\beta_k)$), where A_k^{R} and A_k^{F} denote the probabilities of the typical UE being a CRU and an ERU, respectively. This is to ensure that the resources available to each region is proportional to its area, given that UEs are distributed in the network following a homogeneous PPP. In

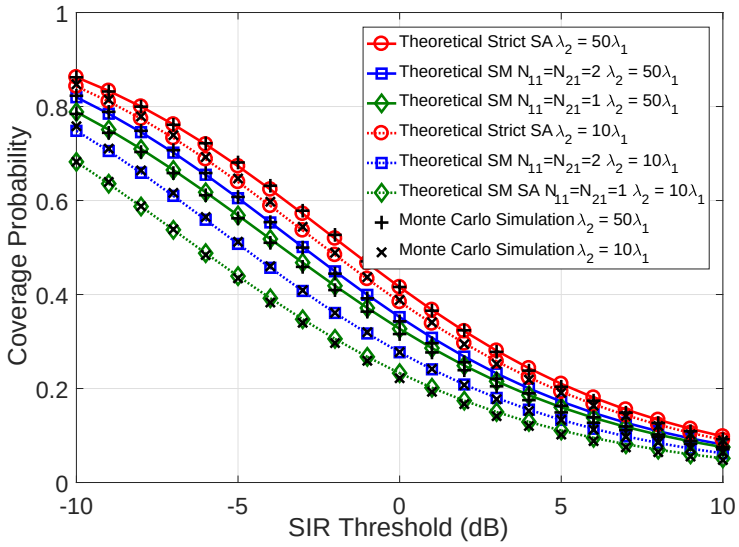

Fig. 4.2 Coverage probability validation of a typical UE under SM ©2018 IEEE

our simulation, the centre region biases are chosen as $[M_1^2, M_2^1] = [20, 1]$. The corresponding ratios between the probabilities of being a CRU and being an ERU are obtained as:

$$\begin{cases} \dfrac{A_1^{\mathrm{R}}}{A_1^{\mathrm{F}}} = 0.9428 \\ \dfrac{A_2^{\mathrm{R}}}{A_2^{\mathrm{F}}} = 1.0593 \end{cases} \text{for } \lambda_2 = 10\lambda_1, \quad \begin{cases} \dfrac{A_1^{\mathrm{R}}}{A_1^{\mathrm{F}}} = 0.7580 \\ \dfrac{A_2^{\mathrm{R}}}{A_2^{\mathrm{F}}} = 1.3199 \end{cases} \text{for } \lambda_2 = 50\lambda_1 \,, \tag{4.33}$$

which are all close to $[\frac{\beta_1}{1-\beta_1}, \frac{\beta_2}{1-\beta_2}] = [1, 1]$.

Fig. 4.2 plots the analytical and simulated coverage probabilities of a typical UE versus the SIR thresholds for the strict SA case ($N_{11} = \infty$) and the SM cases with $N_{11} = 1, 2$, under the low ($\lambda_2 = 10\lambda_1$) and the high ($\lambda_2 = 50\lambda_1$) SC density scenarios. It shows that the theoretical results closely match the simulation results, proving the correctness of our proposed SM model for analysing the coverage probability under SM. We can see that the SM causes severe coverage probability losses, especially in a low SC density scenario, in which the coverage probability declines approximately by 17% at 0 dB SIR threshold. In addition, the coverage losses caused by SM diminish with the increase of SC density.

Fig. 4.3 illustrates the coverage probabilities of the VUs with varieties of the MSMO N_1 in terms of two SIR thresholds (0, 3 dB). It is shown that the SM has remarkable effect on the coverage probabilities of VUs, especially the tier-2 ERUs in the low density scenario who suffer maximumly 20% ($\lambda_2 = 10\lambda_1$, $\tau = 0$ dB) coverage probability reduction. Moreover,

the increasing of SIR threshold τ decreases the coverage probabilities of VUs but has limited effect on the trend of these coverage probabilities.

Fig. 4.4 illustrates the theoretical coverage probabilities of VUs of both tiers versus N_{11} for $\rho_1 = \{0.1, 0.3, 0\}$ under $\lambda_2 = 10\lambda_1$ and $\lambda_2 = 50\lambda_1$. Note that RPSs transfer to ABSs when $\rho_1 = 0$, and tier-1 VUs disappear as all tier-1 UEs use FPSs. The results show that SM decreases coverage probabilities of VUs remarkably, and by using RPSs instead of ABSs can alleviate the SM effect on decreasing the coverage probability. In a low SC density scenario ($\lambda_2 = 10\lambda_1$) the tier-2 VU using ABSs suffers a maximum 45% coverage probability reduction, meanwhile the tier-2 VU using RPSs suffers a maximization of 20% coverage probability reduction. Moreover, a larger power reduction factor ρ_1 alleviates the coverage probability degradation of VUs of both tiers caused by SM, but the coverage probability of a tier-2 VU becomes undesirably poor. In addition, the coverage probabilities of VUs decrease with the increase of the MSMO, regardless of the SC density. According to the coverage probabilities of VUs of both tiers with $\rho_1 = 0.1$ and $\lambda_2 = 10\lambda_1$, in which the effect of SM is the most significant for using RPSs as observed in Fig. 4.4, we can see that the strict SA requirement can be relaxed by up to 20% of a subframe duration, while ensuring the coverage losses caused by SM below 5%.

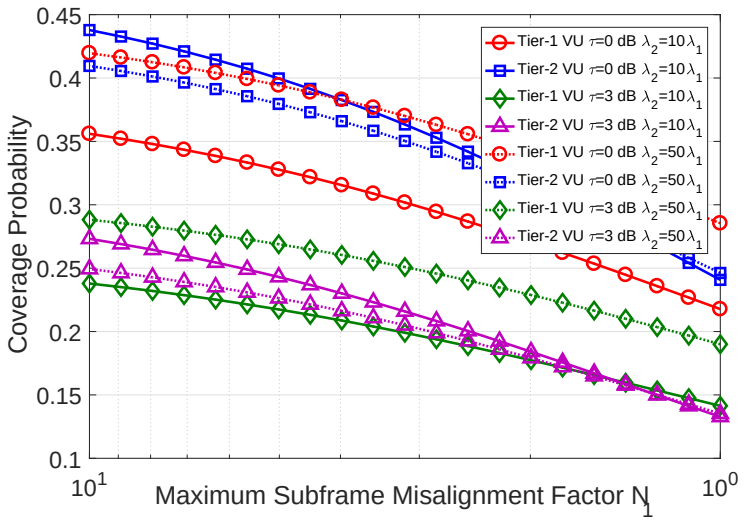

Fig. 4.3 The theoretical coverage probabilities of VUs versus the maximum SM factor N_1 with τ being 0 dB and 3 dB

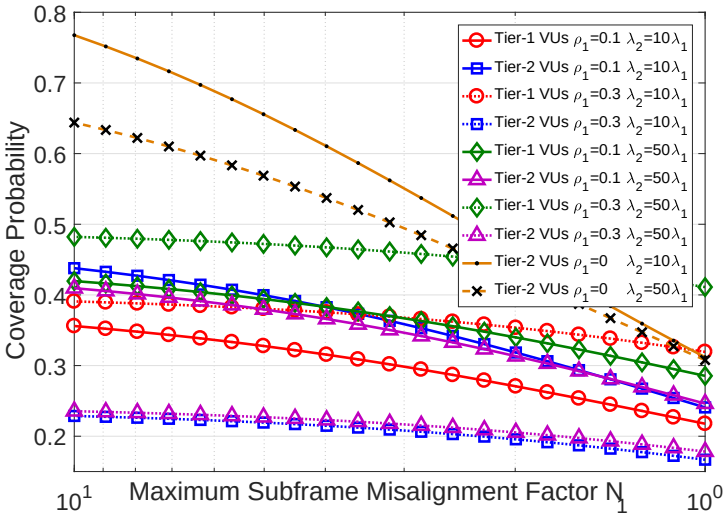

Fig. 4.4 The theoretical coverage probabilities of VUs versus the maximum SM factor N_1 with ρ_1 being 0, 0.1, and 0.3

4.5 Conclusion

In this chapter, we have analysed the downlink coverage probability for a two-tier HetNet employing RPSs under SM. Our analytical and simulation results show that the SM will significantly decrease the coverage probability of a typical UE, which can be mitigated by increasing the SC density. However, the coverage losses of VUs of both tiers caused by SM cannot be mitigated by increasing the SC density, but it can be reduced by increasing the tier-1 power reduction factor. Unfortunately, the coverage probability of a SC CRE UE will be degraded if the tier-1 power reduction factor increases. For protecting the VUs with below 5% coverage reduction caused by SM, the SA requirement can be relaxed by up to 20% of the subframe duration.

Chapter 5

Multi-Unlicensed-Channel Analysis of Coexisting LTE-LAA and WiFi Networks

5.1 Introduction

[1]As aforementioned in Chapter 1, the LTE-U scheme encourages LTE APs to access the 5 GHz unlicensed band, which has already been used by WiFi networks. This scheme can potentially improve the SE of the WiFi only network. In Release 13 of the 3GPP standards, LTE-LAA requires LBT mechanism in LAPs to provide a unified framework for the LTE-U to comply with the regulations worldwide.

Recall that, to our best knowledge, [89] is the only work that has analysed the performance for large-scale coexisting LTE-LAA and WiFi networks with multiple UCs under a stochastic-geometry framework, where both LAPs and WAPs accessed UCs via the CSMA protocol, ignoring collision avoidance. Therefore, the performance of large-scale coexisting LTE-LAA and WiFi networks both deploying the CSMA/CA protocol to access multiple UCs has not been sufficiently studied. Furthermore, the influence of the sensing-region radius of an LAP, which is determined by the sensing threshold of the received power in the CSMA/CA protocol that adopted in the LBT-based LTE-LAA network, has not been investigated in the coexisting LTE-LAA and WiFi networks with multiple UCs. Additionally, it is difficult to generalise the medium access probability (MAP), which is defined as the probability of a typical AP being granted transmission, under a single-UC scenario in [83, 84] to a general

[1]The content of this chapter is based on a slightly revised version of our preprint manuscript [106], which is under review in *IEEE Transaction on Wireless Communication* .

multi-UC case. Therefore, the coexisting LTE-LAA and WiFi networks under a multi-UC scenario need further investigation.

In this work, we provide performance analysis for a large-scale HetNet comprising of LAPs and WAPs that share multiple UCs both using the the CSMA/CA protocol, where LAPs use the LBT-based coexisting mechanism that adopts the CSMA/CA protocol [83]. The main contributions of this work can be summarised as follows: 1) The MAPs of both LAPs and WAPs are obtained in closed form, using tools from stochastic geometry. 2) Based on the closed-from MAPs, analytical expressions of downlink successful transmission probabilities (STPs), which are jointly determined by the downlink coverage probability of a UE and the MAP of the serving AP, are derived for both LTE-LAA and WiFi UEs and validated by Monte Carlo simulations. To reduce the computational complexity in numerical search of the optimal LAP density that maximises the LTE-LAA UE (LUE) throughput, a low-calculation-complexity lower bound (LB) of STP is obtained for LUEs and WiFi UEs (WUEs), respectively. 3) Based on the STPs, we numerically analyse the effects of LAP density and the number of UCs on the throughput and SE. Moreover, by deriving the asymptotic throughput and SE as the LAP density approaches infinity, we provide insights into how the deployment density of LAPs should be selected according to the number of UCs. 4) The fairness between the LTE-LAA and WiFi networks is analysed as a function of the radius of LAP's sensing region.

The rest of this chapter is organised as follows: Section 5.2 introduces the system model, including the network spatial distribution, propagation model, medium access scheme and the defined performance metrics (i.e., STP, UE throughput, spatial throughput (STH) and spatial spectral efficiency (SSE)). In this section, the closed-form MAPs are also derived and validated. Section 5.3 gives the analytical results of the defined performance metrics, and we validate the analytical STPs by Monte Carlo simulations. Only the STPs are validated because other performance metrics (i.e., UE throughput, STH and SSE) are derived based on the STPs. Section 5.4 presents the numerical analysis before concluding the paper in Section 5.5.

5.2 System Model

We consider a two-tier HetNet consisting of LAPs and WAPs, where LAPs form tier-L and WAPs form tier-W. LAPs and WAPs may vary in terms of density (λ_{L} and λ_{W}), sensing threshold (γ_{L} and γ_{W}), and transmit power (P_{L} and P_{W}). We assume that each AP in both tiers transmits in a full buffer mode, i.e., each AP always has data to transmit. We also assume perfect time synchronization throughout the two-tier HetNet. In the following subsections,

Table 5.1 NOTATIONS AND SIMULATION VALUES

Symbol	Definition	Simulation Value
Φ_{L}, Φ_{W}	Spatial PPPs of LAPs and WAPs	
λ_{L}, λ_{W}	Densities of LAPs and WAPs	
P_{L}, P_{W}	Transmission powers of LAPs and WAPs	23 dBm, 23 dBm
Λ_c	Wavelength of carrier frequency	0.06 m
α	Pathloss exponent	4
M	Non-overlapping channel number	3
μ	Rayleigh fading parameter	1
σ^2	Thermal noise power	0
γ_{L}, γ_{W}	Sensing threshold of signal strength of LAPs and WAPs	$\gamma_{\mathrm{W}} = -82$ dBm
κ_{L}	LAP sensing region factor	1.3
R_{L}, R_{W}	Sensing radiuses of LAPs and WAPs	$R_{\mathrm{L}} = \kappa_{\mathrm{L}} R_{\mathrm{W}}$
T, B	SINR threshold, Bandwidth per channel	5 dB, 20 MHz
$t_{\mathbf{x}}$, $t_{\mathbf{y}}$	Back-off timers of LAPs and WAPs	
$e_{\mathbf{x}}^{\mathrm{L}}$, $e_{\mathbf{y}}^{\mathrm{W}}$	Medium access indicators of LAPs and WAPs	
$\widetilde{\Phi}_{\mathrm{L}}$, $\widetilde{\Phi}_{\mathrm{W}}$	Retained interfering LAPs and WAPs	
$\tilde{e}_{\mathbf{x}}^{\mathrm{LL}}$, $\tilde{e}_{\mathbf{y}}^{\mathrm{LW}}$ ($\tilde{e}_{\mathbf{x}}^{\mathrm{WL}}$, $\tilde{e}_{\mathbf{y}}^{\mathrm{WW}}$)	Modified retaining indicators of interfering LAPs and WAPs for a tagged LAP (WAP)	
ξ	Tier-ξ AP is LAP if $\xi = \mathrm{L}$ and WAP if $\xi = \mathrm{W}$	
h_i^{LL}, h_j^{LW} (h_i^{WL}, h_j^{WW})	Fading of the channel from the LAP $\mathbf{x}_i$ and the WAP $\mathbf{y}_j$ to the LAP (WAP) user	
$\mathcal{B}(\mathbf{z}, r)$	Open ball with center $\mathbf{z}$ and radius r	
$\mathcal{B}^c(\mathbf{z}, r)$	Complement of $B(\mathbf{z}, r)$	

the spatial locations of APs and UEs, the radio propagation model, the medium access scheme, and the defined performance metrics will be introduced. The symbols used in this paper are summarised in Table 5.1 together with their definitions and values used in simulation where applicable.

5.2.1 Spatial Locations

The LAPs and WAPs are distributed following two independent PPPs [22], denoted by $\Phi_{\mathrm{L}} = \{\mathbf{x}_1, \mathbf{x}_2, \cdots \mathbf{x}_i, \cdots\}$ and $\Phi_{\mathrm{W}} = \{\mathbf{y}_1, \mathbf{y}_2, \cdots \mathbf{y}_j, \cdots\}$ with densities λ_{L} and λ_{W}, respectively. For analytical tractability, we assume that there are two independent groups of UEs, i.e., LUEs that each served by its closest LAP, and WUEs that each served by its closest WAP. A user association scheme across LTE-LAA and WiFi networks is out of the scope of this chapter. LUEs and WUEs are distributed following two independent PPPs, with densities

much larger than those of LAPs and WAPs. Thus, we can assume that each AP has at least one associated UE [83]. Note that if the UE density is comparable to the AP density, the network performance can be analysed in a way similar as in [107] by excluding the void APs, which are defined as APs without any associated UE.

5.2.2 Propagation Model

We assume that each link between a UE and an AP experiences pathloss and small scale fading. The shadowing is neglected to ensure analytical tractability [9]. The pathloss follows a log-distance model given in dB as $l(d) = 20\log_{10}(\frac{4\pi}{\Lambda_c}) + 10\alpha\log_{10}(d)$, where d is the distance between the transmitter and receiver, Λ_c is the wavelength, and α is the pathloss exponent ($2 < \alpha \leq 6$) [108]. Note that the system model used in this chapter differs from that in the previous two chapters. The main reason is that the carrier frequency of the 5 GHz unlicensed spectrum band is higher than that of the licensed spectrum band, and by using such a pathloss model, the obtained results may be comparable to the results in actual network. It is worthy mentioning that the pathloss model in Chapter 5 is also applicable for Chapter 3 and Chapter 4. For the small scale fading, Rayleigh fading is assumed, thus the received power attenuation caused by it is modelled as an independent exponential distribution with a rate parameter μ. Specifically, the small scale fading of the link between an LAP $\mathbf{x}_i$ or a WAP $\mathbf{y}_j$ and a typical LUE (WUE) is denoted by h_i^{LL} or h_i^{WL} (h_i^{LW} or h_i^{WW}), respectively.

5.2.3 Medium Access Scheme with Multiple Unlicensed Channels

According to the IEEE 802.11 a/n/ac, the 5 GHz unlicensed bands, i.e., $5.15-5.35$ GHz and $5.47-5.825$ GHz, is divided into a number of UCs, each with a bandwidth of 20, 40, 80, or 160 MHz [109]. Since a maximum of 100 MHz bandwidth in the licensed or unlicensed bands can be supported by carrier aggregation [110], we assume that the entire 5 GHz unlicensed band is divided into M non-overlapping UCs, and there is no mutual interference between any two different UCs. The value of M is influenced by the bandwidth of an UC. In the 5 GHz unlicensed band with an approximate total bandwidth of 490 MHz, a maximum of 24 non-overlapping UCs (each with a bandwidth of 20 MHz) can be supported [109].

As the LBT-based medium access scheme is deployed in LAPs, we assume that both WAPs and LAPs adopt CSMA/CA protocol to access the M UCs [89]. The sensing thresholds in the CSMA/CA protocol used by LAPs and WAPs are denoted by γ_{L} and γ_{W}, respectively, which determine their sensing regions. To our best knowledge, there is no closed-form expression of the number of interfering APs if small-scale fading is considered in the area of sensing region. For analytical tractability of the MAP for each AP, we ignore the effect

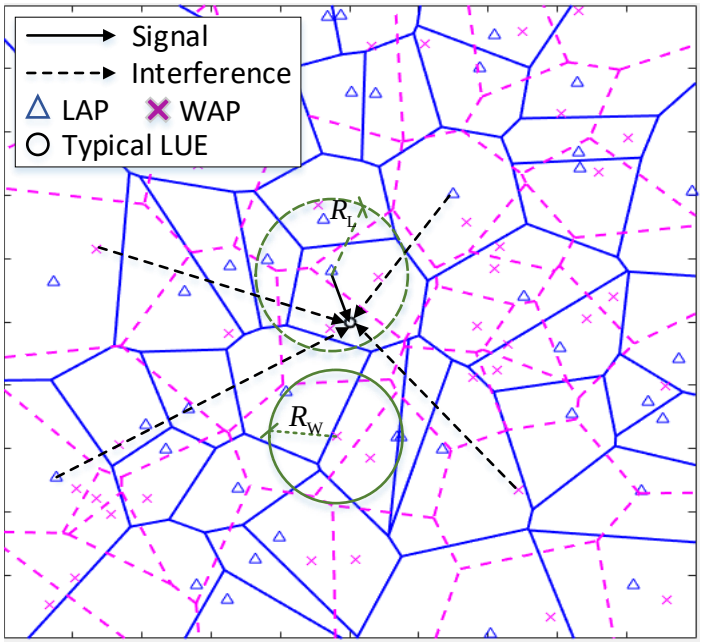

Fig. 5.1 Illustration of the sysyem model for a typical LUE

of small scale fading on the sensing regions [87, 89, 111–113]. , thus the radius R_{W} of the sensing region of a WAP is given by $R_{\mathrm{W}} = \left(\frac{P_{\mathrm{W}}\Lambda_c^2}{\gamma_{\mathrm{W}}(4\pi)^2}\right)^{\frac{1}{\alpha}}$. Since the differences between the carrier frequencies in different UCs in the 5 GHz unlicensed band are much smaller than 5 GHz, we use 5 GHz as the approximate common carrier frequency for all the M UCs. As a result, the wavelength Λ_c is 0.06 m. Similarly, the radius R_{L} of the sensing region of an LAP is given by $R_{\mathrm{L}} = \left(\frac{P_{\mathrm{L}}\Lambda_c^2}{\gamma_{\mathrm{L}}(4\pi)^2}\right)^{\frac{1}{\alpha}}$. Defining $\kappa_{\mathrm{L}} = R_{\mathrm{L}}/R_{\mathrm{W}}$ as the LAP sensing region factor, we have $R_{\mathrm{L}} = \kappa_{\mathrm{L}} R_{\mathrm{W}}$. The spatial locations and the sensing radiuses of LAPs and WAPs are illustrated in Fig. 5.1. Moreover, we assume that each AP in both tiers is able to detect all the idle UCs, and will randomly select one of them to access if there are more than one idle UCs [114].

If APs start to transmit instantly after detecting an idle UC, collisions between simultaneous data transmissions on the same channel from several APs may occur. In order to reduce such collisions, a back-off timer, which is independently and uniformly distributed in the range of $[0,1]$, is employed at each AP in both tiers. The back-off timer decides the time period that the AP should wait before transmission on an idle UC. The back-off timers are respectively denoted by $\{t_{\mathbf{x}_1}, t_{\mathbf{x}_2}, \cdots, t_{\mathbf{x}_i}, \cdots\}$ and $\{t_{\mathbf{y}_1}, t_{\mathbf{y}_3}, \cdots, t_{\mathbf{y}_j}, \cdots\}$ for LAPs and WAPs. Although the simple uniform distribution of the back-off timer ignores its exponentially increasing characteristic related to the collision time, it can still provide reasonable results in modeling the CSMA/CA protocol [115], which grants access of an idle channel to the

AP with the minimum back-off timer. Accordingly, the medium access scheme for APs in both tiers can be described as follows: For a specific AP, its neighbouring APs are defined as the set of WAPs and LAPs in its sensing region. If the number of neighbouring APs is smaller than the UC number M, then this specific AP will be granted transmission, as there is at least one available UC to access. Otherwise, this AP will be granted transmission on an idle UC only if its back-off timer is among the lowest M ones of all the neighbouring APs. A medium access indicator, which is configured as 1 if the AP is granted transmission and as 0 otherwise, is assigned to each AP. A transmission-granted AP is also namely as a retained AP. The medium access indicators of the i-th LAP and the j-th WAP are denoted by $e^{\mathrm{L}}_{\mathbf{x}_i}$ and $e^{\mathrm{W}}_{\mathbf{y}_j}$, respectively, which can be calculated as:

$$e^{\mathrm{L}}_{\mathbf{x}_i} = (\mathcal{N}(\mathbf{x}_i, R_{\mathrm{L}}) < M) + (\mathcal{N}(\mathbf{x}_i, R_{\mathrm{L}}) \geq M) \cdot (t_{\mathbf{x}_i} < \min(\mathcal{T}(\mathbf{x}_i, R_{\mathrm{L}})), M), \tag{5.1}$$

$$e^{\mathrm{W}}_{\mathbf{y}_j} = (\mathcal{N}(\mathbf{y}_j, R_{\mathrm{W}}) < M) + (\mathcal{N}(\mathbf{y}_j, R_{\mathrm{W}}) \geq M) \cdot (t_{\mathbf{y}_j} < \min(\mathcal{T}(\mathbf{y}_j, R_{\mathrm{W}})), M), \tag{5.2}$$

where $\mathcal{N}(\mathbf{z}, \varepsilon)$ and $\mathcal{T}(\mathbf{z}, \varepsilon)$ denote the number and the set of back-off timers of neighbouring APs around a typical AP locating at $\mathbf{z}$ with a sensing region radius ε, respectively. The function $\min(\mathbf{S}, n)$ returns the n-th smallest element in set $\mathbf{S}$. Accordingly, the MAP, which is defined as the the probability of a typical AP being granted transmission, is given in Lemma 5.1.

Lemma 5.1. *Assuming that LAPs and WAPs have the same channel access priority, and each AP can detect the transmitting behaviours of all other APs in its sensing region with radius R_ξ, the MAP ϑ_ξ of a tier-ξ AP located at the origin is given as:*

$$\vartheta_\xi = \mathcal{A}(N_{o,\xi}, M), \tag{5.3}$$

where $\xi \in \{\mathrm{L}, \mathrm{W}\}$, the tier-$\xi$ AP is an LAP if $\xi = \mathrm{L}$ and it is a WAP if $\xi = \mathrm{W}$. $N_{o,\xi}$ is the expected number of neighbouring APs in the sensing region of $\mathcal{B}(o, R_\xi)$, in which o denotes the origin and $\mathcal{B}(\mathbf{z}, \varepsilon)$ denotes a two-dimensional (2D) open ball centred at $\mathbf{z}$ with a sensing radius ε. The function $\mathcal{A}(a,b)$ is defined as:

$$\mathcal{A}(a,b) = \frac{1}{a}\left[b + \frac{\Gamma(b+1,a)}{\Gamma(b+1,0)} + (a-1-b)\frac{\Gamma(b+2,a)}{\Gamma(b+2,0)} - e^{-a}\frac{a^{b+1}}{\Gamma(b+2,0)}\right], \tag{5.4}$$

where a and b are two arbitrary parameters, and the terms $\Gamma(b+1,a)$ and $\Gamma(b+2,a)$ are the upper incomplete Gamma function, which is defined as $\Gamma(\widehat{b},a) = \int_a^\infty u^{\widehat{b}-1}e^{-u}du$, with $\widehat{b} = b+1$, or $b+2$.

Proof. According to Slivnyak's theorem [23], the typical tier-ξ AP can be positioned at origin without loss of generality because the positions of APs belong to a PPP. Based on the definition of the medium access indicators in (5.1) and (5.2), the MAP of the typical tier-ξ AP can be calculated as below:

$$\vartheta_\xi = \mathbb{P}(\mathcal{N}(o,R_\xi) < M) + \mathbb{P}(\mathcal{N}(o,R_\xi) \geq M) \cdot \mathbb{P}(t_o < \min(\mathcal{T}(o,R_\xi),M). \tag{5.5}$$

The probability $\mathbb{P}(N(o,R_\xi) < M)$, which means the probability of the number of neighbouring APs being less than M, can be calculated depended on the probability mass function of point number in a certain area for a PPP. The second term in the right hand side (r.h.s) of (5.5) indicates that the MAP when the number of neighbouring APs is larger than M. Because of the assumption of independent identically distributed back-off timer in each AP, the typical tier-ξ AP will be retained if the value of its back-off timer is among the lowest M ones of all the neighbouring APs plus itself. Consequently, the MAP ϑ_ξ can be transformed as:

$$\begin{aligned}\vartheta_\xi &= \sum_{n=0}^{M-1} \frac{N_{o,\xi}^n \exp(-N_{o,\xi})}{n!} + \sum_{n=M}^{\infty} \frac{M}{n+1} \frac{N_{o,\xi}^n \exp(-N_{o,\xi})}{n!} \\ &= \exp(-N_{o,\xi}) \left[\sum_{n=0}^{M-1} \frac{N_{o,\xi}^n}{n!} + \frac{M}{N_{o,\xi}} \sum_{n=0}^{\infty} \frac{N_{o,\xi}^{n+1}}{(n+1)!} - \frac{M}{N_{o,\xi}} \sum_{n=0}^{M-1} \frac{N_{o,\xi}^{n+1}}{(n+1)!} \right]\end{aligned} \tag{5.6}$$

By calculating the finite series in Wolfram Mathematica [116], we have

$$\begin{aligned}\vartheta_\xi &= \frac{\exp(-N_{o,\xi})}{N_{o,\xi}} \left[M(\exp(N_{o,\xi}) - 1) - \sum_{n=1}^{M} \frac{(M-n){N_{o,\xi}}^n}{n!} \right] \\ &\overset{(a)}{=} \frac{\exp(-N_{o,\xi})}{N_{o,\xi}} \left[M(\exp(N_{o,\xi}) - 1) + \exp(N_{o,\xi}) \frac{\Gamma(M+1, N_{o,\xi})}{\Gamma(M+1)} \right. \\ &\left. + (N_{o,\xi} - M - 1)\exp(-N_{o,\xi}) \frac{\Gamma(M+2, N_{o,\xi})}{\Gamma(M+2)} + M - \frac{N_{o,\xi}^{M+2}}{\Gamma(M+2)} \right] \triangleq \mathcal{A}(N_{o,\xi}, M).\end{aligned} \tag{5.7}$$

Thus the result in Lemma 5.1 has been obtained. A similar derivation can be found in [117] and we move a step further to obtain the MAP in closed form. □

Fig. 5.2 illustrates the theoretical and simulated MAPs of a typical LAP and a typical WAP versus the WAP density for three different values of LAP density: $400, 800$ and 1200 LAPs per km^2. Each simulation curve is obtained by averaging over $10,000$ realizations of LAP and WAP locations following two independent PPPs in a square area of 25 km^2, where the typical LAP or WAP is located at the origin. The simulation values of parameters are

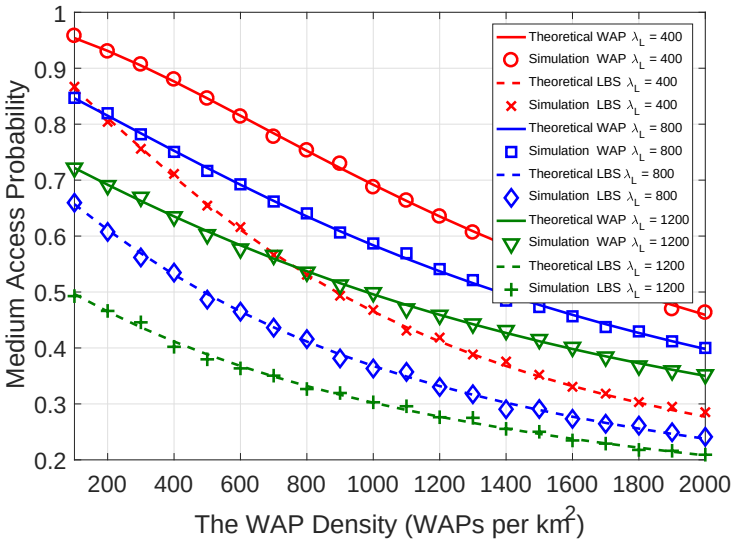

Fig. 5.2 The MAP validation versus the WAP density

listed in Table 5.1. The theoretical curves are obtained following (5.3). The results show that the theoretical MAPs closely match the simulation results for both tiers of APs. This verifies the accuracy of our derived MAP expression in (5.3). In addition, we can see that the MAP of the typical LAP is lower than that of the WAP, because the sensing region of an LAP is larger than that of a WAP ($\kappa_{\mathrm{L}} = 1.3$).

5.2.4 Performance Metrics

In this work, we mainly analyse the STP, the UE throughput, the STH and the SSE. These performance metrics will be respectively defined in the following.

Successful Transmission Probability

The STP of a typical UE is defined as the probability of the typical UE simultaneously satisfying the following two conditions: a) Its serving AP is retained; b) Its SINR is larger than a threshold T. Denoting the medium access indicators of the nearest LAP and the nearest WAP as e_0^{L} and e_0^{W}, respectively, the STPs of a typical LUE and a typical WUE are given as follows:

$$\mathcal{P}_{\mathrm{st}}^{\mathrm{L}}(\lambda_{\mathrm{L}}, \lambda_{\mathrm{W}}, T, M) = \mathbb{E}[e_0^{\mathrm{L}}]\mathbb{P}(\mathrm{SINR}_0^{\mathrm{L}} > T | e_0^{\mathrm{L}} = 1), \tag{5.8}$$

$$\mathcal{P}_{\mathrm{st}}^{\mathrm{W}}(\lambda_{\mathrm{L}}, \lambda_{\mathrm{W}}, T, M) = \mathbb{E}[e_0^{\mathrm{W}}]\mathbb{P}(\mathrm{SINR}_0^{\mathrm{W}} > T | e_0^{\mathrm{W}} = 1). \tag{5.9}$$

The SINR expressions of the typical LUE and the typical WUE are respectively given as follows:

$$\mathrm{SINR}_0^{\mathrm{L}} = \frac{P_{\mathrm{L}} h_0^{\mathrm{LL}} l_{\mathrm{L}}(||\mathbf{x}_0||)}{\sum_{\mathbf{x}_i \in \widetilde{\Phi}_{\mathrm{L}}/\mathbf{x}_0} P_{\mathrm{L}} h_i^{\mathrm{LL}} l_{\mathrm{L}}(||\mathbf{x}_i||) + \sum_{\mathbf{y}_j \in \widetilde{\Phi}_{\mathrm{W}}} P_{\mathrm{W}} h_j^{\mathrm{LW}} l_{\mathrm{W}}(||\mathbf{y}_j||) + \sigma^2}, \tag{5.10}$$

$$\mathrm{SINR}_0^{\mathrm{W}} = \frac{P_{\mathrm{W}} h_0^{\mathrm{WW}} l_{\mathrm{W}}(||\mathbf{y}_0||)}{\sum_{\mathbf{y}_j \in \widetilde{\Phi}_{\mathrm{W}}/\mathbf{y}_0} P_{\mathrm{W}} h_j^{\mathrm{WW}} l_{\mathrm{W}}(||\mathbf{y}_j||) + \sum_{\mathbf{x}_i \in \widetilde{\Phi}_{\mathrm{L}}} P_{\mathrm{L}} h_i^{\mathrm{WL}} l_{\mathrm{L}}(||\mathbf{x}_i||) + \sigma^2}, \tag{5.11}$$

where $\widetilde{\Phi}_{\mathrm{W}}$ and $\widetilde{\Phi}_{\mathrm{L}}$ respectively denote the retained interfering WAPs and LAPs which use the same channel as the serving AP, and $||\mathbf{z}||$ is the Euclidean distance between the location $\mathbf{z}$ and the origin.

UE Throughput

The UE throughput is defined as the throughput of a typical UE. As the UE locations in the same tier follow a homogeneous PPP, the throughputs of contending UEs associated with the same AP follow the same distribution. Thus without loss of generality, we assume the typical UE is allocated with all the radio resources. The UE throughput can be considered as the aggregate throughput of associated UEs for an AP. Note that when the serving AP of this typical UE is not retained, i.e., the serving AP is not granted transmission on any UC, the UE throughput equals 0. As aforementioned, each AP in both tiers can access only one of the idle UCs, thus the throughputs of an LUE and a WUE are given respectively by:

$$\mathcal{C}_{\mathrm{L}}(\lambda_{\mathrm{L}}, \lambda_{\mathrm{W}}, T_{\mathrm{L}}, M) = \mathbb{E}[e_0^{\mathrm{L}}] B \log(1 + T_{\mathrm{L}}) \mathbb{P}(\mathrm{SINR}_0^{\mathrm{L}} > T_{\mathrm{L}} | e_0^{\mathrm{L}} = 1), \tag{5.12}$$

$$\mathcal{C}_{\mathrm{W}}(\lambda_{\mathrm{L}}, \lambda_{\mathrm{W}}, T_{\mathrm{W}}, M) = \mathbb{E}[e_0^{\mathrm{W}}] B \log(1 + T_{\mathrm{W}}) \mathbb{P}(\mathrm{SINR}_0^{\mathrm{W}} > T_{\mathrm{W}} | e_0^{\mathrm{W}} = 1), \tag{5.13}$$

where T_{L} and T_{W} are the SINR thresholds respectively for the typical LTE-LAA and WiFi UEs, and B is the bandwidth per UC.

Spatial Throughput and Spatial Spectral Efficiency

The STH is defined as the aggregate throughput of all UEs served by the retained APs of both tiers in a unit square area [84], which can be expressed as follows:

$$\mathcal{C}_{\mathrm{STH}}(\lambda_{\mathrm{L}}, \lambda_{\mathrm{W}}, T_{\mathrm{L}}, T_{\mathrm{W}}, M) = \lambda_{\mathrm{L}} \mathcal{C}_{\mathrm{L}}(\lambda_{\mathrm{L}}, \lambda_{\mathrm{W}}, T_{\mathrm{L}}, M) + \lambda_{\mathrm{W}} \mathcal{C}_{\mathrm{W}}(\lambda_{\mathrm{L}}, \lambda_{\mathrm{W}}, T_{\mathrm{W}}, M). \tag{5.14}$$

We define that SSE as the STH achieved per hertz (Hz), i.e., the aggregate throughput provided by the retained APs of both tiers in a unit square area per Hz. The SSE can be

expressed as:

$$\Theta(\lambda_{\mathrm{L}},\lambda_{\mathrm{W}},T_{\mathrm{L}},T_{\mathrm{W}},M)=\mathcal{C}_{\mathrm{STH}}(\lambda_{\mathrm{L}},\lambda_{\mathrm{W}},T_{\mathrm{L}},T_{\mathrm{W}},M)/MB. \tag{5.15}$$

5.3 Performance Analysis

In this section, firstly we derive the MAP of the serving AP and the Palm coverage probability [23] to obtain the STP. Secondly, the UE throughput, the STH and the SSE are analysed based on the STP. Without loss of generality, we place the typical UE at the origin, which is justified by the Slivnyak's theorem [9] since the LUEs and the WUEs are distributed following two independent homogeneous PPPs.

5.3.1 The MAP of the Serving AP

The MAP of the serving AP of the typical UE differs from that of a typical AP because it considers the distance between the typical UE and its serving AP. Note that each LUE and each WUE is served by its closest LAP and WAP, respectively. As a result, the distances between the typical UE and other APs, which are in the same tier as the serving AP, must be larger than that between the typical UE and the serving AP. Denoting the position of the serving AP by $(r_0^{\xi},0)$, where r_0^{ξ} is the distance between the serving LAP and the typical LUE if $\xi=\mathrm{L}$, and is the distance between the serving WAP and the typical WUE otherwise, $\xi\in\{\mathrm{L},\mathrm{W}\}$. Conditioned on this, the MAP of the serving AP is given in Lemma 5.2.

Lemma 5.2. *For a tier-ξ serving AP $\mathbf{z}_0^{\xi}$ located at $(r_0^{\xi},0)$ with M accessible UCs, its MAP is given by:*

$$\mathbb{P}(e_0^{\xi}=1|\mathbf{z}_0^{\xi}=(r_0^{\xi},0))=\mathcal{A}(N_{o,\xi}-\lambda_{\xi}\mathcal{V}_{int}(r_0^{\xi},R_{\xi},r_0^{\xi}),M), \tag{5.16}$$

where $\xi\in\{\mathrm{L},\mathrm{W}\}$, R_{ξ} is the sensing radius of the tier-ξ AP, and the function $\mathcal{V}_{int}(r_m,r_n,d)$ denotes the intersection area of two circles, where r_m and r_n are the radius of the two circles and d is the distance between the centres of the two circles. The expression of $\mathcal{V}_{int}(r_m,r_n,d)$ is given as:

$$\mathcal{V}_{int}(r_m,r_n,d)=\begin{cases}\pi(\min(\{r_m,r_n\},1))^2, & d\le\max(r_m,r_n)-\min(\{r_m,r_n\},1),\\ 0, & d\ge r_m+r_n,\\ a^2(\beta_{r_m}-\sin 2\beta_{r_m})+b^2(\beta_{r_n}-\sin 2\beta_{r_n}), & \textit{Otherwiese},\end{cases} \tag{5.17}$$

where $\beta_{r_m}=\arccos\frac{{r_m}^2+d^2-{r_n}^2}{2r_md}$ and $\beta_{r_n}=\arccos\frac{r_n^2+d^2-r_m^2}{2r_nd}$.

Proof. According to the assumption that a typical tier-ξ UE is always tagged to its closest tier-ξ AP, there will be no other tier-ξ APs in the 2D ball of $\mathcal{B}(o, r_0^{\xi})$. As a result, the MAP of this tier-ξ serving AP can be calculated based on the result in Lemma 5.1 by excluding the tier-ξ APs from the intersection region of $\mathcal{B}(o, r_0^{\xi})$ and $\mathcal{B}(\mathbf{z}_0^{\xi}, R_{\xi})$, leading to the expression in (5.16). □

Based on the PDF of the closest tier-ξ AP [9], i.e., $f_{r_0^{\xi}}(r) = 2\pi\lambda_{\xi} r \exp(-\pi\lambda_{\xi} r^2)$, the MAP of the serving tier-ξ AP is given in Corollary 5.1.

Corollary 5.1. *The MAP of the serving tier-ξ AP is:*

$$\mathbb{P}(e_0^{\xi}=1) = 2\pi\lambda_{\xi}\left(\int_0^{\frac{R_{\xi}}{2}} \mathcal{A}(N_{o,\xi}-\lambda_{\xi}\pi r^2, M) r e^{-\lambda_{\xi}\pi r^2} dr + \int_{\frac{R_{\xi}}{2}}^{\infty} \mathcal{A}(N_{o,\xi}-\lambda_{\xi}\mathcal{V}_{int}(r,R_{\xi},r), M) r e^{-\lambda_{\xi}\pi r^2} dr\right). \tag{5.18}$$

Proof. By definition, we have

$$\mathbb{P}(e_0^{\xi}=1) = \mathbb{E}_{r_0^{\xi}}\left[\mathbb{P}(e_0^{\xi}=1|\upsilon_0^{\xi}=(r_0^{\xi},0))\right] = \int_0^{\infty} \mathcal{A}(N_{o,\xi}-\lambda_{\xi}\mathcal{V}_{int}(r,R_{\xi},r), M) f_{r_0^{\xi}}(r) dr. \tag{5.19}$$

Note that the area of the intersection region, obtained in $\mathcal{V}_{int}(r,R_{\xi},r)$, is πr^2 when $r \leq \frac{R_{\xi}}{2}$, thus the MAP of the tier-ξ AP is obtained. □

5.3.2 The Palm Coverage Probability

The Palm coverage probability is defined as the probability of the SINR of a typical UE being larger than a threshold T, conditioned on the known location of the serving AP. For a tier-ξ serving AP $\mathbf{z}_0^{\xi}$ locating at $(r_0^{\xi}, 0)$, the Palm coverage probability of the typical UE is denoted by $\mathbb{P}_{\mathbf{z}_0^{\xi}}(\mathrm{SINR}_0^{\xi} > T | e_0^{\xi}=1, \mathbf{z}_0=(r_0^{\xi},0))$, which can be transformed as follows:

$$\begin{aligned}
&\mathbb{P}_{\mathbf{z}_0^{\xi}}(\mathrm{SINR}_0^{\xi} > T | e_0^{\xi}=1, \mathbf{z}_0=(r_0^{\xi},0)) \\
=&\mathbb{P}(\mathrm{SINR}_0^{\xi} > T | \mathbf{z}_0=(r_0^{\xi},0), \Phi_{\xi}(B(o,r_0^{\xi}))=0, e_0^{\xi}=1) \\
=&\mathbb{P}\left(\frac{P_{\xi} h_0^{\xi \mathrm{L}} l_{\xi}(||\mathbf{z}_0^{\xi}||)}{\widetilde{I}_{\xi \mathrm{L}} + \widetilde{I}_{\xi \mathrm{W}} + \sigma^2)} > T | e_0^{\xi}=1\right),
\end{aligned} \tag{5.20}$$

where $\widetilde{I}_{\xi \mathrm{L}} = \sum_{\mathbf{x}_i \in \widetilde{\Phi}_{\xi \mathrm{L}}/\mathbf{x}_0} P_{\mathrm{L}} h_i^{\xi \mathrm{L}} l_{\mathrm{L}}(||\mathbf{x}_i||)$ and $\widetilde{I}_{\xi \mathrm{W}} = \sum_{\mathbf{y}_j \in \widetilde{\Phi}_{\xi \mathrm{W}}} P_{\mathrm{W}} h_j^{\xi \mathrm{W}} l_{\mathrm{W}}(||\mathbf{y}_j||)$. Thus in order to obtain the Palm coverage probability, the distribution of the aggregate interference, i.e., $\widetilde{I}_{\xi \mathrm{L}}$ and $\widetilde{I}_{\xi \mathrm{W}}$, should be derived first. According to [23], the retained interfering LAPs and WAPs form a Matern hard core process (MHCP), but the closed-form LT of the aggregate

interference power based on an MHCP is still unknown. Fortunately, an approximation method, which treats the MHCP as an independent inhomogeneous thinning process by decoupling the thinning dependence between the interfering APs, has been proven effective for performance analysis in [83, 84, 89, 117]. Based on the approximation method, the retaining probability of an interfering AP correlates only with the transmission state of the serving AP. Accordingly, we give the retaining probability of an interfering LAP or WAP conditioned on a location-known serving tier-ξ AP being retained in Proposition 5.1.

Proposition 5.1. *Conditioned on the serving tier-ξ AP $\mathbf{z}_0^{\xi}$ transmitting at $(r_0^{\xi},0)$, the retaining probabilities of an interfering LAP $\mathbf{x}_i$ and WAP $\mathbf{y}_j$ are respectively given as follows:*

$$\mathcal{R}_{\xi \mathrm{L}}(\mathbf{x}_i,\lambda_{\mathrm{L}},\lambda_{\mathrm{W}},M) \approx \begin{cases} \mathcal{A}(N_{\mathbf{x}_i,\mathrm{L}},M)/M, \mathbf{x}_i \in V_0^{\xi}(\mathrm{L}) \cap V_1^{\xi}(\mathrm{L}), \\ \dfrac{\mathcal{A}(N_{\mathbf{x}_i,\mathrm{L}} - \lambda_{\xi}\mathcal{V}_{int}(R_{\mathrm{L}},r_0^{\xi},||\mathbf{x}_i||),M)}{M}, \mathbf{x}_i \in V_0^{\xi}(\mathrm{L}) \cap V_2^{\xi}(\mathrm{L}), \\ 0, \quad \textit{Otherwise}, \end{cases} \tag{5.21}$$

$$\mathcal{R}_{\xi \mathrm{W}}(\mathbf{y}_j,\lambda_{\mathrm{L}},\lambda_{\mathrm{W}},M) \approx \begin{cases} \mathcal{A}(N_{\mathbf{y}_j,\mathrm{W}},M)/M, \mathbf{y}_j \in V_0^{\xi}(\mathrm{W}) \cap V_1^{\xi}(\mathrm{W}), \\ \dfrac{\mathcal{A}(N_{\mathbf{y}_j,\mathrm{W}} - \lambda_{\xi}\mathcal{V}_{int}(R_{\mathrm{W}},r_0^{\xi},||\mathbf{y}_j||),M)}{M}, \mathbf{y}_j \in V_0^{\xi}(\mathrm{W}) \cap V_2^{\xi}(\mathrm{W}), \\ 0, \quad \textit{Otherwise}, \end{cases} \tag{5.22}$$

where $V_0^{\xi}(\widehat{\xi}) = \mathcal{B}^c(\mathbf{z}_0^{\xi},\max\{R_{\widehat{\xi}},R_{\xi}\})$, $V_1^{\xi}(\widehat{\xi}) = \mathcal{B}^c(o,r_0^{\xi}+R_{\widehat{\xi}})$, and $V_2^{\xi}(\widehat{\xi}) = \mathcal{B}(o,r_0^{\xi}+R_{\widehat{\xi}})$, if $\xi = \widehat{\xi}$, otherwise, $V_2^{\xi}(\widehat{\xi}) = \mathcal{B}(o,r_0^{\xi}+R_{\widehat{\xi}}) \cap \mathcal{B}^c(o,r_0^{\xi})$, $\widehat{\xi} \in \{\mathrm{L},\mathrm{W}\}$.

Proof. Without loss of generality, we give the derivation of the retaining probability of an interfering LAP $\mathbf{x}_i$. Due to the interfering LAP must use the same UC as the serving tier-ξ AP, the distance between them must be larger than the maximum radius of their sensing regions, i.e., $||\mathbf{x}_i - \mathbf{z}_0^{\xi}|| \geq \max\{R_{\mathrm{L}},R_{\xi}\}$, which can be denoted as $\mathbf{x}_i \in V_0^{\xi}(\mathrm{L})$. As a consequence, the retaining probability of the interfering LAP, which follows $\mathbf{x}_i \in \mathcal{B}(\mathbf{z}_0^{\xi},\max\{R_{\mathrm{L}},R_{\xi}\})$, equals 0. Note that no other tier-ξ APs exist in $\mathcal{B}(o,r_0^{\xi})$ because the serving tier-ξ AP is assumed as the nearest tier-ξ AP. Consequently, if the sensing region of the interfering LAP intersects with $\mathcal{B}(o,r_0^{\xi})$, the expected number of interfering APs in this sensing region will be affected by the area of the intersection between $\mathcal{B}(o,r_0^{\xi})$ and $\mathcal{B}(\mathbf{x}_i,R_{\mathrm{L}})$, which eventually influences the retaining probability of the interfering LAP. Accordingly, as illustrated in Fig. 5.3, the entire plane has been divided into three regions conditioned on that the serving AP is an LAP or a WAP. The outer region, i.e., $V_0^{\xi}(\mathrm{L}) \cap \mathrm{V}_1^{\xi}(\mathrm{L})$, represents no intersection occurs between $\mathcal{B}(o,r_0^{\xi})$ and $\mathcal{B}(\mathbf{x}_i,R_{\mathrm{L}})$; The middle region, i.e., $V_0^{\xi}(\mathrm{L}) \cap \mathrm{V}_2^{\xi}(\mathrm{L})$, represents

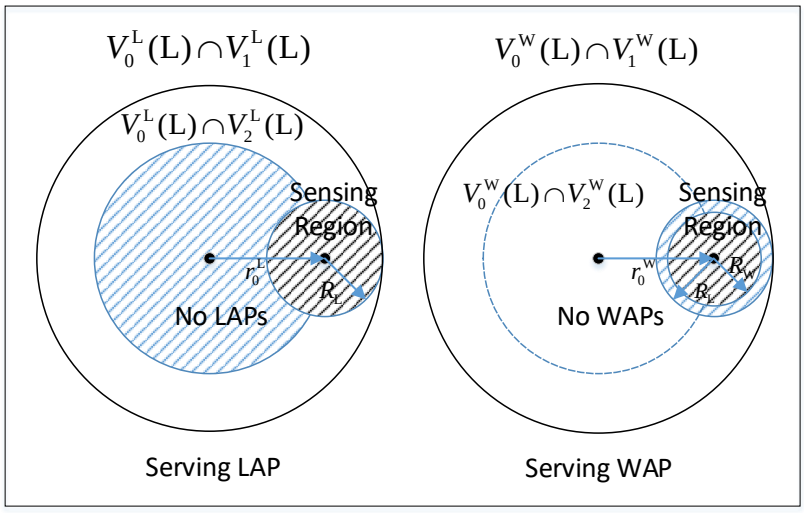

Fig. 5.3 Illustration of the regions for interfering LAPs with serving LAP and WAP

intersection occurs between $\mathcal{B}(o, r_0^{\xi})$ and $\mathcal{B}(\mathbf{x}_i, R_{\mathrm{L}})$. Note that the interfering LAP cannot exist in $\mathcal{B}(o, r_0^{\xi})$ when the serving AP is an LAP, thus $V_2^{\mathrm{L}}(\mathrm{L})$ excludes this circle for the interfering LAPs, differing from $V_2^{\mathrm{W}}(\mathrm{L})$; The inner region, which is the complementary of the two other regions, represents the locations that interfering LAPs cannot occur. By assuming the retaining LAPs have equal probability (i.e., $1/M$) to access one of the M UCs, the retaining probability of an interfering LAP $\mathbf{x}_i$ can be achieved as the result in (5.21). The result for an interfering WAP can be obtained in a way similar to the interfering LAP, which is omitted in this work. It is worthy mentioning that this result is an approximation as we ignores the transmission state of APs in the intersection of $B(\mathbf{x}_i, R_{\mathrm{L}})$ and $B(\mathbf{x}_0, R_{\mathrm{L}})$. If some of these APs are granted transmission, the probability of the interfering AP being retained, which uses the same UC as the serving AP, increases because of less accessible UCs. □

Equipped with the retaining probabilities of the two-tier interfering APs, the Palm coverage probabilities of the LTE-LAA and the WiFi users are given in Lemma 5.3.

Lemma 5.3. *In coexisting LTE-LAA and WiFi networks with M UCs and an SINR threshold of T, conditioned on the serving LAP $\mathbf{x}_0$ located at $(r_0^{\mathrm{L}}, 0)$, the Palm coverage probability of the LUE, denoted by $p_{\mathbf{x}_0}(r_0^{\mathrm{L}}, \lambda_{\mathrm{W}}, \lambda_{\mathrm{L}}, T, M)$, can be approximately obtained as the expression in* (5.23)*. For the WUE, its Palm coverage probability $p_{\mathbf{y}_0}(r_0^{\mathrm{W}}, \lambda_{\mathrm{W}}, \lambda_{\mathrm{L}}, T, M)$ can be approximately obtained as the expression in* (5.24) *conditioned on the serving WAP $\mathbf{y}_0$ located at $(r_0^{\mathrm{W}}, 0)$. $\mathsf{p}(\rho, \theta)$ denotes a point in the Cartesian coordinate system with radius of ρ and angle of θ in the polar coordinate system, which translates the locations of retained interfering APs from the the polar coordinate system into the Cartesian coordinate system, which can be expressed as $\mathsf{p}(\rho, \theta) = (\rho\cos(\theta), \rho\sin(\theta))$.*

$$
\begin{aligned}
p_{\mathbf{x}_0}(r_0^{\mathrm{L}},\lambda_{\mathrm{W}},\lambda_{\mathrm{L}},T,M) &\approx \exp\left(-\int_0^{2\pi}\int_{r_0^{\mathrm{L}}}^{\infty}\frac{\mathcal{R}_{\mathrm{LL}}(\mathsf{p}(\rho,\theta),\lambda_{\mathrm{L}},\lambda_{\mathrm{W}},M)\lambda_{\mathrm{L}}}{1+\frac{l_{\mathrm{L}}(r_0^{\mathrm{L}})}{Tl_{\mathrm{L}}(\rho)}}\rho d\rho d\theta\right)\\
&\times\exp\left(-\int_0^{2\pi}\int_0^{\infty}\frac{\mathcal{R}_{\mathrm{LW}}(\mathsf{p}(\rho,\theta),\lambda_{\mathrm{L}},\lambda_{\mathrm{W}},M)\lambda_{\mathrm{W}}}{1+\frac{P_{\mathrm{L}}l_{\mathrm{L}}(r_0^{\mathrm{L}})}{P_{\mathrm{W}}Tl_{\mathrm{W}}(\rho)}}\rho d\rho d\theta\right)\times\exp\left(-\frac{\mu T\sigma^2}{P_{\mathrm{L}}l_{\mathrm{L}}(r_0^{\mathrm{L}})}\right)
\end{aligned}
\tag{5.23}
$$

$$
\begin{aligned}
p_{\mathbf{y}_0}(r_0^{\mathrm{W}},\lambda_{\mathrm{W}},\lambda_{\mathrm{L}},T,M) &\approx \exp\left(-\int_0^{2\pi}\int_{r_0^{\mathrm{W}}}^{\infty}\frac{\mathcal{R}_{\mathrm{WW}}(\mathsf{p}(\rho,\theta),\lambda_{\mathrm{W}},\lambda_{\mathrm{W}},M)\lambda_{\mathrm{W}}}{1+\frac{l_{\mathrm{W}}(r_0^{\mathrm{W}})}{Tl_{\mathrm{W}}(\rho)}}\rho d\rho d\theta\right)\\
&\times\exp\left(-\int_0^{2\pi}\int_0^{\infty}\frac{\mathcal{R}_{\mathrm{WL}}(\mathsf{p}(\rho,\theta),\lambda_{\mathrm{L}},\lambda_{\mathrm{W}},M)\lambda_{\mathrm{L}}}{1+\frac{P_{\mathrm{W}}l_{\mathrm{W}}(r_0^{\mathrm{W}})}{P_{\mathrm{L}}Tl_{\mathrm{L}}(\rho)}}\rho d\rho d\theta\right)\times\exp\left(-\frac{\mu T\sigma^2}{P_{\mathrm{W}}l_{\mathrm{W}}(r_0^{\mathrm{W}})}\right)
\end{aligned}
\tag{5.24}
$$

Proof. As the Palm coverage probability for a typical WUE can be obtained by some certain parameter exchanges in that of a typical LUE, thus we can focus on the derivation of a typical LUE. According to (5.20), the Palm coverage probability of a typical LUE can be transformed as

$$
p_{\mathbf{x}_0}(r_0^{\mathrm{L}},\lambda_{\mathrm{W}},\lambda_{\mathrm{L}},T,M)=\mathbb{P}\left(\frac{P_{\mathrm{L}}h_0^{\mathrm{LL}}l_{\mathrm{L}}(||\mathbf{x}_0||)}{\widetilde{I}_{\mathrm{LL}}+\widetilde{I}_{\mathrm{LW}}+\sigma^2)}>T|e_0^{\mathrm{L}}=1\right). \tag{5.25}
$$

By incorporating the definition of $\widetilde{I}_{\mathrm{LL}}$ and $\widetilde{I}_{\mathrm{LW}}$, this result can be calculated as follows:

$$
\begin{aligned}
&p_{\mathbf{x}_0}(r_0^{\mathrm{L}},\lambda_{\mathrm{W}},\lambda_{\mathrm{L}},T,M)\\
&=\mathbb{P}\left(\frac{P_{\mathrm{L}}h_0^{\mathrm{LL}}l_{\mathrm{L}}(||\mathbf{x}_0||)}{\sum_{\mathbf{x}_i\in\widetilde{\Phi}_{\mathrm{LL}}/\mathbf{x}_0}P_{\mathrm{L}}h_i^{\mathrm{LL}}l_{\mathrm{L}}(||\mathbf{x}_i||)+\sum_{\mathbf{y}_j\in\widetilde{\Phi}_{\mathrm{LW}}}P_{\mathrm{W}}h_j^{\mathrm{LW}}l_{\mathrm{W}}(||\mathbf{y}_j||)+\sigma^2)}>T|e_0^{\mathrm{L}}=1\right)\\
&=\exp\left(-\frac{\mu T\sigma^2}{P_{\mathrm{L}}l_{\mathrm{L}}(r_0^{\mathrm{L}})}\right)\mathbb{E}_{\widetilde{I}_{\mathrm{LL}}}\left[\exp\left(-\frac{\mu T}{l_{\mathrm{L}}(r_0^{\mathrm{L}})}\sum_{\mathbf{x}_i\in\Phi_{\mathrm{L}}\cap B^c(o,r_0^{\mathrm{L}})}h_i^{\mathrm{LL}}l_{\mathrm{L}}(||\mathbf{x}_i||)e_{\mathbf{x}_i)}^{\mathrm{LL}}\,\middle|\,e_0^{\mathrm{L}}=1\right)\right]\\
&\times\mathbb{E}_{\widetilde{I}_{\mathrm{LW}}}\left[\exp\left(-\frac{\mu T}{l_{\mathrm{L}}(r_0^{\mathrm{L}})}\frac{P_{\mathrm{W}}}{P_{\mathrm{L}}}\sum_{\mathbf{y}_j\in\Phi_{\mathrm{W}}}h_j^{\mathrm{LW}}l_{\mathrm{W}}(||\mathbf{y}_j||)e_{\mathbf{y}_j)}^{\mathrm{LW}}\,\middle|\,e_0^{\mathrm{L}}=1\right)\right],
\end{aligned}
\tag{5.26}
$$

where $e_{\mathbf{x}_i}^{\mathrm{LL}}$ and $e_{\mathbf{y}_j}^{\mathrm{LW}}$ respectively denote the retaining indicators of the interfering LAP $\mathbf{x}_i$ and the interfering WAP $\mathbf{y}_j$, which equals 1 when the AP retains and equals 0 otherwise. Based on the retaining probability of the interfering LAP in (5.21), the expectation of the aggregate

interference power $\widetilde{I}_{\mathrm{LL}}$ generated by the retained interfering LAPs can be approximated as:

$$\begin{aligned}&\mathbb{E}_{\widetilde{I}_{\mathrm{LL}}}\left[\exp\left(-\frac{\mu T}{l_{\mathrm{L}}(r_0^{\mathrm{L}})}\sum_{\mathbf{x}_i\in\Phi_{\mathrm{L}}\cap B^c(o,r_0^{\mathrm{L}})}h_i^{\mathrm{LL}}l_{\mathrm{L}}(||\mathbf{x}_i||)e_{\mathbf{x}_i)}^{\mathrm{LL}}\,|e_0^{\mathrm{L}}=1\right)\right]\\ \approx&\exp\left(-\lambda_{\mathrm{L}}\int_{\mathbb{R}^2/B(0,r_0^{\mathrm{L}})}\mathcal{V}_{\mathrm{LL}}(x,\lambda_{\mathrm{L}},\lambda_{\mathrm{W}},M)\left(1-\mathbb{E}_{h_i^{\mathrm{LL}}}\left[\exp(-h_i^{\mathrm{LL}}\frac{\mu T}{l_{\mathrm{L}}(r_0^{\mathrm{L}})}l_{\mathrm{L}}(x))\right]\right)dx\right),\end{aligned} \tag{5.27}$$

which is obtained by the moment generating function for an inhomogeneous PPP [115]. By calculating the expectation of h_i^{LL}, we have:

$$\begin{aligned}&\mathbb{E}_{\widetilde{I}_{\mathrm{LL}}}\left[\exp\left(-\frac{\mu T}{l_{\mathrm{L}}(r_0^{\mathrm{L}})}\sum_{\mathbf{x}_i\in\Phi_{\mathrm{L}}\cap B^c(o,r_0^{\mathrm{L}})}h_i^{\mathrm{LL}}l_{\mathrm{L}}(||\mathbf{x}_i||)e_{\mathbf{x}_i)}^{\mathrm{LL}}\,|e_0^{\mathrm{L}}=1\right)\right]\\ =&\exp\left(-\int_{\mathbb{R}^2/B(0,r)}\frac{\mathcal{V}_{\mathrm{LL}}(x,\lambda_{\mathrm{L}},\lambda_{\mathrm{W}},M)\lambda_{\mathrm{L}}}{1+\frac{l_{\mathrm{L}}(r)}{Tl_{\mathrm{L}}(||x||)}}dx\right)\\ \overset{(a)}{=}&\exp\left(-\int_0^{2\pi}\int_r^{\infty}\frac{\mathcal{V}_{\mathrm{LL}}(\mathrm{p}(\rho,\theta),\lambda_{\mathrm{L}},\lambda_{\mathrm{W}},M)\lambda_{\mathrm{L}}}{1+\frac{l_{\mathrm{L}}(r)}{Tl_{\mathrm{L}}(\rho)}}\rho d\rho d\theta\right),\end{aligned} \tag{5.28}$$

where step (a) is obtained by transforming an arbitrary point in the Cartesian coordinate system into the Polar coordinate system. Consequently, the expectation of the aggregate interference power $\widetilde{I}_{\mathrm{LL}}$ is achieved. Similarly, the expectation of the aggregate interference power from WAPs can be obtained as follows:

$$\begin{aligned}&\mathbb{E}\left[\exp\left(-\frac{\mu T}{l_{\mathrm{L}}(r_0^{\mathrm{L}})}\frac{P_{\mathrm{W}}}{P_{\mathrm{L}}}\sum_{\mathbf{y}_j\in\Phi_{\mathrm{W}}}h_j^{\mathrm{LW}}l_{\mathrm{W}}(||\mathbf{y}_j||)\tilde{e}_{\mathbf{y}_j)}^{\mathrm{LM}}\,|\tilde{e}_0^{\mathrm{L}}=1\right)\right]\\ =&\exp\left(-\int_0^{2\pi}\int_0^{\infty}\frac{\mathcal{V}_{\mathrm{LW}}(\mathrm{p}(\rho,\theta),\lambda_{\mathrm{L}},\lambda_{\mathrm{W}},M)\lambda_{\mathrm{W}}}{1+\frac{P_{\mathrm{L}}l_{\mathrm{L}}(r_0^{\mathrm{L}})}{P_{\mathrm{W}}Tl_{\mathrm{W}}(\rho)}}\rho d\rho d\theta\right).\end{aligned} \tag{5.29}$$

Combining the results in (5.28) and (5.29), we can obtain the Palm coverage probability of the LUE. As aforementioned, the Palm coverage probability of a typical WUE can be obtained in a way similar as the LUE. Thus the final results in Lemma 5.3 have been yielded. □

The Palm coverage probability can be utilised to obtain the coverage probability of a UE if the location of its serving AP is known. As the PDF of the distance between a UE and its serving AP has already been obtained in Section 5.3.1, the coverage probability of a UE can be obtained by removing the condition on the serving AP location from the results in

Lemma 5.3. The coverage probability is critical for the STP, which will be discussed in the next subsection.

5.3.3 The Successful Transmission Probability

Recall that the STP of a typical UE is defined as the probability of the UE's SINR being larger than a threshold T while its serving AP being retained. Combining the results in Corollary 5.1 with those in Lemma 5.3, we present the the STPs of the LUE and the WUE in Theorem 5.1.

Theorem 5.1. *In coexisting LTE-LAA and WiFi networks with M UCs and an SINR threshold of T, the STPs of an LUE and a WUE, denoted respectively by $p_0^{\mathrm{L}}(\lambda_{\mathrm{W}},\lambda_{\mathrm{L}},T,M)$ and $p_0^{\mathrm{W}}(\lambda_{\mathrm{W}},\lambda_{\mathrm{L}},T,M)$, can be approximated as follows:*

$$\mathcal{P}_{\mathrm{st}}^{\mathrm{L}}(\lambda_{\mathrm{W}},\lambda_{\mathrm{L}},T,M) \approx \mathbb{P}(e_0^{\mathrm{L}}=1)\int_0^{\infty} p_{\mathbf{x}_0}(r,\lambda_{\mathrm{W}},\lambda_{\mathrm{L}},T,M) f_{r_0^{\mathrm{L}}}(r)dr, \tag{5.30}$$

$$\mathcal{P}_{\mathrm{st}}^{\mathrm{W}}(\lambda_{\mathrm{W}},\lambda_{\mathrm{L}},T,M) \approx \mathbb{P}(e_0^{\mathrm{W}}=1)\int_0^{\infty} p_{\mathbf{y}_0}(r,\lambda_{\mathrm{W}},\lambda_{\mathrm{L}},T,M) f_{r_0^{\mathrm{W}}}(r)dr. \tag{5.31}$$

Since the terms $\mathbb{P}(e_0^{\mathrm{L}}=1)$, $\mathbb{P}(e_0^{\mathrm{W}}=1)$, $p_{\mathbf{x}_0}(r,\lambda_{\mathrm{W}},\lambda_{\mathrm{L}},T,M)$, and $p_{\mathbf{y}_0}(r,\lambda_{\mathrm{W}},\lambda_{\mathrm{L}},T,M)$ correlate with the function $\mathcal{A}(\cdot)$ given in (5.4), which contains the upper incomplete Gamma function, closed-form results of the STPs are difficult to obtain. The accuracy of the STPs in (21) and (22) is validated through comparison with simulation results, which are based on $10,000$ realizations of random locations of LAPs and WAPs with the typical LUE or WUE at the origin. In each realization, the closest LAP and WAP are selected as the serving AP for the LUE and the WUE, respectively, and the retaining states of all APs are determined according to our proposed medium access scheme in Section 5.2.3. If the serving AP is not retained, then the SINR of the typical UE is set as 0. We assume that the retained LAPs and WAPs each independently have the probability of $1/M$ to access the same channel as the serving AP. The simulation parameters are listed in Table 5.1 unless otherwise specified.

Fig. 5.4a and Fig. 5.4b respectively plot the theoretical and simulated STPs of a typical LUE and a typical WUE, versus the SINR threshold for $\lambda_{\mathrm{L}} = \{400,800,1200\}$ LAPs per km^2 and $\lambda_{\mathrm{W}} = \{400,800\}$ WAPs per km^2. Firstly, the results show that the theoretical STPs closely match the simulated STPs, validating the accuracy of our analytical expressions of the STPs. Secondly, the STP of an LUE does not always increase with the LAP density. This is because the increased coverage probability, due to the shorter serving-LAP distance, cannot compensate for the decreased serving-LAP MAP for low to medium values of the SINR thresholds. Thirdly, the STP of a WUE degrades significantly with the increase of the LAP density. This degradation can be reduced by deploying more WAPs in the network.

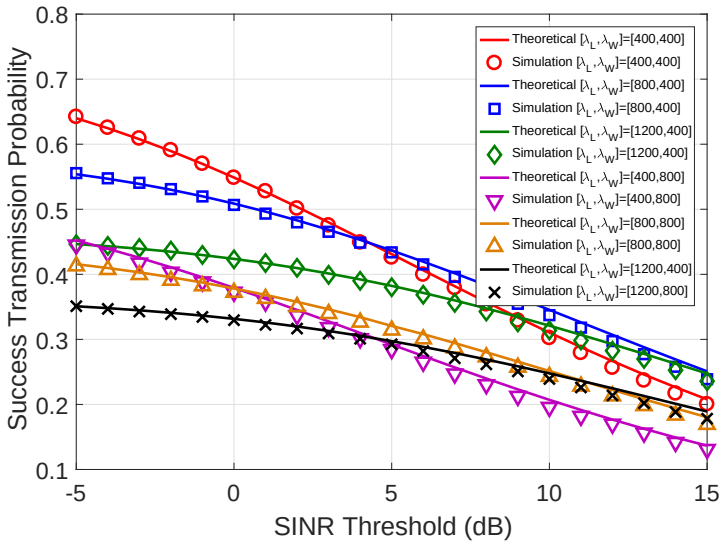

(a) The STP of the LUE

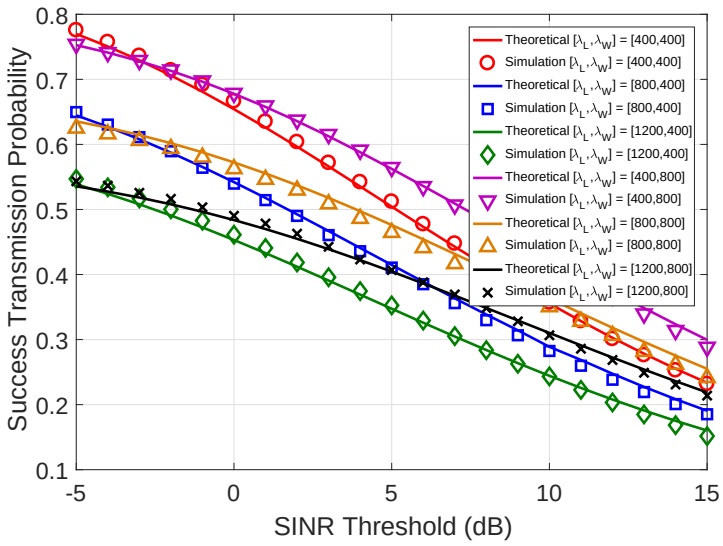

(b) The STP of the WUE

Fig. 5.4 The validation of STPs versus the SINR threshold

In order to reduce the computational complexity of STPs in numerical analysis, we derive a closed-form lower bound (LB) of the coverage probability, which is then combined with (14) to obtain the LBs of STPs. The LBs of STPs are provided in Corollary 5.2.

Corollary 5.2. *Assuming the thermal noise power $\sigma^2 = 0$, the lower bounds of the STPs for the typical LUE and the typical WUE are respectively obtained as follows:*

$$\mathcal{P}_{\mathrm{st}}^{\mathrm{L}}(\lambda_{\mathrm{L}},\lambda_{\mathrm{W}},T,M) \geq \frac{M\cdot\mathbb{P}(e_0^{\mathrm{L}}=1)}{M+T^{\frac{2}{\alpha}}(\mathrm{sinc}^{-1}(\frac{2\pi}{\alpha})-{}_2F^1(1,\frac{2}{\alpha};1+\frac{2}{\alpha};-\frac{1}{T})+\frac{\lambda_{\mathrm{W}}}{\lambda_{\mathrm{L}}}(\frac{P_{\mathrm{W}}}{P_{\mathrm{L}}})^{\frac{2}{\alpha}}\mathrm{sinc}^{-1}(\frac{2\pi}{\alpha}))}, \tag{5.32}$$

$$\mathcal{P}_{\mathrm{st}}^{\mathrm{W}}(\lambda_{\mathrm{L}},\lambda_{\mathrm{W}},T,M) \geq \frac{M\cdot\mathbb{P}(e_0^{\mathrm{W}}=1)}{M+T^{\frac{2}{\alpha}}(\mathrm{sinc}^{-1}(\frac{2\pi}{\alpha})-{}_2F^1(1,\frac{2}{\alpha};1+\frac{2}{\alpha};-\frac{1}{T})+\frac{\lambda_{\mathrm{L}}}{\lambda_{\mathrm{W}}}(\frac{P_{\mathrm{L}}}{P_{\mathrm{W}}})^{\frac{2}{\alpha}}\mathrm{sinc}^{-1}(\frac{2\pi}{\alpha}))}. \tag{5.33}$$

Proof. According to Theorem 5.1, the STP of a typical LUE can be expressed as follows with $\sigma^2 = 0$:

$$\mathcal{P}_{\mathrm{st}}^{\mathrm{L}}(\lambda_{\mathrm{W}},\lambda_{\mathrm{L}},T,M) \approx \mathbb{P}(e_0^{\mathrm{L}}=1)\int_0^{\infty}\mathcal{L}_{\widetilde{I}_{\mathrm{LL}}}(\frac{T_{\mathrm{L}}}{l_{\mathrm{L}}(r)})\mathcal{L}_{\widehat{I}_{\mathrm{LW}}}(\frac{T_{\mathrm{L}}}{l_{\mathrm{L}}(r)})f_{r_0^{\mathrm{L}}}(r)dr, \tag{5.34}$$

where the functions $\mathcal{L}_{\widetilde{I}_{\mathrm{LL}}}(\frac{T_{\mathrm{L}}}{l_{\mathrm{L}}(r)})$ and $\mathcal{L}_{\widehat{I}_{\mathrm{LW}}}(\frac{T_{\mathrm{L}}}{l_{\mathrm{L}}(r)})$ denote the Laplace transforms of the aggregate interference power from retained interfering LAPs and WAPs, respectively. Note that the value of function $\mathcal{A}(\cdot)$ is always smaller than $1/M$, then we have:

$$\mathcal{L}_{\widetilde{I}_{\mathrm{LL}}}(\frac{T}{l_{\mathrm{L}}(r)}) \geq \exp\left(-\int_0^{2\pi}\int_r^{\infty}\frac{\lambda_{\mathrm{L}}/M}{1+\frac{l_{\mathrm{L}}(r)}{Tl_{\mathrm{L}}(\rho)}}\rho d\rho d\theta\right). \tag{5.35}$$

According to [99], the expression in (5.36) can be translated into the following form as:

$$\mathcal{L}_{\widetilde{I}_{\mathrm{LL}}}(\frac{T}{l_{\mathrm{L}}(r)}) \geq \exp\left(-\pi\frac{\lambda_{\mathrm{L}}}{M}r^2T^{\frac{2}{\alpha}}(\mathrm{sinc}^{-1}(\frac{2\pi}{\alpha})-{}_2F^1(1,\frac{2}{\alpha};1+\frac{2}{\alpha};-\frac{1}{T}))\right) \triangleq \mathcal{H}_{\mathrm{LL}}(\frac{T}{l_{\mathrm{L}}(r)}). \tag{5.36}$$

Similarly, the LB of $\mathcal{L}_{\widehat{I}_{\mathrm{LW}}}(\frac{T_{\mathrm{L}}}{l_{\mathrm{L}}(r)})$ can be obtained as:

$$\begin{aligned}\mathcal{L}_{\widehat{I}_{\mathrm{LW}}}(\frac{T}{l_{\mathrm{L}}(r)}) &\geq \exp\left(-\int_0^{2\pi}\int_0^{\infty}\frac{\lambda_{\mathrm{W}}/M}{1+\frac{P_{\mathrm{L}}l_{\mathrm{L}}(r)}{P_{\mathrm{W}}Tl_{\mathrm{W}}(\rho)}}\rho d\rho d\theta\right)\\ &= \exp\left(-\pi\frac{\lambda_{\mathrm{W}}}{M}r^2\left(\frac{P_{\mathrm{W}}}{P_{\mathrm{L}}}T_{\mathrm{L}}\right)^{\frac{2}{\alpha}}\mathrm{sinc}^{-1}(\frac{2\pi}{\alpha})\right) \triangleq \mathcal{H}_{\mathrm{LW}}(\frac{T}{l_{\mathrm{L}}(r)}).\end{aligned} \tag{5.37}$$

By incorporating the expressions in (5.36) and (5.37) into (5.34), we can achieve the LB of the STP for an LUE as the result in Corollary 5.2. The LB of the STP for a WUE can be obtained correspondingly, which is thus omitted in this work. □

5.3.4 UE Throughput, Spatial Throughput and Spatial Spectrum Efficiency

In this subsection, the UE throughput, the STH and the SSE are analysed based on the STP. Moreover, the asymptotic STH and SSE with the LAP density approaching infinity in a multi-UC scenario is derived. The LUE and WUE throughputs, which are respectively defined as the expressions in (5.12) and (5.13), are given in Corollary 5.3.

Corollary 5.3. *In coexisting LTE-LAA and WiFi networks with M UCs, LTE-LAA SINR threshold of T_L, and WiFi SINR threshold of T_W, the LUE and WUE throughputs, respectively denoted by $\mathcal{C}_{\mathrm{L}}(\lambda_{\mathrm{L}},\lambda_{\mathrm{W}},T_{\mathrm{L}},M)$ and $\mathcal{C}_{\mathrm{W}}(\lambda_{\mathrm{L}},\lambda_{\mathrm{W}},T_{\mathrm{W}},M)$, are given by:*

$$\mathcal{C}_{\mathrm{L}}(\lambda_{\mathrm{L}},\lambda_{\mathrm{W}},T_{\mathrm{L}},M) = B\log(1+T_{\mathrm{L}})\mathcal{P}_{\mathrm{st}}^{\mathrm{L}}(\lambda_{\mathrm{L}},\lambda_{\mathrm{W}},T_{\mathrm{L}},M), \tag{5.38}$$

$$\mathcal{C}_{\mathrm{W}}(\lambda_{\mathrm{L}},\lambda_{\mathrm{W}},T_{\mathrm{W}},M) = B\log(1+T_{\mathrm{W}})\mathcal{P}_{\mathrm{st}}^{\mathrm{W}}(\lambda_{\mathrm{L}},\lambda_{\mathrm{W}},T_{\mathrm{W}},M). \tag{5.39}$$

Proof. By substituting the corresponding parts in (5.12) and (5.13) with the STPs in (5.30) and (5.31) given in Theorem 5.1, the final results can be achieved. □

The STH and the SSE can be obtained by incorporating the results in Corollary 5.3 into their definitions in (5.14) and (5.15). In the following, we will give the asymptotic STH and SSE with LAP density approaching infinity.

Corollary 5.4. *When the LAP density becomes very large ($\lambda_{\mathrm{L}} \to \infty$), the STH and the SSE converge to $\frac{MB\log(1+T_{\mathrm{L}})}{\pi R_{\mathrm{L}}^2}$ and $\frac{\log(1+T_{\mathrm{L}})}{\pi R_{\mathrm{L}}^2}$, respectively, where R_L is the sensing radius of an LAP, T_{L} is the LTE-LAA SINR threshold, M is the number of UCs, and B is the bandwidth per UC.*

Proof. By definition, the STH can be expressed as:

$$\mathcal{C}_{\mathrm{STH}}(\lambda_{\mathrm{L}},\lambda_{\mathrm{W}},T_{\mathrm{L}},T_{\mathrm{W}},M) = \lambda_{\mathrm{L}}\mathcal{C}_{\mathrm{L}}(\lambda_{\mathrm{L}},\lambda_{\mathrm{W}},T_{\mathrm{L}},M) + \lambda_{\mathrm{W}}\mathcal{C}_{\mathrm{W}}(\lambda_{\mathrm{L}},\lambda_{\mathrm{W}},T_{\mathrm{L}},M). \tag{5.40}$$

The first term on the r.h.s of (5.40) is calculated as follows when $\lambda_{\mathrm{L}} \to \infty$:

$$\begin{aligned}
&\lim_{\lambda_{\mathrm{L}}\to\infty} \lambda_{\mathrm{L}} \mathcal{C}_{\mathrm{L}}(\lambda_{\mathrm{L}}, \lambda_{\mathrm{W}}, T_{\mathrm{L}}, M) \\
=&B\log(1+T_{\mathrm{L}}) \lim_{\lambda_{\mathrm{L}}\to\infty} \lambda_{\mathrm{L}} \mathbb{E}_{r_0^{\mathrm{L}}} \left[\mathbb{P}(\mathbf{e}_0^{\mathrm{L}}=1|\mathbf{x}_0=(r_0^{\mathrm{L}},0))\mathbb{P}(\mathrm{SINR}_0^{\mathrm{L}} > T_{\mathrm{L}}|\mathbf{e}_0^{\mathrm{L}}=1, \mathbf{x}_0=(r_0^{\mathrm{L}},0))\right] \\
=&B\log(1+T_{\mathrm{L}}) \int_0^{\infty} \lim_{\lambda_{\mathrm{L}}\to\infty} \lambda_{\mathrm{L}} \mathbb{P}(\mathbf{e}_0^{\mathrm{L}}=1|\mathbf{x}_0=(r,0))\mathbb{P}(\mathrm{SINR}_0^{\mathrm{L}} > T_{\mathrm{L}}|\mathbf{e}_0^{\mathrm{L}}=1, \mathbf{x}_0=(r,0)) f_{r_0^{\mathrm{L}}}(r) dr.
\end{aligned} \tag{5.41}$$

Note that $\lim_{\lambda_{\mathrm{L}}\to\infty} f_{r_0^{\mathrm{L}}}(r) = \lim_{\lambda_{\mathrm{L}}\to\infty} 2\pi\lambda_{\mathrm{L}} r \exp(-\pi\lambda_{\mathrm{L}} r^2) = \delta(r)$, where $\delta(\cdot)$ is the Dirac delta function. This is because $f_{r_0^{\mathrm{L}}}(r)$ is the serving-LAP-distance PDF function, we have $\int_0^{\infty} \lim_{\lambda_{\mathrm{L}}\to\infty} f_{r_0^{\mathrm{L}}}(r) dr = 1$, and $\lim_{\lambda_{\mathrm{L}}\to\infty} 2\pi\lambda_{\mathrm{L}} r \exp(-\pi\lambda_{\mathrm{L}} r^2)$ equals zero if $r > 0$. As a result, $\lim_{\lambda_{\mathrm{L}}\to\infty} f_{r_0^{\mathrm{L}}}(r)$ matches the property of the Dirac delta function. Moreover, the term $\lim_{\lambda_{\mathrm{L}}\to\infty} \lambda_{\mathrm{L}} \mathbb{P}(\mathbf{e}_0^{\mathrm{L}}=1|\mathbf{x}_0=(r,0))$ in (5.41) can be transformed as follows:

$$\begin{aligned}
&\lim_{\lambda_{\mathrm{L}}\to\infty} \lambda_{\mathrm{L}} \mathbb{P}(\mathbf{e}_0^{\mathrm{L}}=1|\mathbf{x}_0=(r,0)) \overset{(a)}{=} \lim_{\lambda_{\mathrm{L}}\to\infty} \lambda_{\mathrm{L}} \mathcal{A}(N_{o,\mathrm{L}} - \lambda_{\mathrm{L}} \mathcal{V}_{\mathrm{int}}(r, R_{\mathrm{L}}, r), M) \\
&= \lim_{\lambda_{\mathrm{L}}\to\infty} \lambda_{\mathrm{L}} \mathcal{A}((\lambda_{\mathrm{L}}+\lambda_{\mathrm{W}})\pi R_{\mathrm{L}}^2 - \lambda_{\mathrm{L}} \mathcal{V}_{\mathrm{int}}(r, R_{\mathrm{L}}, r), M).
\end{aligned} \tag{5.42}$$

By denoting the term $(\lambda_{\mathrm{L}}+\lambda_{\mathrm{W}})\pi R_{\mathrm{L}}^2 - \lambda_{\mathrm{L}} \mathcal{V}_{\mathrm{int}}(r, R_{\mathrm{L}}, r)$ as $N'_{o,\mathrm{L}}$, and combining with the expression of function $\mathcal{A}(\cdot)$ in (5.4), we have

$$\begin{aligned}
&\lim_{\lambda_{\mathrm{L}}\to\infty} \lambda_{\mathrm{L}} \mathbb{P}(\mathbf{e}_0^{\mathrm{L}}=1|\mathbf{x}_0=(r,0)) \\
&= \lim_{\lambda_{\mathrm{L}}\to\infty} \frac{\lambda_{\mathrm{L}}}{N'_{o,\mathrm{L}}} \left[M + \frac{\Gamma(M+1, N'_{o,\mathrm{L}})}{\Gamma(M+1,0)} + (N'_{o,\mathrm{L}} - 1 - M) \frac{\Gamma(M+2, N'_{o,\mathrm{L}})}{\Gamma(M+2,0)} - e^{-N'_{o,\mathrm{L}}} \frac{N'^{M+1}_{o,\mathrm{L}}}{\Gamma(M+2,0)} \right].
\end{aligned} \tag{5.43}$$

We first note that $\lim_{\lambda_{\mathrm{L}}\to\infty} \frac{N'_{o,\mathrm{L}}}{\lambda_{\mathrm{L}}} = \pi R_{\mathrm{L}}^2 - \mathcal{V}_{\mathrm{int}}(r, R_{\mathrm{L}}, r)$. Then based on the property of the upper incomplete Gamma function $\Gamma(\widehat{b}, a)$, we have $\lim_{\lambda_{\mathrm{L}}\to\infty} \Gamma(\widehat{b}, N'_{o,\mathrm{L}}) = 0$. Moreover, according to Wolfram Mathematica, the function $\Gamma(\widehat{b}, a)$ can be expanded as the following expression when $a \to \infty$:

$$\lim_{a\to\infty} \Gamma(\widehat{b}, a) = \exp(-a) a^{\widehat{b}} \left(\frac{1}{a} + \frac{\widehat{b}-1}{a^2} + O((\frac{1}{a})^3) \right). \tag{5.44}$$

Based on the L'Hospital's rule, we can have $\lim_{a\to\infty} a^{M+1} e^{-a} = 0$ and $\lim_{a\to\infty} a\Gamma(\widehat{b}, a) = 0$. Therefore, the result in (5.43) can be obtained as $\frac{M}{\pi R_{\mathrm{L}}^2 - \mathcal{V}_{\mathrm{int}}(r, R_{\mathrm{L}}, r)}$. After this, we derive the upper and lower bounds of the term $\lim_{\lambda_{\mathrm{L}}\to\infty} \mathbb{P}\left(\mathrm{SINR}_0^{\mathrm{L}} > T_{\mathrm{L}}|\mathbf{e}_0^{\mathrm{L}}=1, \mathbf{x}_0=(r,0)\right)$, which can

be expressed as follows based on (5.36) and (5.37) in the proof of Corollary 5.2:

$$\mathcal{H}_{\mathrm{LL}}(\frac{T_{\mathrm{L}}}{l_{\mathrm{L}}(r)})\mathcal{H}_{\mathrm{LW}}(\frac{T_{\mathrm{L}}}{l_{\mathrm{L}}(r)}) \leq \mathbb{P}\left(\mathrm{SINR}_0^{\mathrm{L}} > T_{\mathrm{L}} | \mathbf{e}_0^{\mathrm{L}} = 1, \mathbf{x}_0 = (r,0)\right) \leq 1. \tag{5.45}$$

According to the property of the Dirac delta function, which satisfies $\int_0^\infty f(r)\delta(r)dr = f(0)$ where $f(\cdot)$ is an arbitrary continuous compactly supported function, the lower bound and upper bound of the STH provided by LAPs are expressed as follows:

$$\frac{M}{\pi R_{\mathrm{L}}^2} \leq \lim_{\lambda_{\mathrm{L}}\to\infty} \lambda_{\mathrm{L}} C_{\mathrm{L}}(\lambda_{\mathrm{L}}, \lambda_{\mathrm{W}}, T_{\mathrm{L}}, M) \leq \frac{M}{\pi R_{\mathrm{L}}^2}. \tag{5.46}$$

Due to the values of the upper and lower bounds are identical, the STH provided by LAPs converges to $\frac{M}{\pi R_{\mathrm{L}}^2}$. On the other hand, the STH provided by WAPs equals 0 with λ_{L} approaching infinity because the MAP of a typical WAP and the coverage probability of its serving UE are both close to 0. Consequently, the STH of the two-tier HetNet yields to $\frac{MB\log(1+T_{\mathrm{L}})}{\pi R_{\mathrm{L}}^2}$ with $\lambda_{\mathrm{L}} \to \infty$. Accordingly, the SSE converges to $\frac{\log(1+T_{\mathrm{L}})}{\pi R_{\mathrm{L}}^2}$. □

We can see that the asymptotic STH increases with the total bandwidth and T_{L} and decrease with R_{L}, this is because that the coverage probability of the LUE is close to 1 for an arbitrary finite threshold when the LAP density approaches infinity, while the asymptotic SSE increases with T_{L} and decrease with R_{L}. Both STH and SSE are mainly influenced by the parameters in the LTE-LAA network. This is because that the STH provided by WAPs is negligible when the LAP density approaches infinity. The results in Corollary 5.4 can be used to provide design insights into how the deployment density of LAPs should be selected according to the number of available UCs.

5.4 Numerical Results and Discussions

In this section, we present numerical results to how the LUE and WUE throughputs, as well as the STH and SSE, are affected by the SINR thresholds, the LAP density, and the number of UCs. The fairness between the LUEs and the WUEs is analysed with respect to the LAP sensing region factor κ_{L}. The values of parameters used in the numerical results are listed in Table 5.1 unless otherwise specified.

5.4.1 Analysis of LUE and WUE Throughputs

Fig. 5.5a and Fig. 5.5b respectively plot the LUE throughput and the WUE throughput versus the SINR threshold. In Fig. 5.5a, conditioned on the same LAP density, the LUE

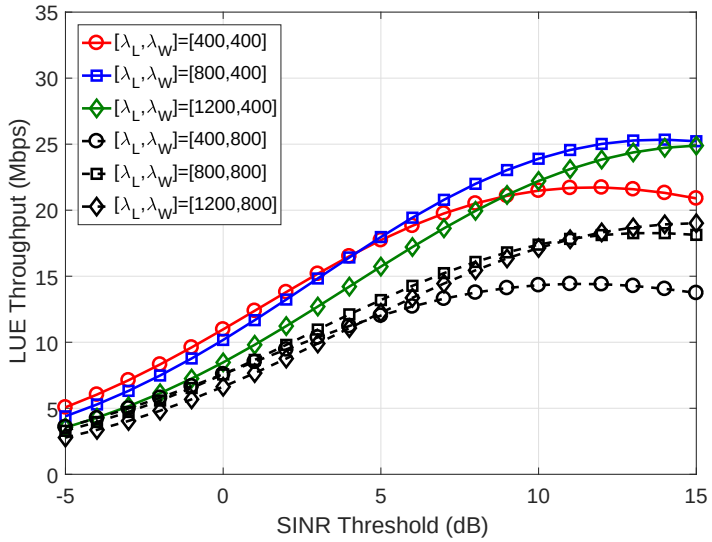

(a) The LUE throughput

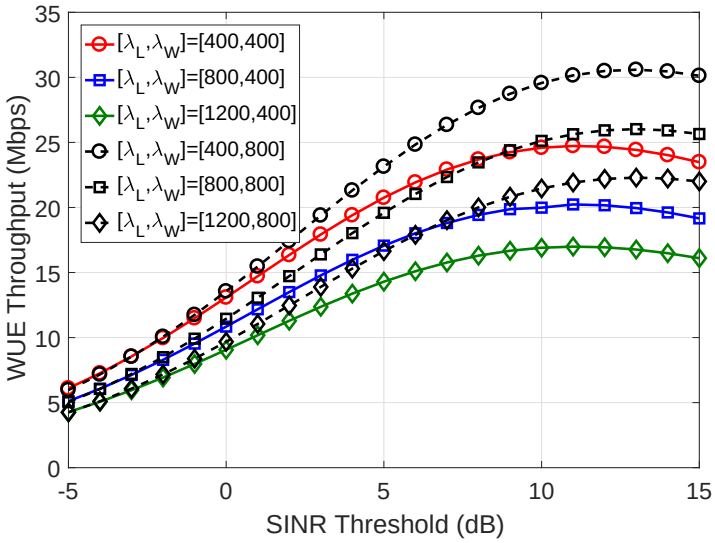

(b) The WUE throughput

Fig. 5.5 The UE throughputs versus the SINR threshold

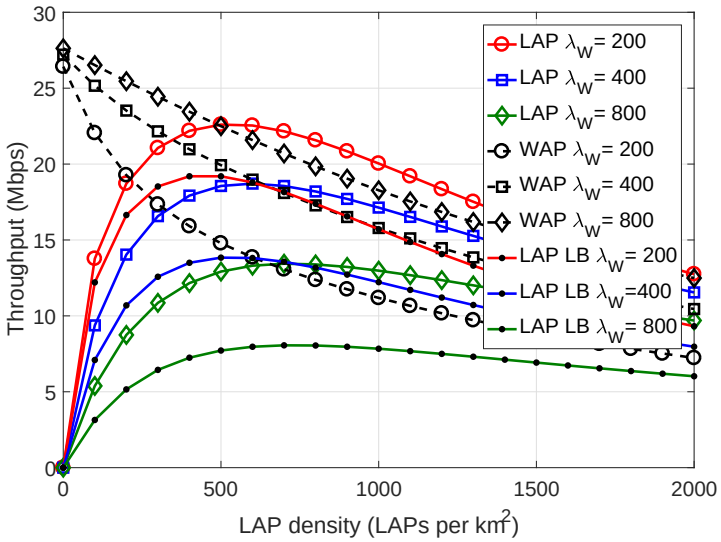

Fig. 5.6 The LUE and WUE throughputs versus the LAP density for several WAP densities (200, 400, and 800 WAPs per km^2)

throughput obtained in a higher WAP density is always smaller than that in a lower WAP density. In Fig. 5.5b, conditioned on the same LAP or WAP density, the WUE throughput obtained in a higher LAP or WAP density is always smaller than that in a lower LAP or WAP density, respectively. Accordingly, the SINR threshold has limited effect on the trend of UE throughput, i.e., under the same AP density of a specific tier, the throughput curves for a high AP density of the other tier are always above those for a low AP density of the other tier. In this paper, we set the SINR threhold as 5 dB without loss of generality, where a relative average UE throughput is achieved.

Fig. 5.6 illustrates both the LUE and WUE throughputs versus the LAP density for WAP density of 200, 400 and 800 WAPs per km^2. The result shows that, with the increase of LAP density, the WUE throughput decreases monotonically, while the LUE throughput increases with the LAP density under low LAP densities and decreases under high LAP densities. The main reason for the decrease of LUE throughput is that the coverage probability enhancement for the LUE is negligible under a high LAP density but the MAP of the serving-AP decreases with the increase of LAP density. The LUE throughput curves indicate that the optimal LAP density for maximizing the LUE throughput exists. Additionally, the LB of LUE throughput, which is obtained based on the LB of the STP of the LUE, is also illustrated in Fig. 5.6. We can see that the optimal LAP density maximizing the LUE throughput obtained by the LB result is very close to that obtained by the theoretical expression in (5.38). This shows that the LB of LUE throughput can be used to find the optimal LAP density with a low computational complexity.

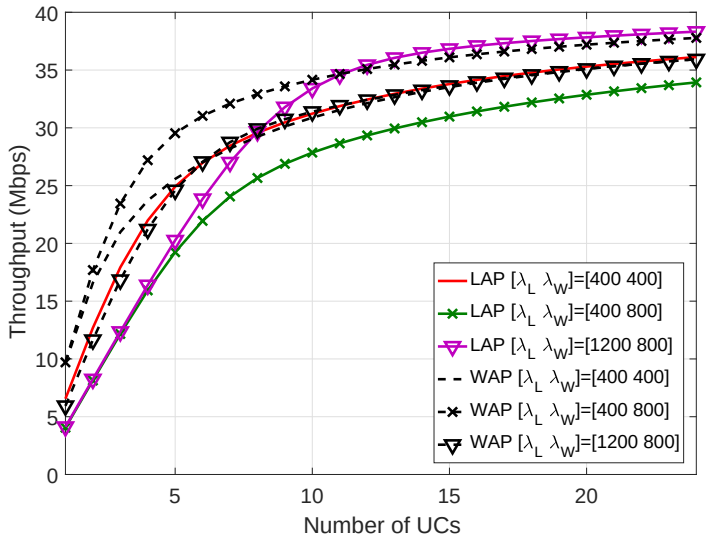

Fig. 5.7 The LUE and WUE throughputs versus the number of UCs for several typical densities of LAPs and WAPs

In Fig. 5.7, the LUE and WUE throughputs are both plotted versus the number of UCs for several typical LAP and WAP densities. The results show that both throughputs increase monotonically with more UCs. In the high density scenario with $\lambda_{\mathrm{L}} = 1200$ LAPs per km^2 and $\lambda_{\mathrm{W}} = 800$ WAPs per km^2, the LUE throughput with 10 UCs approximately increases 6 times as compared with that with single UC, while the WUE throughput with 10 UCs are 5 times greater than that with single UCs. However, even with 24 UCs, the LUE throughput and the WUE throughput can only increase 6.5 times and 6 times as compared with those with single UC, respectively, which are close to the throughput enhancement provided by 10 UCs. In the low density scenario with $\lambda_{\mathrm{L}} = 400$ LAPs per km^2 and $\lambda_{\mathrm{W}} = 400$ WAPs per km^2, as compared with the LUE and WUE throughputs with single UC, the throughput enhancements for the LUE and the WUE provide with 24 UCs are close to those with 5 UCs, respectively. Accordingly, appropriate number of UCs shared among LTE-LAA and WiFi networks should be determined based on the LAP and WAP density, and more number of UCs should be allocated in a scenario with higher density of APs.

5.4.2 Analysis of Spatial Throughput and Spatial Spectral Efficiency

Fig. 5.8a and Fig. 5.8b respectively depict the STH and the SSE of the whole two-tier HetNet versus the LAP density with the WAP density being 200, 400 and 800 WAPs per km^2 for $M = 1, 3$. In most cases, the STH and SSE both increase monotonically with the increase of LAP density. Exceptions occur within the range of $[0, 300]$ LAPs per km^2, in which both of

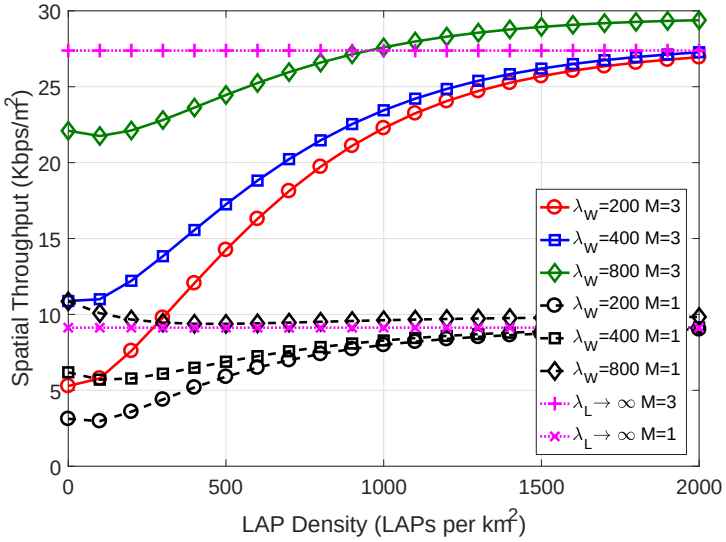

(a) The STH of the two-tier HetNet

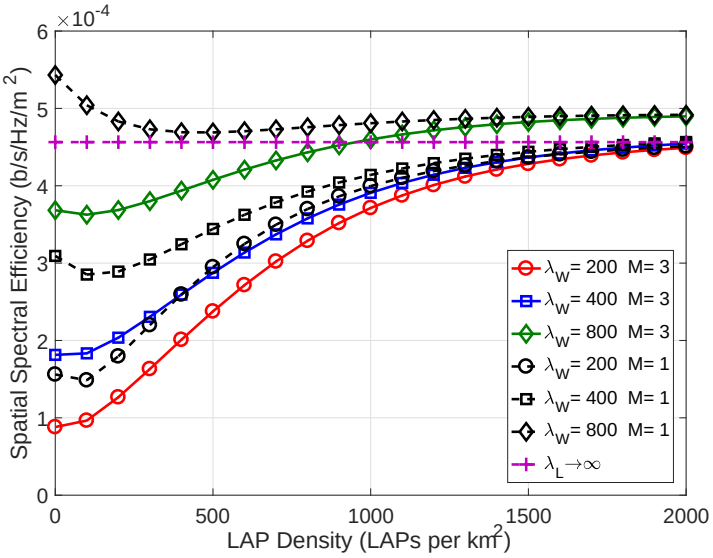

(b) The SSE of the two-tier HetNet

Fig. 5.8 The STH and SSE of the two-tier HetNet versus the LAP density for WAP density being 200, 400, and 800 WAPs per km^2 with $M = 1, 3$.

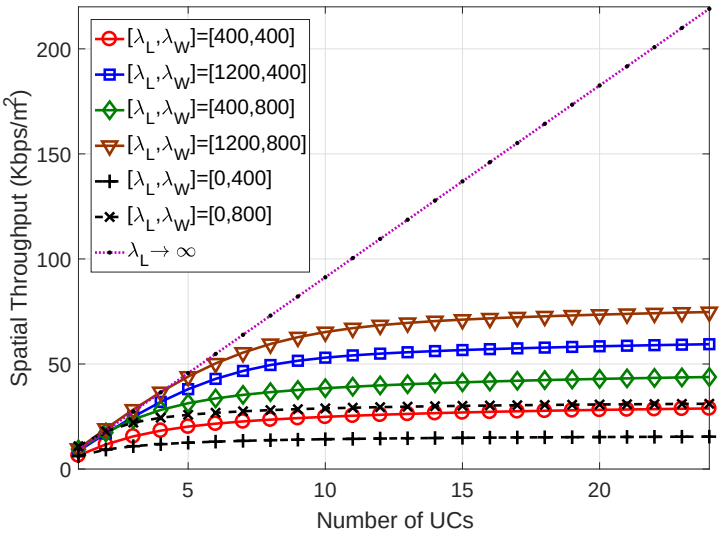

(a) The STH of the two-tier HetNet

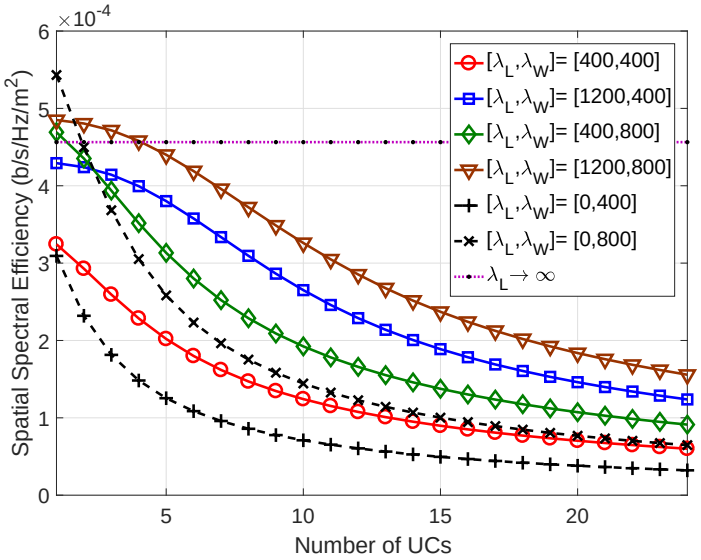

(b) The SSE of the two-tier HetNet

Fig. 5.9 The STH and SSE of the two-tier HetNet versus the number of UCs for several typical LAP and WAP densities.

STH and SSE first decrease then increase with the increase of the LAP density. This indicates that the LAP density should be relatively large to increase the performance of the two-tier HetNet. This is mainly because in a relative low LAP density, LAPs are unable to provide better throughput than WAPs, then the additional STH provided by LAPs cannot make up the loss in STH provided by WAPs. Interestingly, when the LAP density is relatively low (i.e., $\lambda_{\mathrm{L}} \leq 1000$ LAPs per km^2, $\lambda_{\mathrm{W}} = 200,400$ WAPs per km^2, $M = 1,3$), there is always a large gap between the SSE and the corresponding asymptotic SSE in Fig. 5.8b, and the STH or SSE can be improved significantly by deploying more LAPs with the LAP density in the range of $[0,1000]$ LAPs per km^2. Accordingly, the gap between the current SSE and the asymptotic SSE can be used to decide whether to deploy more LAPs or not. As all SSEs for $\lambda_{\mathrm{L}} = 1000$ LAPs per km^2, $\lambda_{\mathrm{W}} = 200,400$ WAPs per km^2 and $M = 1,3$ are approximate 85% of the asymptotic SSE, deploying more LAPs can efficiently improve the STH and SSE of the two-tier HetNet when the current SSE is lower more than 15% of the asymptotic SSE. Note that we only consider single input single output antenna in our system model, thus the spatial spectrum efficiency is lower than that in a system equipped with multiple antennas.

In Fig. 5.9a and Fig. 5.9b, the STH and SSE versus the UC number are illustrated for several LAP and WAP densities. The results show that there is a trade-off between the STH and the SSE when the UC number increases, i.e., with the increase of the number of UCs, the STH increases whereas the SSE decreases. By increasing the accessible UCs, the MAP of the serving AP improves, thus the STH increases. Nevertheless, this MAP does not increase linearly with the number of channels, e.g., the MAP obtained with 5 UCs is smaller than 5 times of the MAP obtained with single UC. As a result, the STH obtained with M accessible UCs is smaller than M times of that obtained with single UC. Therefore, the SSE decreases with the increase of the number of UCs. Moreover, Fig. 5.9b shows that for $\lambda_{\mathrm{W}} = 800$ WAPs per km^2 the SSE of the two-tier HetNet cannot be improved by deploying LAPs if there is only one or two accessible UCs, whereas for other cases, this SSE improves significantly. This indicates that sufficient number of UCs are prerequisite to improve the SSE for the deployment of LAPs. In addition, the gap between the SSE and the corresponding asymptotic SSE becomes larger with the increase of the UC number. This also validates our proposal of using the gap between the current SSE and the asymptotic SSE to decide whether to deploy more LAPs or not to share UCs.

5.4.3 Fairness Analysis

In Fig. 5.10, the fairness between the LUE and the WUE is analysed in terms of their throughputs against the LAP sensing region factor κ_{L} for several WAP densities and the LAP density of 800 LAPs per km^2. The fairness can be treated as the minimum throughput of the

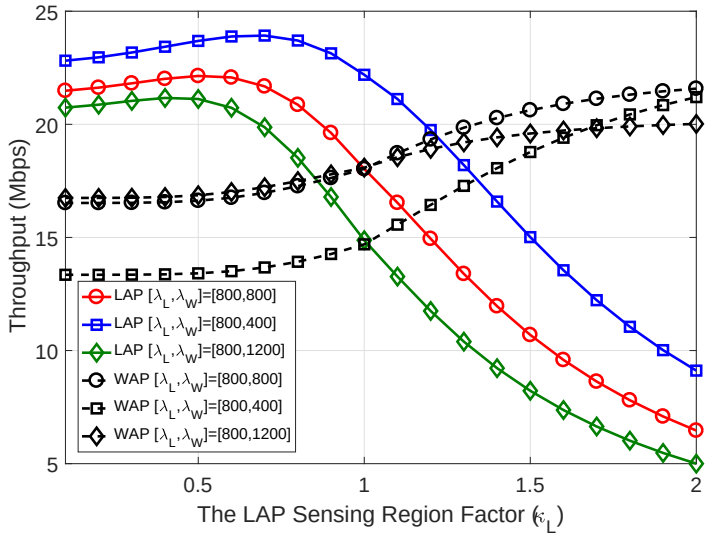

Fig. 5.10 The LUE and WUE throughputs versus the LAP sensing region factor for several LAP and WAP densities with $M = 3$.

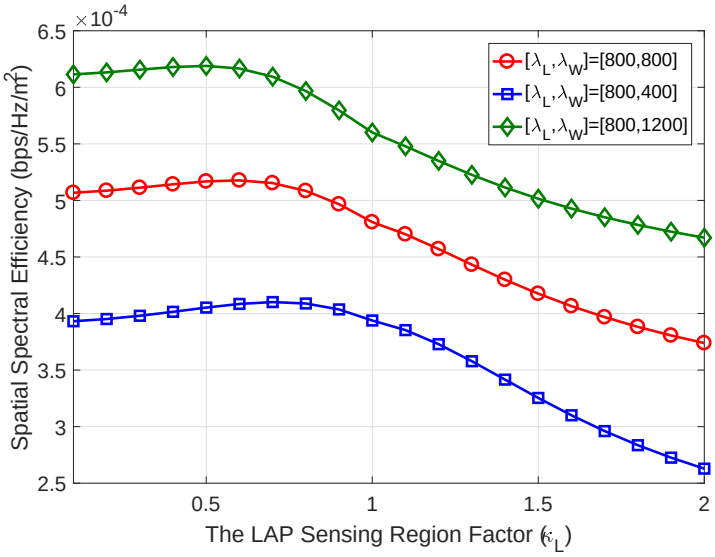

Fig. 5.11 The SSE versus the the LAP sensing region factor for several LAP and WAP densities.

LUE and the WUE, and a better fairness means a larger minimum throughput. Firstly, the results show that both LUE and WUE throughputs remain nearly constant when κ_{L} is smaller than 0.65. This is because the MAP of an LAP is larger than 90%, and the limited variance of MAP has a trivial effect on the throughput. However, such a high MAP of the LAP will cause catastrophic degradation for the WUE throughput. As a result, the LUE throughput is much better than the WUE throughput, and the fairness between the LUE and the WUE is poor. Secondly, the best fairness is achieved at $\kappa_{\text{L}} = 0.85, 1$, and 1.3 for WAP density of 400, 800, and 1200, respectively. This indicates that the fairness between the LUE and the WUE in terms of their throughputs can be improved by expanding the LAP sensing region if the LUE throughput outperforms the WUE throughput, but this will decrease the LUE throughput significantly. The SSE of the two-tier HetNet is plotted in Fig. 5.11. The results show the SSE severely decreases with the increase of κ_{L} for $\kappa_{\text{L}} > 0.65$. This indicates that the fairness is achieved by sacrificing the SSE of the whole HetNet.

5.5 Conclusion

In this chapter, we have derived analytical expressions for STPs for both LTE-LAA and WiFi UEs in coexistence sharing unlicensed spectrum, which are validated by the Monte Carlo simulation. Based on the STP, the UE throughput, spatial throughput and spatial spectral efficiency are obtained and analysed numerically versus the LAP density and the number of UCs. We have also derived lower bounds of the STPs, which can be used to find the optimal LAP density that maximises the LUE throughput at a low computational complexity. The results show that the deployment of LAPs can improve the overall STH and SEE of the coexisting LTE-LAA and WiFi networks. However, if the unlicensed channels are in scarcity, the STH or SSE may be degraded as compared with that in a one-tier WiFi only network. Having more accessible UCs can increase the STH but will always decrease the SSE. Additionally, the asymptotic STH and SSE are calculated with the LAP density approaching infinity. We have found that the asymptotic SSE can be utilised to determine whether to deploy more LAPs or not based on the gap between the achieved SSE and the asymptotic SSE. Finally, the fairness between LUEs and WUEs in terms of their throughputs can be achieved by expanding the LAP sensing region when the LUE throughput outperforms the WUE throughput at the cost of reduced SSE.

Chapter 6

Conclusion and Future Works

6.1 Conclusion

In this dissertation, we have investigated the large-scale performance of applying two interference coordination schemes (i.e., FeICIC and LTE-LAA) in randomly-deployed HetNets to provide guidelines for the system design in reality.

In the first-stage work as illustrated in Chapter 3, we have analysed the coverage probability and the rate coverage probability for a large-scale two-tier HetNet consisting of macro BSs and pico BSs (with CRE) with RPSs adopted in macrocells, which was proposed in Release 11 of the 3GPP standards. To obtain the analytical results, the positions of MBSs and PBSs are assumed following two independent PPPs. Based on the analytical results, we have proposed an effective single-iteration method to obtain the NO values of macrocell centre region bias and picocell range expansion bias by observing the fact that resource allocation contributes more than SINR for maximizing the rate coverage probability. According to our simulation results, it is found that the optimal power reduction factor is in the range of $[0, 0.1]$, and when the picocell range expansion bias is relatively low (under 7 dB), the power reduction factor has negligible effect on the rate coverage probability when the RPS duty cycle is optimised. In addition, as compared with ABSs, RPSs have poorer coverage probability and rate coverage probability with optimal macrocell centre region bias and picocell range expansion bias, but the optimal biases cause a heavier burden on the picocell backhaul as more UEs are associated with picocell expanded regions. If the range expansion bias is static without optimisation, RPSs in turn outperform ABSs in terms of rate coverage probability. The usage of conventional RPSs were only discussed in macrocells, which ignores the potential usage in femtocells to improve the coverage probability of edge MUEs. Consequently, in the second part in Chapter 3, we have proposed the scheme to apply RPSs in both tiers of a two-tier HetNet without CRE comprising of MBSs and FBSs. Different from

the first work in Chapter 3, we have proposed a novel SIR-based user association strategy. By assuming that the positions of MBSs and FBSs follow two independent PPPs, we have achieved the closed-form coverage probability and rate coverage probabilities of UEs in each group. The results showed that a maximum of 20% coverage-probability gain can be yielded for the macrocell edge-region UEs by introducing RPSs in femtocells, and the rate coverage probability of the two-tier HetNet can also be increased by up to 15%. Nevertheless, there are four main ideal assumptions made in these two works: 1) Strict synchronization is assumed throughout the whole HetNet. 2) SCs are expected to deploy at the edge of macrocells, which is ignored in our system model. 3) The locations of UEs follow an independent PPP, but in reality, their locations may have certain patterns, such as clustered. 4) There is always data to transmit in all BSs.

Accordingly, in our second-stage work, we have investigated the effect of asychronization on the performance in a HetNet. Specifically, under subframe misaligned interference, the downlink coverage probability of a two-tier HetNet employing CRE and RPSs has been analysed. To analyse the effect of SM, we have proposed an practical SM model with the misalignment offsets restricted in a certain range. The results showed that the SM significantly decreases the coverage probability of a typical UE, which can be mitigated by increasing the SC density. However, an increase of SC density cannot mitigate the coverage-probability degradation of VUs. This coverage-probability degradation of VUs can be reduced by increasing the RPS transmit power in macrocells. Moreover, for protecting the VUs with below 5% coverage-probability reduction caused by SM, the SA requirement can be relaxed by up to 20% of the subframe duration. Furthermore, as compared with ABSs, the application of RPSs relax the requirement of SA. However, the other three aforementioned ideal assumptions were made in this work, which can be investigated in our future work.

In the third-stage of our work, we have investigated the large-scale performance of another interference coordination scheme, i.e., LTE-LAA, for the coexistence of LTE-U/LAA network and WiFi network with multiple UCs. Specifically, analytical expressions of downlink STPs of the typical LUE and WUE, STH and SSE of the whole two-tier HetNet consisting of LAPs and WAPs have been derived. Additionally, the asymptotic STH and SSE have been derived in closed form with the LAP density approaching infinity, which can be utilised to determine whether to deploy more LAPs based on the gap between the achieved SSE and the asymptotic SSE. The results show that by employing the LTE-LAA interference coordination scheme, the deployment of LAPs can improve the STH and SSE of the coexisting LTE-LAA and WiFi networks, and having more accessible UCs can increase the STH but will decrease the SSE. The results also showed that the fairness between LUEs and WUEs in terms of their throughputs can be achieved by expanding the LAP sensing region. However, this work

ignores the case of applying CSAT scheme under a multi-UC case, where practical channel selection scheme should be incorporated.

6.2 Future Works

(a) **Large-scale Performance Analysis of Location-Dependent HetNets with CRE and RPSs**

Recent researches [118–120] show that the independent assumption of the deployment of BSs in different tiers is not so feasible for the HetNet deployment in reality. One reason is that the SC BSs are intended to be deployed at the edge of the macrocells by operators. Therefore, the MBSs have their exclude regions for prohibiting the SC BSs to activate in. Another reason is that the SC BSs are always deployed at work and residential places. This may lead to a quite different density in different areas, which formulates as a clustered point process. Therefore, to further evaluate the performance and to exploit comprehensive design guidelines for FeICIC RPSs, it is worthy taking more practical network models into consideration.

(b) **Large-scale Performance Analysis of User-Centric HetNets with CRE and RPSs**

In reality, there exits correlation between the UE locations and BS locations [121–123], thus introducing this correlation into the analysis of HetNets with CRE and RPSs can provide additional design guidelines for FeICIC RPSs. Furthermore, the traffic pattern and throughput requirement of each UE may vary [124–126]. As a consequence, to analyse a user-centric HetNet with CRE and RPSs becomes critical.

(c) **Large-scale Performance Analysis of Coexisting LTE-U and WiFi networks with CSAT under Multiple Unlicensed Channel**

In Chapter 5, only the LTE-LAA coexisting scheme has been analysed under a multi-UC environment. As CSAT is a popular interference coordination scheme between LTE-U APs without MAC modification and WiFi APs, the comparison between the CSAT and LTE-LAA (LBT-based mechanism) under a multi-UC scenario can provide guidelines for the future deployment of the coexisting LTE-U and WiFi networks. The challenging part for the analysis of CSAT under a multi-UC scenario is the modelling of the channel access scheme for the LTE-U APs.

(d) **Interference Modelling of three-dimensional MIMO enabled HetNets**

The three-dimensional MIMO array antennas has been proposed to reduce the inter-cell interference by adjusting the beam direction at both horizontal and vertical dimensions

[127–129]. To reduce the size of three-dimensional MIMO array antennas, mmWave spectrum band is desirable to be used in the three-dimensional MIMO array antenna. However, existing works currently focus on the link-level analysis, and the interference modelling is remarkably important for the system-level performance analysis of three-dimensional MIMO enabled HetNets.

References

[1] G. Americas, "Meeting the 1000x Challenge: The Need for Spectrum, Technology and Policy Innovation," 4G Americas, Tech. Rep, Tech. Rep., 2013.

[2] C. V. N. Index, "Global Mobile Data Traffic Forecast Update, 2016–2021 White Paper, accessed on May 2, 2017."

[3] Q. C. Li, H. Niu, A. T. Papathanassiou, and G. Wu, "5G Network Capacity: Key Elements and Technologies," *IEEE Vehicular Technology Magazine*, vol. 9, no. 1, pp. 71–78, March 2014.

[4] D. Lopez-Perez, A. Valcarce, G. de la Roche, and J. Zhang, "OFDMA Femtocells: A Roadmap on Interference Avoidance," *IEEE Communications Magazine*, vol. 47, no. 9, pp. 41–48, September 2009.

[5] J. Zhang and G. D. la Roche, *Femtocells: Technologies and Deployment*. John Wiley & Sons, 2011.

[6] D. Lopez-Perez, I. Guvenc, G. de la Roche, M. Kountouris, T. Q. S. Quek, and J. Zhang, "Enhanced Intercell Interference Coordination Challenges in Heterogeneous Networks," *IEEE Wireless Communications*, vol. 18, no. 3, pp. 22–30, June 2011.

[7] D. Lopez-Perez, I. Guvenc, and X. Chu, "Mobility Management Challenges in 3GPP Heterogeneous Networks," *IEEE Communications Magazine*, vol. 50, no. 12, pp. 70–78, December 2012.

[8] A. H. Jafari, D. López-Pérez, H. Song, H. Claussen, L. Ho, and J. Zhang, "Small Cell Backhaul: Challenges and Prospective Solutions," *EURASIP Journal on Wireless Communications and Networking*, vol. 2015, no. 1, p. 206, December 2015.

[9] J. G. Andrews, F. Baccelli, and R. K. Ganti, "A Tractable Approach to Coverage and Rate in Cellular Networks," *IEEE Transactions on Communications*, vol. 59, no. 11, pp. 3122–3134, November 2011.

[10] A. Merwaday, S. Mukherjee, and I. Güvenç, "HetNet capacity with reduced power subframes," in *2014 IEEE Wireless Communications and Networking Conference (WCNC)*, April 2014, pp. 1380–1385.

[11] Panasonic, "Performance Study on ABS with Reduced Macro Power," 3GPP TSG-RAN WG1, Technical Report R1-113806, November 2011.

[12] D. Bladsjö, M. Hogan, and S. Ruffini, "Synchronization aspects in LTE small cells," *IEEE Communications Magazine*, vol. 51, no. 9, pp. 70–77, September 2013.

[13] H. Zhang, X. Chu, W. Guo, and S. Wang, "Coexistence of Wi-Fi and Heterogeneous Small Cell Networks Sharing Unlicensed Spectrum," *IEEE Communications Magazine*, vol. 53, no. 3, pp. 158–164, March 2015.

[14] Y. Wu, W. Guo, H. Yuan, L. Li, S. Wang, X. Chu, and J. Zhang, "Device-to-device Meets LTE-unlicensed," *IEEE Communications Magazine*, vol. 54, no. 5, pp. 154–159, May 2016.

[15] Qualcomm Technologies, Inc., "Qualcomm Research LTE in Unlicensed Spectrum: Harmonious Coexistence with Wi-Fi," June 2014.

[16] B. Chen, J. Chen, Y. Gao, and J. Zhang, "Coexistence of LTE-LAA and Wi-Fi on 5 GHz with Corresponding Deployment Scenarios: A Survey," *IEEE Communications Surveys & Tutorials*, vol. 19, no. 1, pp. 7–32, Firstquarter 2017.

[17] H. Kwon, J. Jeon, A. Bhorkar, Q. Ye, H. Harada, Y. Jiang, L. Liu, S. Nagata, B. L. Ng, T. Novlan *et al.*, "Licensed-assisted Access to Unlicensed Spectrum in LTE Release 13," *IEEE Communications Magazine*, vol. 55, no. 2, pp. 201–207, February 2017.

[18] J. Xu, J. Zhang, and J. G. Andrews, "On the Accuracy of the Wyner Model in Cellular Networks," *IEEE Transactions on Wireless Communications*, vol. 10, no. 9, pp. 3098–3109, September 2011.

[19] J. G. Andrews, "Seven Ways that HetNets are A Cellular Paradigm Shift," *IEEE Communications Magazine*, vol. 51, no. 3, pp. 136–144, March 2013.

[20] M. Haenggi, *Stochastic Geometry for Wireless Networks*, 1st ed. New York, NY, USA: Cambridge University Press, 2012.

[21] C. H. Lee, C. Y. Shih, and Y. S. Chen, "Stochastic Geometry Based Models for Modeling Cellular Networks in Urban Areas," *Wireless networks*, vol. 19, no. 6, pp. 1063–1072, August 2013.

[22] H. S. Dhillon, R. K. Ganti, F. Baccelli, and J. G. Andrews, "Modeling and Analysis of K-tier Downlink Heterogeneous Cellular Networks," *IEEE Journal on Selected Areas in Communications*, vol. 30, no. 3, pp. 550–560, April 2012.

[23] F. Baccelli, B. Błaszczyszyn *et al.*, "Stochastic geometry and wireless networks: Volume II Applications," *Foundations and Trends® in Networking*, vol. 4, no. 1–2, pp. 1–312, 2010.

[24] S. P. Weber, X. Yang, J. G. Andrews, and G. de Veciana, "Transmission Capacity of Wireless Ad Hoc Networks with Outage Constraints," *IEEE Transactions on Information Theory*, vol. 51, no. 12, pp. 4091–4102, December 2005.

[25] H. ElSawy, E. Hossain, and S. Camorlinga, "Characterizing Random CSMA Wireless Networks: A Stochastic Geometry Approach," in *2012 IEEE International Conference on Communications (ICC)*, June 2012, pp. 5000–5004.

[26] W. Lu and M. D. Renzo, "Stochastic Geometry Modeling of Cellular Networks: Analysis, Simulation and Experimental Validation," in *Proceedings of the 18th ACM International Conference on Modeling, Analysis and Simulation of Wireless and Mobile Systems*. ACM, 2015, pp. 179–188.

[27] T. D. Novlan, R. K. Ganti, A. Ghosh, and J. G. Andrews, "Analytical Evaluation of Fractional Frequency Reuse for OFDMA Cellular Networks," *IEEE Transactions on Wireless Communications*, vol. 10, no. 12, pp. 4294–4305, December 2011.

[28] ——, "Analytical Evaluation of Fractional Frequency Reuse for Heterogeneous Cellular Networks," *IEEE Transactions on Communications*, vol. 60, no. 7, pp. 2029–2039, July 2012.

[29] H. S. Jo, Y. J. Sang, P. Xia, and J. G. Andrews, "Heterogeneous Cellular Networks with Flexible Cell Association: A Comprehensive Downlink SINR Analysis," *IEEE Transactions on Wireless Communications*, vol. 11, no. 10, pp. 3484–3495, October 2012.

[30] S. Singh, H. S. Dhillon, and J. G. Andrews, "Offloading in Heterogeneous Networks: Modeling, Analysis, and Design Insights," *IEEE Transactions on Wireless Communications*, vol. 12, no. 5, pp. 2484–2497, 2013.

[31] S. Singh and J. G. Andrews, "Joint Resource Partitioning and Offloading in Heterogeneous Cellular Networks," *IEEE Transactions on Wireless Communications*, vol. 13, no. 2, pp. 888–901, February 2014.

[32] M. Cierny, H. Wang, R. Wichman, Z. Ding, and C. Wijting, "On Number of Almost Blank Subframes in Heterogeneous Cellular Networks," *IEEE Transactions on Wireless Communications*, vol. 12, no. 10, pp. 5061–5073, October 2013.

[33] Q. Cui, H. Wang, P. Hu, X. Tao, P. Zhang, J. Hamalainen, and L. Xia, "Evolution of Limited-Feedback CoMP Systems from 4G to 5G: CoMP Features and Limited-Feedback Approaches," *IEEE Vehicular Technology Magazine*, vol. 9, no. 3, pp. 94–103, Sept 2014.

[34] G. Nigam, P. Minero, and M. Haenggi, "Coordinated multipoint in heterogeneous networks: A stochastic geometry approach," in *2013 IEEE Globecom Workshops (GC Wkshps)*, December 2013, pp. 145–150.

[35] F. Baccelli and A. Giovanidis, "A Stochastic Geometry Framework for Analyzing Pairwise-Cooperative Cellular Networks," *IEEE Transactions on Wireless Communications*, vol. 14, no. 2, pp. 794–808, February 2015.

[36] H. S. Dhillon, M. Kountouris, and J. G. Andrews, "Downlink Coverage Probability in MIMO HetNets," in *2012 Conference Record of the Forty Sixth Asilomar Conference on Signals, Systems and Computers (ASILOMAR)*, November 2012, pp. 683–687.

[37] ——, "Downlink MIMO HetNets: Modeling, Ordering Results and Performance Analysis," *IEEE Transactions on Wireless Communications*, vol. 12, no. 10, pp. 5208–5222, October 2013.

[38] M. D. Renzo and W. Lu, "Stochastic Geometry Modeling and Performance Evaluation of MIMO Cellular Networks Using the Equivalent-in-Distribution (EiD)-Based Approach," *IEEE Transactions on Communications*, vol. 63, no. 3, pp. 977–996, March 2015.

[39] C. Li, J. Zhang, J. G. Andrews, and K. B. Letaief, "Success Probability and Area Spectral Efficiency in Multiuser MIMO HetNets," *IEEE Transactions on Communications*, vol. 64, no. 4, pp. 1544–1556, April 2016.

[40] H. H. Yang, G. Geraci, and T. Q. S. Quek, "Energy-Efficient Design of MIMO Heterogeneous Networks With Wireless Backhaul," *IEEE Transactions on Wireless Communications*, vol. 15, no. 7, pp. 4914–4927, July 2016.

[41] A. He, L. Wang, M. Elkashlan, Y. Chen, and K. K. Wong, "Spectrum and Energy Efficiency in Massive MIMO Enabled HetNets: A Stochastic Geometry Approach," *IEEE Communications Letters*, vol. 19, no. 12, pp. 2294–2297, December 2015.

[42] T. Bai, R. Vaze, and R. W. Heath, "Analysis of Blockage Effects on Urban Cellular Networks," *IEEE Transactions on Wireless Communications*, vol. 13, no. 9, pp. 5070–5083, September 2014.

[43] T. Bai and R. W. Heath, "Coverage and Rate Analysis for Millimeter-Wave Cellular Networks," *IEEE Transactions on Wireless Communications*, vol. 14, no. 2, pp. 1100–1114, February 2015.

[44] R. Wang, X. Peng, J. Zhang, and K. B. Letaief, "Mobility-aware caching for content-centric wireless networks: modeling and methodology," *IEEE Communications Magazine*, vol. 54, no. 8, pp. 77–83, August 2016.

[45] B. Blaszczyszyn and A. Giovanidis, "Optimal Geographic Caching in Cellular Networks," in *2015 IEEE International Conference on Communications (ICC)*, June 2015, pp. 3358–3363.

[46] Y. Cui and D. Jiang, "Analysis and Optimization of Caching and Multicasting in Large-Scale Cache-Enabled Heterogeneous Wireless Networks," *IEEE Transactions on Wireless Communications*, vol. 16, no. 1, pp. 250–264, Jan 2017.

[47] N. Deng, W. Zhou, and M. Haenggi, "A Heterogeneous Cellular Network Model with Inter-tier Dependence," in *2014 IEEE Global Communications Conference*. IEEE, December 2014, pp. 1522–1527.

[48] ——, "Heterogeneous Cellular Network Models With Dependence," *IEEE Journal on Selected Areas in Communications*, vol. 33, no. 10, pp. 2167–2181, October 2015.

[49] Z. Yazdanshenasan, H. S. Dhillon, M. Afshang, and P. H. J. Chong, "Poisson Hole Process: Theory and Applications to Wireless Networks," *IEEE Transactions on Wireless Communications*, vol. 15, no. 11, pp. 7531–7546, Nov 2016.

[50] C. h. Lee and M. Haenggi, "Interference and Outage in Poisson Cognitive Networks," *IEEE Transactions on Wireless Communications*, vol. 11, no. 4, pp. 1392–1401, April 2012.

[51] S. Lee, R. Zhang, and K. Huang, "Opportunistic Wireless Energy Harvesting in Cognitive Radio Networks," *IEEE Transactions on Wireless Communications*, vol. 12, no. 9, pp. 4788–4799, September 2013.

[52] A. H. Sakr and E. Hossain, "Cognitive and Energy Harvesting-Based D2D Communication in Cellular Networks: Stochastic Geometry Modeling and Analysis," *IEEE Transactions on Communications*, vol. 63, no. 5, pp. 1867–1880, May 2015.

[53] H. ElSawy, E. Hossain, and M. S. Alouini, "Analytical Modeling of Mode Selection and Power Control for Underlay D2D Communication in Cellular Networks," *IEEE Transactions on Communications*, vol. 62, no. 11, pp. 4147–4161, November 2014.

[54] S. W. Y. G. X. Z. Z. Lin, Y. Li and D. Yang, "Stochastic geometry analysis of achievable transmission capacity for relay-assisted Device-to-Device networks," in *2014 IEEE International Conference on Communications (ICC), Sydney, NSW*, May 2014, pp. 2251–2256.

[55] J. Liu, S. Zhang, H. Nishiyama, N. Kato, and J. Guo, "A Stochastic Geometry Analysis of D2D Overlaying Multi-channel Downlink Cellular Networks," in *2015 IEEE Conference on Computer Communications (INFOCOM)*, April 2015, pp. 46–54.

[56] R. K. Ganti and M. Haenggi, "Interference and Outage in Clustered Wireless Ad Hoc Networks," *IEEE Transactions on Information Theory*, vol. 55, no. 9, pp. 4067–4086, September 2009.

[57] V. Suryaprakash, J. Møller, and G. Fettweis, "On the Modeling and Analysis of Heterogeneous Radio Access Networks Using a Poisson Cluster Process," *IEEE Transactions on Wireless Communications*, vol. 14, no. 2, pp. 1035–1047, February 2015.

[58] X. Lin, R. K. Ganti, P. J. Fleming, and J. G. Andrews, "Towards Understanding the Fundamentals of Mobility in Cellular Networks," *IEEE Transactions on Wireless Communications*, vol. 12, no. 4, pp. 1686–1698, April 2013.

[59] W. Bao and B. Liang, "Stochastic Geometric Analysis of User Mobility in Heterogeneous Wireless Networks," *IEEE Journal on Selected Areas in Communications*, vol. 33, no. 10, pp. 2212–2225, October 2015.

[60] Y. Hong, X. Xu, M. Tao, J. Li, and T. Svensson, "Cross-tier Handover Analyses in Small Cell Networks: A Stochastic Geometry Approach," in *2015 IEEE International Conference on Communications (ICC)*, June 2015, pp. 3429–3434.

[61] H. ElSawy, E. Hossain, and M. Haenggi, "Stochastic geometry for modeling, analysis, and design of multi-tier and cognitive cellular wireless networks: A survey," *IEEE Communications Surveys Tutorials*, vol. 15, no. 3, pp. 996–1019, Thirdquarter 2013.

[62] H. ElSawy, A. Sultan-Salem, M. S. Alouini, and M. Z. Win, "Modeling and Analysis of Cellular Networks Using Stochastic Geometry: A Tutorial," *IEEE Communications Surveys Tutorials*, vol. 19, no. 1, pp. 167–203, Firstquarter 2017.

[63] B. Soret, H. Wang, K. I. Pedersen, and C. Rosa, "Multicell cooperation for LTE-advanced heterogeneous network scenarios," *IEEE Wireless Communications*, vol. 20, no. 1, pp. 27–34, February 2013.

[64] 3GPP, "Coordinated Multi-point Operation for LTE Physical Layer Aspects," Technical Report TR 36.819, November 2013.

[65] B. Soret and K. I. Pedersen, "Macro Transmission Power Reduction for HetNet Co-channel Deployments," in *2012 IEEE Global Communications Conference (GLOBECOM)*, December 2012, pp. 4126–4130.

[66] F. Alfarhan, R. Lerbour, and Y. L. Helloco, "An Optimization Framework for LTE eICIC and Reduced Power eICIC," in *2015 IEEE Global Communications Conference (GLOBECOM)*, December 2015, pp. 1–6.

[67] A. Merwaday, S. Mukherjee, and I. Güvenç, "HetNet Capacity with Reduced Power Subframes," in *2014 IEEE Wireless Communications and Networking Conference (WCNC)*, April 2014, pp. 1380–1385.

[68] A. Merwaday, S. Mukherjee, and I. Güvenç, "Capacity Analysis of LTE-Advanced HetNets with Reduced Power Subframes and Range Expansion," *EURASIP Journal on Wireless Communications and Networking*, vol. 2014, no. 1, p. 189, November 2014.

[69] Y. Liu, C. S. Chen, C. W. Sung, and C. Singh, "A Game Theoretic Distributed Algorithm for FeICIC Optimization in LTE-A HetNets," *IEEE/ACM Transactions on Networking*, vol. 25, no. 6, pp. 3500–3513, December 2017.

[70] X. Nie, Y. Wang, J. Zhang, and L. Ding, "Performance Analysis of FeICIC and Adaptive Spectrum Allocation in Heterogeneous Networks," in *2017 24th International Conference on Telecommunications (ICT)*, May 2017, pp. 1–6.

[71] X. Nie, Y. Wang, L. Ding, and J. Zhang, "Joint Optimization of FeICIC and Spectrum Allocation for Spectral and Energy Efficient Heterogeneous Networks," *IEICE Transactions on Communications*, vol. advpub, December 2017.

[72] A. Kumbhar, . Güvenç, S. Singh, and A. Tuncer, "Exploiting LTE-Advanced HetNets and FeICIC for UAV-Assisted Public Safety Communications," *IEEE Access*, vol. 6, pp. 783–796, February 2018.

[73] B. Blaszczyszyn and P. Muhlethaler, "Stochastic Analysis of Non-Slotted Aloha in Wireless Ad-Hoc Networks," in *2010 Proceedings IEEE INFOCOM*, March 2010, pp. 1–9.

[74] B. Błaszczyszyn and P. Mühlethaler, "Interference and SINR Coverage in Spatial Non-slotted Aloha Networks," *annals of telecommun.-annales des télécommun.*, vol. 70, pp. 345–358, August 2015.

[75] A. Munari, P. Mähönen, and M. Petrova, "A Stochastic Geometry Approach to Asynchronous Aloha Full-Duplex Networks," *IEEE/ACM Transactions on Networking*, vol. 25, no. 6, pp. 3695–3708, December 2017.

[76] S. Darshi and R. Bhattacharjee, "Outage Analysis of Asynchronized Wireless Networks in Interference-Limited Environment," *IEEE Transactions on Vehicular Technology*, vol. 62, no. 8, pp. 3863–3874, Oct 2013.

[77] X. Lin, L. Jiang, and J. G. Andrews, "Performance Analysis of Asynchronous Multicarrier Wireless Networks," *IEEE Transaction on Communnication*, vol. 63, pp. 3377–3390, September 2015.

[78] M. Speth, S. A. Fechtel, G. Fock, and H. Meyr, "Optimum Receiver Design for Wireless Broad-band Systems Using OFDM. I," *IEEE Transactions on Communications*, vol. 47, no. 11, pp. 1668–1677, November 1999.

[79] V. Naghshin, M. C. Reed, S. V. Hanly, and N. Aboutorab, "Downlink Coverage Analysis of Two-tier Heterogeneous Networks with Asynchronous Slots," in *2016 IEEE International Conference on Communications (ICC)*, May 2016, pp. 1–6.

[80] V. Naghshin, M. C. Reed, and N. Aboutorab, "Coverage Analysis of Packet Multi-Tier Networks With Asynchronous Slots," *IEEE Transactions on Communications*, vol. 65, no. 1, pp. 200–215, January 2017.

[81] F. Liu, E. Bala, E. Erkip, M. C. Beluri, and R. Yang, "Small-Cell Traffic Balancing Over Licensed and Unlicensed Bands," *IEEE Transactions on Vehicular Technology*, vol. 64, no. 12, pp. 5850–5865, December 2015.

[82] C. Cano and D. J. Leith, "Unlicensed LTE/WiFi coexistence: Is LBT inherently fairer than CSAT?" in *2016 IEEE International Conference on Communications (ICC)*, May 2016, pp. 1–6.

[83] Y. Li, F. Baccelli, J. G. Andrews, T. D. Novlan, and J. C. Zhang, "Modeling and Analyzing the Coexistence of Wi-Fi and LTE in Unlicensed Spectrum," *IEEE Transactions on Wireless Communications*, vol. 15, no. 9, pp. 6310–6326, September 2016.

[84] X. Wang, T. Q. S. Quek, M. Sheng, and J. Li, "Throughput and Fairness Analysis of Wi-Fi and LTE-U in Unlicensed Band," *IEEE Journal on Selected Areas in Communications*, vol. 35, no. 1, pp. 63–78, January 2017.

[85] A. k. Ajami and H. Artail, "On The Modeling and Analysis of Uplink and Downlink IEEE 802.11ax Wi-Fi With LTE in Unlicensed Spectrum," *IEEE Transactions on Wireless Communications*, vol. 16, no. 9, pp. 5779–5795, September 2017.

[86] A. Bhorkar, C. Ibars, and P. Zong, "Performance Analysis of LTE and Wi-Fi in Unlicensed Band Using Stochastic Geometry," in *2014 IEEE 25th Annual International Symposium on Personal, Indoor, and Mobile Radio Communication (PIMRC)*, September 2014, pp. 1310–1314.

[87] A. M. Voicu, L. Simić, and M. Petrova, "Inter-Technology Coexistence in a Spectrum Commons: A Case Study of Wi-Fi and LTE in the 5-GHz Unlicensed Band," *IEEE Journal on Selected Areas in Communications*, vol. 34, no. 11, pp. 3062–3077, November 2016.

[88] R. Yin, G. Yu, A. Maaref, and G. Y. Li, "LBT-Based Adaptive Channel Access for LTE-U Systems," *IEEE Transactions on Wireless Communications*, vol. 15, no. 10, pp. 6585–6597, October 2016.

[89] X. Ding, C. H. Liu, L. C. Wang, and X. Zhao, "Coexisting Success Probability and Throughput of Multi-RAT Wireless Networks With Unlicensed Band Access," *IEEE Wireless Communications Letters*, vol. 5, no. 1, pp. 4–7, February 2016.

[90] Q. Chen, G. Yu, A. Maaref, G. Y. Li, and A. Huang, "Rethinking Mobile Data Offloading for LTE in Unlicensed Spectrum," *IEEE Transactions on Wireless Communications*, vol. 15, no. 7, pp. 4987–5000, July 2016.

[91] Y. Zhang, C. Jiang, J. Wang, Z. Han, J. Yuan, and J. Cao, "Coalition Formation Game Based Access Point Selection for LTE-U and Wi-Fi Coexistence," *IEEE Transactions on Industrial Informatics*, vol. 14, no. 6, pp. 2653–2665, June 2018.

[92] L. Li, J. P. Seymour, L. J. Cimini, and C. C. Shen, "Coexistence of Wi-Fi and LAA Networks With Adaptive Energy Detection," *IEEE Transactions on Vehicular Technology*, vol. 66, no. 11, pp. 10 384–10 393, November 2017.

[93] L. Li, A. H. Jafari, X. Chu, and J. Zhang, "Simultaneous Transmission Opportunities for LTE-LAA Small-cells Coexisting with WiFi in Unlicensed Spectrum," in *2016 IEEE International Conference on Communications (ICC)*, May 2016, pp. 1–7.

[94] S. Khairy, L. X. Cai, Y. Cheng, Z. Han, and H. Shan, "A Hybrid-LBT MAC with Adaptive Sleep for LTE LAA Coexisting with Wi-Fi over Unlicensed Band," in *GLOBECOM 2017 - 2017 IEEE Global Communications Conference*, December 2017, pp. 1–6.

[95] S. Sagari, S. Baysting, D. Saha, I. Seskar, W. Trappe, and D. Raychaudhuri, "Coordinated dynamic spectrum management of LTE-U and Wi-Fi networks," in *2015 IEEE International Symposium on Dynamic Spectrum Access Networks (DySPAN)*, September 2015, pp. 209–220.

[96] M. Chen, W. Saad, and C. Yin, "Echo State Networks for Self-Organizing Resource Allocation in LTE-U With Uplink-Downlink Decoupling," *IEEE Transactions on Wireless Communications*, vol. 16, no. 1, pp. 3–16, January 2017.

[97] O. Sandoval, G. D. González, J. Hämäläinen, and S. Yoo, "Indoor Planning and Optimization of LTE-U Radio Access over WiFi," in *2016 IEEE 27th Annual International Symposium on Personal, Indoor, and Mobile Radio Communications (PIMRC)*, September 2016, pp. 1–7.

[98] H. Zhang, Y. Liao, and L. Song, "D2D-U: Device-to-Device Communications in Unlicensed Bands for 5G System," *IEEE Transactions on Wireless Communications*, vol. 16, no. 6, pp. 3507–3519, June 2017.

[99] H. Hu, J. Weng, and J. Zhang, "Coverage Performance Analysis of FeICIC Low-Power Subframes," *IEEE Transactions on Wireless Communications*, vol. 15, no. 8, pp. 5603–5614, August 2016.

[100] H. Hu, J. Weng, J. Zhang, J. Zhang, and Y. Wang, "Modelling and Analysis of Reduced Power Subframes in Two-Tier Femto HetNets," in *2016 IEEE 83rd Vehicular Technology Conference (VTC Spring)*, May 2016, pp. 1–5.

[101] F. Baccelli, B. Błaszczyszyn *et al.*, "Stochastic Geometry and Wireless Networks: Volume I Theorey," *Foundations and Trends® in Networking*, vol. 3, no. 3–4, pp. 249–449, 2009.

[102] T. M. Nico, "Large Parameter Cases of the Gauss Hypergeometric Function," *Journal of Computational and Applied Mathematics*, vol. 153, no. 1–2, pp. 441 – 462, April 2003.

[103] H. Hu, B. Zhang, Q. Hong, X. Chu, and J. Zhang, "Coverage Analysis of Reduced Power Subframes Applied in Heterogeneous Networks with Subframe Misalignment Interference," *IEEE Wireless Communications Letters*, pp. 1–1, 2018.

[104] P. C. Pinto, A. Giorgetti, M. Z. Win, and M. Chiani, "A stochastic geometry approach to coexistence in heterogeneous wireless networks," *IEEE Journal on Selected Areas in Communications*, vol. 27, no. 7, pp. 1268–1282, September 2009.

[105] E. Ferreira, A. Kohara, and J. Sesma, "New properties of the Lerch's transcendent," *Journal of Number Theory*, vol. 172, pp. 21–31, March 2017.

[106] H. Hu, Y. Gao, X. Chu, B. Zhang, and J. Zhang, "On the Performance of LTE-LAA Networks Coexisting with WiFi Networks Sharing Multiple Unlicensed Channels," *ResearchGate preprint 10.13140/RG.2.2.27418.95686*, May 2018.

[107] C. H. Liu and H. C. Tsai, "On the Limits of Coexisting Coverage and Capacity in Multi-RAT Heterogeneous Networks," *IEEE Transactions on Wireless Communications*, vol. 16, no. 5, pp. 3086–3101, May 2017.

[108] T. S. Rappaport *et al.*, *Wireless communications: principles and practice*. prentice hall PTR New Jersey, 1996, vol. 2.

[109] "IEEE Standard for Information technology–Telecommunications and information exchange between systems Local and metropolitan area networks–Specific requirements - Part 11: Wireless LAN Medium Access Control (MAC) and Physical Layer (PHY) Specifications," *IEEE Std 802.11-2016 (Revision of IEEE Std 802.11-2012)*, pp. 1–3534, December 2016.

[110] G. Yuan, X. Zhang, W. Wang, and Y. Yang, "Carrier aggregation for LTE-advanced mobile communication systems," *IEEE Communications Magazine*, vol. 48, no. 2, pp. 88–93, February 2010.

[111] L. A. T. Zhang, J. Zhao and D. Liu, "Energy Efficiency of Base Station Deployment in Ultra Dense HetNets: A Stochastic Geometry Analysis," *IEEE Wireless Communications Letters*, vol. 5, no. 2, pp. 184–187, April 2016.

[112] Y. Zhong, W. Zhang, and M. Haenggi, "Stochastic analysis of the mean interference for the rts/cts mechanism," in *2014 IEEE International Conference on Communications (ICC)*, June 2014, pp. 1996–2001.

[113] A. Mbengue and Y. Chang, "Performance analysis of laa / wi-fi coexistence: Stochastic geometry model," in *2018 IEEE Wireless Communications and Networking Conference (WCNC)*, April 2018, pp. 1–6.

[114] H. Kwon, S. Kim, and B. G. Lee, "Opportunistic multi-channel CSMA protocol for OFDMA systems," *IEEE Transactions on Wireless Communications*, vol. 9, no. 5, pp. 1552–1557, May 2010.

[115] H. Q. Nguyen, F. Baccelli, and D. Kofman, "A Stochastic Geometry Analysis of Dense IEEE 802.11 Networks," in *IEEE INFOCOM 2007 - 26th IEEE International Conference on Computer Communications*, May 2007, pp. 1199–1207.

[116] Wolfram Mathematica 9, "Symbolic Integral Computation," [Online].[Accessed 2 August 2015]. Available form: http://www.wolfram.com/mathematica.

[117] H. ElSawy, E. Hossain, and S. Camorlinga, "Multi-channel design for random CSMA wireless networks: A stochastic geometry approach," in *2013 IEEE International Conference on Communications (ICC)*, June 2013, pp. 1656–1660.

[118] A. Guo and M. Haenggi, "Spatial Stochastic Models and Metrics for the Structure of Base Stations in Cellular Networks," *IEEE Transactions on Wireless Communications*, vol. 12, no. 11, pp. 5800–5812, November 2013.

[119] N. Deng, W. Zhou, and M. Haenggi, "The Ginibre Point Process as a Model for Wireless Networks With Repulsion," *IEEE Transactions on Wireless Communications*, vol. 14, no. 1, pp. 107–121, January 2015.

[120] Y. Li, F. Baccelli, H. S. Dhillon, and J. G. Andrews, "Statistical Modeling and Probabilistic Analysis of Cellular Networks With Determinantal Point Processes," *IEEE Transactions on Communications*, vol. 63, no. 9, pp. 3405–3422, September 2015.

[121] C. Saha, M. Afshang, and H. S. Dhillon, "Enriched K-tier HetNet Model to Enable the Analysis of User-centric Small Cell Deployments," *IEEE Transactions on Wireless Communications*, vol. 16, no. 3, pp. 1593–1608, March 2017.

[122] M. Afshang and H. S. Dhillon, "Poisson Cluster Process Based Analysis of HetNets with Correlated User and Base Station Locations," *IEEE Transactions on Wireless Communications*, vol. 17, no. 4, pp. 2417–2431, April 2018.

[123] M. Haenggi, "User Point Processes in Cellular Networks," *IEEE Wireless Communications Letters*, vol. 6, no. 2, pp. 258–261, April 2017.

[124] M. Mirahsan, R. Schoenen, and H. Yanikomeroglu, "HetHetNets: Heterogeneous Traffic Distribution in Heterogeneous Wireless Cellular Networks," *IEEE Journal on Selected Areas in Communications*, vol. 33, no. 10, pp. 2252–2265, October 2015.

[125] S. Andreev, A. Pyattaev, K. Johnsson, O. Galinina, and Y. Koucheryavy, "Cellular Traffic Offloading onto Network-assisted Device-to-device Connections," *IEEE Communications Magazine*, vol. 52, no. 4, pp. 20–31, April 2014.

[126] Z. Zhao, M. Li, R. Li, and Y. Zhou, "Temporal-spatial Distribution Nature of Traffic and Base Stations in Cellular Networks," *IET Communications*, vol. 11, no. 16, pp. 2410–2416, August 2017.

[127] G. Liu, X. Hou, F. Wang, J. Jin, H. Tong, and Y. Huang, "Achieving 3D-MIMO with Massive Antennas from Theory to Practice with Evaluation and Field Trial Results," *IEEE Systems Journal*, vol. 11, no. 1, pp. 62–71, March 2017.

[128] X. Cheng and B. Yu and L. Yang and J. Zhang and G. Liu and Y. Wu and L. Wan, "Communicating in the Real World: 3D MIMO," *IEEE Wireless Communications*, vol. 21, no. 4, pp. 136–144, August 2014.

[129] T. E. Bogale and L. B. Le, "Massive MIMO and Millimeter Wave for 5G Wireless HetNet: Potentials and Challenges," *arXiv preprint arXiv:1510.06359*, 2015.

Title: Coverage Performance Analysis of FeICIC Low-Power Subframes

Author: Haonan Hu; Jialai Weng; Jie Zhang

Publication: Wireless Communications, IEEE Transactions on

Publisher: IEEE

Date: Aug. 2016

Thesis / Dissertation Reuse

The IEEE does not require individuals working on a thesis to obtain a formal reuse license, however, you may print out this statement to be used as a permission grant:

Requirements to be followed when using any portion (e.g., figure, graph, table, or textual material) of an IEEE copyrighted paper in a thesis:

1) In the case of textual material (e.g., using short quotes or referring to the work within these papers) users must give full credit to the original source (author, paper, publication) followed by the IEEE copyright line © 2011 IEEE.
2) In the case of illustrations or tabular material, we require that the copyright line © [Year of original publication] IEEE appear prominently with each reprinted figure and/or table.
3) If a substantial portion of the original paper is to be used, and if you are not the senior author, also obtain the senior author's approval.

Requirements to be followed when using an entire IEEE copyrighted paper in a thesis:

1) The following IEEE copyright/ credit notice should be placed prominently in the references: © [year of original publication] IEEE. Reprinted, with permission, from [author names, paper title, IEEE publication title, and month/year of publication]
2) Only the accepted version of an IEEE copyrighted paper can be used when posting the paper or your thesis on-line.
3) In placing the thesis on the author's university website, please display the following message in a prominent place on the website: In reference to IEEE copyrighted material which is used with permission in this thesis, the IEEE does not endorse any of [university/educational entity's name goes here]'s products or services. Internal or personal use of this material is permitted. If interested in reprinting/republishing IEEE copyrighted material for advertising or promotional purposes or for creating new collective works for resale or redistribution, please go to http://www.ieee.org/publications_standards/publications/rights/rights_link.html to learn how to obtain a License from RightsLink.

If applicable, University Microfilms and/or ProQuest Library, or the Archives of Canada may supply single copies of the dissertation.

Title:	Modelling and Analysis of Reduced Power Subframes in Two-Tier Femto HetNets
Conference Proceedings:	2016 IEEE 83rd Vehicular Technology Conference (VTC Spring)
Author:	Haonan Hu; Jialai Weng; Jiliang Zhang; Jie Zhang; Yang Wang
Publisher:	IEEE
Date:	15-18 May 2016

Thesis / Dissertation Reuse

The IEEE does not require individuals working on a thesis to obtain a formal reuse license, however, you may print out this statement to be used as a permission grant:

Requirements to be followed when using any portion (e.g., figure, graph, table, or textual material) of an IEEE copyrighted paper in a thesis:

1) In the case of textual material (e.g., using short quotes or referring to the work within these papers) users must give full credit to the original source (author, paper, publication) followed by the IEEE copyright line © 2011 IEEE.
2) In the case of illustrations or tabular material, we require that the copyright line © [Year of original publication] IEEE appear prominently with each reprinted figure and/or table.
3) If a substantial portion of the original paper is to be used, and if you are not the senior author, also obtain the senior author's approval.

Requirements to be followed when using an entire IEEE copyrighted paper in a thesis:

1) The following IEEE copyright/ credit notice should be placed prominently in the references: © [year of original publication] IEEE. Reprinted, with permission, from [author names, paper title, IEEE publication title, and month/year of publication]
2) Only the accepted version of an IEEE copyrighted paper can be used when posting the paper or your thesis on-line.
3) In placing the thesis on the author's university website, please display the following message in a prominent place on the website: In reference to IEEE copyrighted material which is used with permission in this thesis, the IEEE does not endorse any of [university/educational entity's name goes here]'s products or services. Internal or personal use of this material is permitted. If interested in reprinting/republishing IEEE copyrighted material for advertising or promotional purposes or for creating new collective works for resale or redistribution, please go to http://www.ieee.org/publications_standards/publications/rights/rights_link.html to learn how to obtain a License from RightsLink.

If applicable, University Microfilms and/or ProQuest Library, or the Archives of Canada may supply single copies of the dissertation.

BACK CLOSE WINDOW

Title: Coverage Analysis of Reduced Power Subframes Applied in Heterogeneous Networks with Subframe Misalignment Interference

Author: Haonan Hu; Baoling Zhang; Qi Hong; Xiaoli Chu; Jie Zhang

Publication: IEEE Wireless Communications Letters (L-WC)

Publisher: IEEE

Date: Dec 31, 1969

Thesis / Dissertation Reuse

The IEEE does not require individuals working on a thesis to obtain a formal reuse license, however, you may print out this statement to be used as a permission grant:

Requirements to be followed when using any portion (e.g., figure, graph, table, or textual material) of an IEEE copyrighted paper in a thesis:

1) In the case of textual material (e.g., using short quotes or referring to the work within these papers) users must give full credit to the original source (author, paper, publication) followed by the IEEE copyright line © 2011 IEEE.
2) In the case of illustrations or tabular material, we require that the copyright line © [Year of original publication] IEEE appear prominently with each reprinted figure and/or table.
3) If a substantial portion of the original paper is to be used, and if you are not the senior author, also obtain the senior author's approval.

Requirements to be followed when using an entire IEEE copyrighted paper in a thesis:

1) The following IEEE copyright/ credit notice should be placed prominently in the references: © [year of original publication] IEEE. Reprinted, with permission, from [author names, paper title, IEEE publication title, and month/year of publication]
2) Only the accepted version of an IEEE copyrighted paper can be used when posting the paper or your thesis on-line.
3) In placing the thesis on the author's university website, please display the following message in a prominent place on the website: In reference to IEEE copyrighted material which is used with permission in this thesis, the IEEE does not endorse any of [university/educational entity's name goes here]'s products or services. Internal or personal use of this material is permitted. If interested in reprinting/republishing IEEE copyrighted material for advertising or promotional purposes or for creating new collective works for resale or redistribution, please go to http://www.ieee.org/publications_standards/publications/rights/rights_link.html to learn how to obtain a License from RightsLink.

If applicable, University Microfilms and/or ProQuest Library, or the Archives of Canada may supply single copies of the dissertation.